Russian Chemical Reviews **70** (3) 177 – 210 (2001) © 2001 Russian Academy of Sciences and Turpion Ltd

DOI 10.1070/RC2001v070n03ABEH000627

Nanoclusters and nanocluster systems. Assembling, interactions and properties

I P Suzdalev, P I Suzdalev

Contents

I.	Introduction	177
II.	Synthesis and classification of nanoclusters and nanocluster structures	177
III.	Properties of isolated nanoclusters	179
IV.	Cluster nanosystems and nanostructures	185
V.	Conclusion	206

Abstract. Data on the structures and properties of nanoclusters and nanocluster systems are analysed. A classification of nanoclusters and nanosystems based on the method of their preparation is proposed. Methods for assembling nanoclusters to give nanostructures, the main principles of assembling and the types of nanosystems are described. The appearance of new properties upon combination of nanoclusters into a nanosystem is noted. The bibliography includes 274 references.

I. Introduction

The properties of a material are known to change significantly on passing from macrostructures to the microstructures the size of which lies in the nanometer range. Thus the crystal lattice parameters, the heat capacity, the melting point and the electrical conductivity of nanoclusters in the condensed state differ from those of the corresponding macrocrystals. In addition, they acquire new optical, magnetic, and electronic characteristics; their reactivity and catalytic properties also change.[1–10] The properties of nanostructures are determined by not only the cluster size but also the mode of their organisation or self-organisation into a nanocluster structure in which the clusters act as separate atoms. Nanostructures, in turn, can form supramolecular structures.

The ways of assembly of nanoclusters into nanostructures depend not only on the properties of separate nanoclusters and intercluster interactions but also on the methods used to prepare nanoclusters. Thus, several main trends can be distinguished in research on nanoclusters and cluster nanosystems

— methods for the preparation and classification of nanoclusters;
— properties of isolated nanoclusters;
— ways of assembly (self-assembly) of cluster nanosystems;
— properties of nanocluster systems.

Great progress in studies of nanoclusters and nanostructures has been achieved in the last decade. An enormous number of publications have appeared, devoted both to fundamental research on nanoclusters and nanostructures and to the ways of using them in nanotechnologies (design of magnetic recording devices, nanodiodes, nanowires, and single-electron transfer devices tuned by changing the size of the nanolaser; production of new nanomaterials with specific mechanical, thermal, electronic, optical, and magnetic properties).

In this review, we present data on nanoclusters and nanostructures obtained both by methods of inorganic, physical, and solid-state chemistry and by methods of condensed-state physics and the physics of gases, using diverse calculation procedures and experimental equipment. We have not intended to give an exhaustive review on the published data concerning all the properties of nanoclusters, but considered only those of them that are of fundamental importance in the formation of cluster systems. Some of the problems considered in the review related to the interpretation of experimental facts and, especially, classification of clusters and nanoparticles are debatable. In addition, not all the cluster effects are considered. Nevertheless, we hope that the information we present would be of interest for researchers engaged in the chemistry or nanotechnologies and in physics.

II. Synthesis and classification of nanoclusters and nanocluster structures

As noted above, many properties of nanoclusters and nanosystems depend on the method used to prepare them. Therefore, we attempted to classify the clusters in terms of the method of synthesis. With this empirical approach, the diversity of properties of clusters and cluster systems can be represented on the basis of their origin. In terms of the preparation method, clusters can be classified into six groups: molecular, gas-phase, colloid, solid-state, matrix and film clusters. Isolated nanoclusters can be prepared by chemical reactions (molecular clusters), laser vaporisation (gas-phase clusters) or by matrix isolation (solid-state and colloid syntheses). Nanosystems are mainly formed in solid-state and colloid syntheses.

1. Molecular ligand metal clusters

Molecular metal clusters are multinuclear complex compounds the molecular structure of which is based on a core (cell) of metal atoms (their number should be greater than two) bound directly to one another and surrounded by ligands. The metal–metal distances in these clusters are usually shorter than those in the bulk metal.[11] The metal core consists of chains of different lengths and different branching types, rings or polyhedra or combinations of these structural units. Both homo- and heterometallic clusters are known.

I P Suzdalev, P I Suzdalev N N Semenov Institute of Chemichal Physics, Russian Academy of Sciences, ul. Kosygina 4, 117977 Moscow, Russian Federation. Fax (7-095) 137 83 18. Tel. (7-095) 939 71 01.
E-mail: suzdalev@chph.ras.ru

Received 9 October 2000
Uspekhi Khimii **70** (3) 203 – 240 (2001); translated by Z P Bobkova

Molecular ligand metal clusters are produced from metal complexes upon various chemical reactions. An enormous number of publications have been devoted to the synthesis, structure and properties of molecular metal clusters (see, for example, a monograph [11] and references therein).

2. Gaseous ligand-free clusters

Ligand-free clusters of metals or metal oxides can be prepared, for example, by laser vaporisation of metals from a substrate followed by separation according to size (or weight) in a time-of-flight mass-spectrometer. The clusters formed upon vaporisation are fixed in traps (or on substrates) and then their electronic, optical, and other properties are studied.[12] The clusters obtained in this way contain from several dozens to several hundreds of atoms. The synthesis of big nanoclusters ($\geqslant 100$ nm) is performed by heating and vaporisation of metals in a radio-frequency electromagnetic field *in vacuo* or under an inert gas followed by deposition of clusters onto a substrate or a filter.[13] The use of a substrate is necessary because nanoparticles are highly reactive and stick together upon collisions, while the substrate stabilises them.

Yet another method for the preparation of gas-phase metal clusters is vaporisation of metals in an inert gas followed by the formation of metal clusters in a low-temperature matrix (cryochemical method).[14]

Gas-phase methods of synthesis are also used for the preparation of carbon clusters (in particular, fullerenes). Thus C_{60} fullerene was prepared for the first time by laser vaporisation of graphite in 1985.[15] Fullerenes with the compositions C_{36}, C_{70}, C_{82}, C_{84}, C_{90} and C_{96} have also been synthesised.[16–19]

Among other gas-phase ligand-free clusters, van der Waals clusters of noble gases and water should be mentioned.

The evaporation–condensation technique allows the preparation of the purest metal particles; therefore, nowadays, this method is still finding application. However, when using this method, it is difficult to control the size of the resulting metal clusters. The clusters obtained in this way are characterised by broad size distributions.

3. Colloid clusters and nanosystems

Colloid solutions containing metal nanoclusters and their compounds have long been known; however, in connection with the task of preparing assembled nanostructures, it became necessary to synthesise monodisperse colloid systems with a controlled cluster size. Monodisperse colloid systems are usually synthesised using sol–gel technology,[20] which includes preparation of a sol and its transformation into a gel. Sols are prepared using dispersion and condensation (physical and chemical) methods. Thus hydrolysis of metal salts or metal alkoxides gives rise to sols of metal oxides or hydroxides characterised by high excess energy. Owing to the excess energy, aggregation of sols takes place in these systems, accompanied by the formation of a gel. This process affords nanostructures with a size of up to 100 nm.

In recent years, the use of microemulsion systems (direct and reverse micelles) for the preparation of nanoclusters with a narrow size distributions of particles has started.† Many metal clusters with particle size of 1 to 10 nm have been prepared in this way.[21,22]

4. Solid-state clusters

Solid-state clusters are formed as a result of diverse transformations of the solid phase: chemical reactions in the solid phase, crystallisation of an amorphous phase, mechanochemical transformations, *etc*.[23] Many chemical reactions in the solid state for example, thermal decomposition of metal salts and complexes are accompanied by the formation of metal or metal oxide nuclei, which then grow due to sintering. The size of nanoclusters thus formed varies over a very broad range — from one to hundreds of nanometers.

Crystallisation is employed to prepare nanoclusters from amorphous alloys. The crystallisation conditions are maintained in such a way as to generate as many crystallisation centres as possible; the growth of nanoclusters should occur at a low rate.

Solid-state nanoclusters can also be prepared *via* photochemical reactions, for example, those involving silver halides. These reactions, too, start with the formation of nuclei, which are then enlarged giving rise to nanoclusters with sizes ranging from tens to hundreds of nanometers.[7]

Apart from chemical reactions in solids, mechanochemical transformations can also be used to prepare solid-state clusters. Thus mechanical grinding of a bulk solid permits one to prepare nanoclusters the size of which does not exceed several nanometers. Due to the activation of the newly formed surface, new nanocluster compounds differing from the initial ones can arise.[6,8]

Yet another method for the preparation of solid-state nanoclusters consists in nanostructurisation of a material on exposure to pressure with shear.[6] By increasing pressure to 5 GPa and shear to 1000 °C, one can prepare nanoclusters with a grain size reaching several nanometers the properties of which differ sharply from those of the initial material. Nanoclusters are also produced when other methods of plastic yield are employed.

5. Matrix clusters

Methods for the preparation of nanoclusters which make use of various inorganic and organic matrices and matrix isolation constitute a self-dependent group, although they can include some features of the gas-phase, solid-state and other methods. The point is that nanoclusters prepared using matrix methods differ from those formed, for example, in solid-state chemical reactions because they are isolated from one another by the matrix and, therefore, heating of the whole nanosystem does not result in an increase in the cluster size due to sintering. The originality of this approach is that it provides the possibility of restricting size dispersion of the nanoclusters and of changing the intercluster interactions in a required manner. Thus microencapsulation of nanoclusters in inert gases at low temperatures is used to prepare gas-phase metal clusters.

Clusters and cluster systems are often prepared by chemical reactions in solution followed by precipitation of the resulting compounds in the pores of a solid. Nanoclusters and nanosystems can also be prepared by impregnating porous matrices with solutions and performing chemical reactions in the pore acting as a micro- or a nanoreactor. This procedure is used, for example, to prepare metal and metal oxide clusters in zeolites, the cluster size being determined by the size of zeolite cells (1–2 nm). In this case, aluminosilicates promote the formation of assembled cluster structures.

Broad opportunities for the variation of the size and composition of clusters are provided by using inorganic and organic sorbents (for example, silica gels and aluminogels, ion exchange resins and polysorbs).[3] In this case, the change in the cluster size and cluster organisation takes place due to both the change in the pore size and the variation of the surface hydrophilicity (or hydrophobicity), the concentration of initial components, temperature, *etc*.

6. Nanofilms

When nanoclusters are formed in nanofilms, the mechanism of nucleation and growth differs from those in the formation of solid-state clusters because the synthesis is related to the surface chemistry (the formation of two-dimensional structures). Epitaxial nanofilms on an oriented crystalline surface are prepared using laser vaporisation and molecular beams.[17]

In recent years, the CVD method has started to be widely used to apply nanocluster nanofilms on the surface.[24] According to this

† Procedures for the synthesis of ultradisperse particles based on the sol–gel method and microemulsion systems are described in the recent review by B D Summ, N I Ivanova *Usp. Khim.* **69** 995 (2000). [*Russ. Chem. Rev.* **69** 911 (2000)]

method, the initial substances are first evaporated and then transferred through the gas phase and deposited in a required proportion onto a chosen substrate.

To produce molecular layers with controlled composition and thickness, the method of molecular layering is used, the essence of which is to induce surface chemical reactions separated in space and time.[25–27] Nanofilms containing one to ten monolayers have been prepared in this way.

The technology of synthesis of Langmuir–Blodgett films, which has been developed in recent years, makes it possible to introduce metal ions and metal complexes into the surfactant film being formed on the surface of water and thus to prepare nanoclusters. The use of this approach results in the formation of Langmuir–Blodgett films with an ordered monolayer of clusters, which can then be applied onto a solid substrate using a special technique. This procedure can be repeated thus forming multilayer films and superstructures.[28]

III. Properties of isolated nanoclusters

Clusters occupy an intermediate position between separate molecules and macro-solids. Therefore, the properties of a single isolated cluster can be compared both with the properties of separate atoms or molecules and with the properties of a bulk solid.

The notion 'isolated cluster' is rather abstract because it is virtually impossible to obtain a cluster not interacting with the environment. In addition, when investigating the properties of isolated clusters, one should take into account their interaction with the measuring instrument, which can change the properties of the cluster during the measurements. This is especially true for contact techniques of measurement (for example, tunnelling microscopy). However, these changes are relatively insignificant and we shall not consider this type of interaction in this review. Since molecular metal clusters, van der Waals noble gas and water clusters, gas-phase metal clusters, and fullerenes are subject only to weak intercluster interactions, they can conventionally be considered as isolated clusters.

In this Section, we shall consider the structure, the atomic dynamics, and the electronic, optical, and magnetic properties of isolated clusters.

1. Molecular ligand clusters in solutions

Molecular clusters are important objects of coordination, inorganic and structural chemistry. The unusual features of their structures and properties caused by the presence of a core of metal atoms have stimulated the development of a separate branch of science — cluster chemistry — possessing its own calculation, synthesis and investigation methods. Since the number of metal atoms forming the cluster core can vary from a few to hundreds or even thousands, a specific approach to the choice of the investigation method for each particular cluster is required. The methods range from those designed for separate atoms (for example, atomic molecular spectroscopy), used in the case of small clusters, to those developed to study the collective and dynamic properties, which are used for big clusters.

In this Section we consider specific quantum-size properties of molecular clusters, which display themselves when the size of the metal core of the cluster ranges from 1 to 3 nm. The properties of bigger clusters (3 to 20 nm) are discussed in the Section devoted to colloid clusters.

The core of a molecular cluster is formed in accordance with the close-packing pattern of metal atoms, similarly to the bulk metal.[29,30] The number of metal atoms in a close-packed core constructed as a regular 12-vertex polyhedron (cubooctahedron, icosahedron, or anticubooctahedron) can be found from the formula

$$N = \frac{1}{3}(10n^3 + 15n^2 + 11n + 3),$$

where n is the number of layers around the central atom. Thus, the smallest close-packed core contains 13 atoms: one central atom and 12 first-layer atoms. This gives a set of 'magic' numbers $N = 13, 55, 147, 309, 561, 923, 1415, 2057, 2869$, *etc*. corresponding to the most stable cores of metal clusters. Indeed, the following clusters are known: 13-atomic (single-layer) clusters $[Au_{13}(diphos)_6](NO_3)_4$ (diphos is $PPh_2CH_2CH_2PPh_2$)[31] and $[Rh_{13}(CO)_{24}H_3]^{2-}$ (see Ref. 32) with icosahedral and cuboocta-hedral cores, respectively, 55-atomic (two-layer) clusters $Au_{55}(PPh_3)_{12}Cl_6$,[33,34] $Rh_{55}(PPh_3)_{12}Cl_6$, $Pt_{55}(AsBu^t_3)_{12}$,[35,36] $Ru_{55}(PBu^t_3)_{12}Cl_{20}$ (see Ref. 37) with cubooctahedral cores, a 309-atomic (four-layer) cluster $Pt_{309}Phen'_{36}O_{30\pm10}$ [Phen′ is the sodium salt of 4,7-bis(phenylsulfate)-1,10-phenanthroline] with a cubooctahedral core,[38] a 561-atomic (five-layer) cluster $Pd_{561}Phen_{60}(OAc)_{180}$ (Phen is phenanthroline) with an icosahedral core,[39,40] 1415-atomic (seven-layer) cluster $Pd_{1415}Phen_{60}O_{\sim1100}$ and a 2057-atomic (eight-layer) $Pd_{2057}Phen_{84}O_{\sim1600}$ cluster.[10] It should be noted that, in addition to stable clusters, with 'magic' numbers of metal atoms, intermediate clusters with other numbers of atoms are also inevitably formed.

For the Au_{55} and Pd_{561} clusters, electrical conductivity, heat capacity, and magnetic susceptibility were measured. These characteristics proved to differ substantially from those of the bulk metal. The electrons of the metal atoms forming the cluster core are not delocalised, unlike the collectivised electrons in a bulk metal sample; instead, they form discrete energy levels differing from molecular orbitals. On passing from the bulk metal to a cluster and then to a molecule, delocalised *s*- and *d*-electrons forming the conduction band in the bulk metal are replaced by non-delocalised electrons, which form discrete energy levels in a cluster, and then by molecular orbitals.

The appearance of discrete electron bands in metal clusters with a size ranging from 1 to 4 nm should be accompanied by the appearance of single-electron transitions. An efficient technique for observing effects of this type is tunnelling microscopy (TM), which provides voltammetric characteristics when the tip of the microscope is fixed on a molecular cluster. Upon transition from the cluster to the tip of the tunnelling microscope, an electron overcomes a Coulomb barrier the height of which is equal to the electrostatic energy $\Delta E = e^2/2C$ (C is the nanocluster capacity proportional to its size). For small clusters, the electrostatic energy of an electron becomes greater than its kinetic energy kT; therefore, steps corresponding to the single-electron transition appear on the voltammetric curve $U = f(I)$. Thus, a decrease in the cluster size and in the temperature of the single-electron transition results in violation of the linear dependence $U = f(I)$, typical of the bulk metal. A stepwise dependence has been observed for the $Au_{55}(PPh_3)_{12}Cl_6$ molecular cluster with a size of 1.4 nm even at room temperature.[41] As the temperature further decreases to 90 K, several Coulomb steps appear on the voltammetric curve (Fig. 1 *a*,*b*).

Quantum-size effects were observed in the measurements of the magnetic susceptibility and the heat capacity of the molecular clusters $Pd_{561}Phen_{60}(OAc)_{180}$, $Pd_{561}Phen_{36}O_{200}$, $Pd_{1415}Phen_{54}$. O_{1000} and $Pd_{2057}Phen_{78}O_{1600}$ (see Ref. 42) at ultralow temperatures. Bulk Pd exhibits Pauli paramagnetism, which is provided by electrons with an energy E_F near the Fermi energy; therefore, its magnetic susceptibility barely depends on the temperature down to the liquid-helium temperature.

Calculations show that on passing from Pd_{2057} to Pd_{561}, *i.e*., as the size of Pd clusters diminishes, the density of states near E_F decreases, resulting in a change in the magnetic susceptibility. The calculation predicts that upon a decrease in the temperature ($T \to 0$), the susceptibility should either drop to zero or increase to infinity for even and odd numbers of electrons, respectively. Since the study was performed for clusters containing an odd number of electrons, the magnetic susceptibility was actually found to increase. The increment is substantial for Pd_{561} (with a maximum at $T < 2$ K) and slight for Pd_{1415}. In the case of Pd_{2057}, virtually no temperature variation is observed, which is typical of

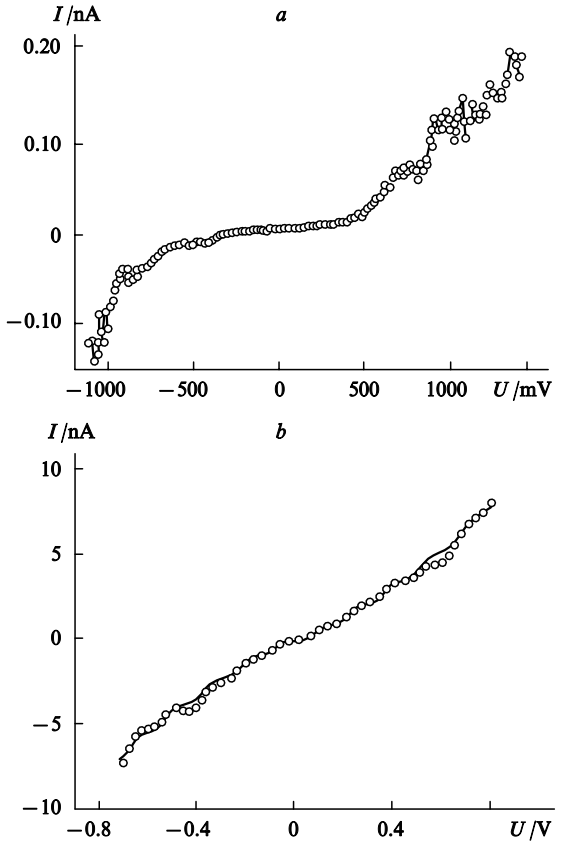


Figure 1. Voltammetric characteristics of the $Au_{55}(PPh_3)_{12}Cl_6$ cluster at $T = 300$ (*a*) and 90 K (*b*).[41]

bulk Pd, although, as noted above, the values of magnetic susceptibility found for Pd_{2057} are much lower than those for bulk Pd.

Heat capacity measurements for giant Pd molecular clusters have revealed equally interesting features. Bulk solids are characterised by a linear temperature dependence of electron heat capacity, $C \sim T$. The transition from the bulk solid to nanoclusters gives rise to quantum-size effects,[42] which are manifested as a deviation of the $C = f(T)$ plot from linearity following a decrease in the cluster size. Thus the greatest deviation from the linear dependence is observed for Pd_{561}. With a correction for the ligand dependence ($C \sim T^3$), a $C \sim T^2$ dependence was obtained for nanoclusters at ultralow temperatures $T < 1$ K. The heat capacity of a cluster is known to be $C = kT/\delta$ (δ is the mean distance between energy levels, $\delta = E_F/N$, where N is the number of electrons in the cluster). Calculations of the δ/k value carried out for Pd_{561}, Pd_{1415} and Pd_{2057}, and for the colloid Pd cluster with a size of $\sim$15 nm, gave values of 12, 4.5, 3.0 and 0.06 K, respectively. Thus, the unusual $C \sim T^2$ dependence in the region of $T < 1$ K indicates that quantum-size effects are involved. Note that the $C \sim T^2$ dependence is also typical of amorphous solids and is attributable to tunnelling effects.[43]

Quantum-size effects have also been observed in non-metal and metal oxide and chalcogenide ligand clusters.[44–46] The internal metallic core in the molecular cluster $[Mn_{12}(CH_3COO)_{16}.(H_2O)_4O_{12}]\cdot 2CH_3COOH\cdot 4H_2O$ (Mn_{12}^*) has a tetragonal two-layer structure: the Mn^{4+} atoms of the inner cubane structure of Mn_4O_4 have total spin $S = 3/2$, and the eight outer Mn^{3+} atoms have spin $S = 2$.[45] The exchange interactions within the cluster stabilise the ferromagnetic ground state with a collective spin $S = 10$ (parallel and antiparallel alignment of the individual spins of Mn^{4+} and Mn^{3+}). A single crystal constructed from Mn_{12}^* clusters was placed in an external magnetic field ($H = 5$ T) and its magnetisation at $T = 1.55 - 3.2$ K was measured.[45]

The Mn_{12}^* cluster with the spin $S = 10$ forms energy levels in an external magnetic field. Electronic transitions between these levels can be either induced by thermal fluctuations or occur *via* quantum tunnelling. A thermally activated transition can be due to superparamagnetism (superparamagnetic relaxation), when the total magnetic moment of the cluster fluctuates as a whole. In this case, the magnetisation curves vary smoothly. For a single crystal constructed from Mn_{12}^* clusters, unusual 'stepwise' hysteresis curves (Fig. 2) resembling single-electron conductivity curves have been obtained. A magnetisation curve has steps in the case where the quantum mechanism of tunnelling is involved. This effect takes place when the magnetic field strength is such that the energy levels coincide. At these H values, the relaxation by a tunnelling mechanism from one spin state to another is accelerated compared to the superparamagnetic relaxation. As a consequence, at low temperatures, discontinuous changes in the magnetisation by $H_{n+1} - H_n = \Delta H = 0.44$ T are observed in the region of H from 0 to 2.64 T, in accordance with quantisation of the spin levels in a magnetic field.

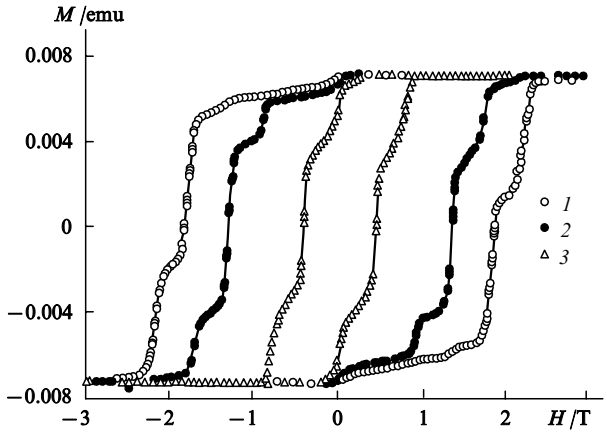


Figure 2. Magnetisation curves for a single crystal of the Mn_{12}^* acetate cluster at different temperatures.[45]
Temperature /K: 1.77 (*1*), 2.10 (*2*) and 2.64 (*3*).

Semiconductor molecular clusters also exhibit a number of remarkable properties. Since semiconductor clusters acquire discrete energy levels in the valence band and in the conduction band, and the energy gap between them increases (with respect to that in the bulk sample), the optical transitions between these levels are characterised by greater energies. The smaller the cluster, the greater the energy of optical transitions. This is the so-called blue shift of the radiation frequency observed upon a decrease in the cluster size. A similar effect has been observed for the $Cd_{32}S_{17}(SC_6H_5)_{36}(DMF)_4$ clusters with a semiconductor CdS nucleus having a size of $\sim$1.5 nm.[46] The increase in the radiation frequency is accompanied by an increase in the oscillator strength, which is now concentrated on several transitions.

A decrease in the cluster size also restricts the wavelength of carriers in semiconductors. The appearance of discrete levels in the clusters characterises them as quantum dots with zero dimensionality.

Examples of semiconductor clusters with specific optical properties will be considered in the Section devoted to colloid clusters.

Thus, the molecular ligand clusters of metals and metal oxides and chalcogenides possessing quantum-size properties can underlie the design of materials with new electronic, magnetic, and optical properties.

2. Gaseous ligand-free clusters

Ligand-free clusters are devoid of a ligand shell influencing the properties of the surface atoms of the core; in this respect, they

differ from molecular clusters. Ligand-free clusters have been obtained for almost each element of the Periodic System. Several groups of ligand-free clusters possessing characteristic properties can be distinguished: alkali metal clusters, carbon clusters, rare gas clusters and van der Waals clusters.

a. Alkali metal clusters

The properties of alkali metal clusters are well described in terms of the jellium model or, what is the same, the drop shell model. According to this model, a cluster is considered as two subsystems: positively charged ions forming the core and delocalised *s*-electrons, which can form shells similar to the electron shells in atoms. The electron shell in an atom is occupied by the numbers of electrons $n_e = 2, 8, 18, 20, 34, 40$, *etc*., which corresponds to the filling of $1s$, $1p$, $1d$, $2s$, $1f$, $2p$, *etc*. shells.[47,48] The number of metal atoms in a cluster that corresponds to the number of electrons in the filled shells is called the 'magic' number. The 'electronic magic numbers'‡ correspond to the most stable electronic configurations of clusters with filled shells. They were discovered experimentally during measurements of ionisation potentials and electron affinities.[49]

Calculations carried out in terms of the jellium model made it possible to explain the shell structure of the clusters. The classical expression for the electron work function in the jellium model (drop model) of the cluster[50]

$$W(R,z) = W_\infty + \frac{(z + 3/8)e^2}{R}, \qquad (1)$$

[W_∞ is the electron work function for the bulk metal, z is the charge of the cluster (spherical), and R is the cluster radius] predicts higher ionisation potentials for clusters compared to bulk solids. In the case of nanoclusters, a stepwise dependence of the ionisation potential on the number of atoms is observed (the steps occur at points corresponding to 'magic' numbers). The stability of charged clusters is determined by the dissociation energy. Thus the dissociation energies for Na_n^+ and K_n^+ pass through maxima at $n = 9$ and 21, which corresponds to filled shells containing 8 and 20 electrons.[51,52]

The quantum-size effects manifest themselves in the optical properties of clusters, which is expressed as the appearance of a discrete structure and broadening of spectral lines.[53] An interesting effect is giant resonance associated with oscillations and polarisability of the cluster electrons. Similar giant resonance effects have also been observed for atomic nuclei, in which they are related to the collective motion of protons relative to neutrons. The optical absorption in a cluster is calculated using the Mie equation,[54] derived for a spherical cluster. According to Mie, light absorption cross-section (σ) has a resonance form

$$\sigma = \frac{ne^2}{mc\Gamma\varepsilon_0} \frac{\omega^2}{\omega^2 - \omega_0^2 + (\omega\Gamma)^2}, \qquad (2)$$

where n is the number of electrons, e and m is the charge and the mass of an electron, c is the velocity of sound, Γ is the damping coefficient for the oscillation of electrons in an electromagnetic field (line width), ε_0 is polarisability in vacuum, ω is the oscillation frequency, and $\omega_0 = \omega_p/\sqrt{3}$ is the resonance oscillation frequency constituting a part of the plasmon frequency (ω_p) of electron oscillations in the bulk metal ($\omega_p = e^2/4\pi\varepsilon_0 V$, $V = 4/3\pi r_s^3$, r_s is the Wigner – Seitz radius).

Calculation of the cluster polarisability in terms of the jellium model predicts that the cluster polarisability $\alpha = (ne^2/m\varepsilon_0)\omega_0^2$ should be greater than that of a bulk sample, which is actually observed for Na and K clusters with $n \leqslant 40$.[55] Ellipsoidal clusters have two resonance frequencies, longitudinal and transverse ones; this makes it possible to estimate the cluster shape. Figure 3 shows

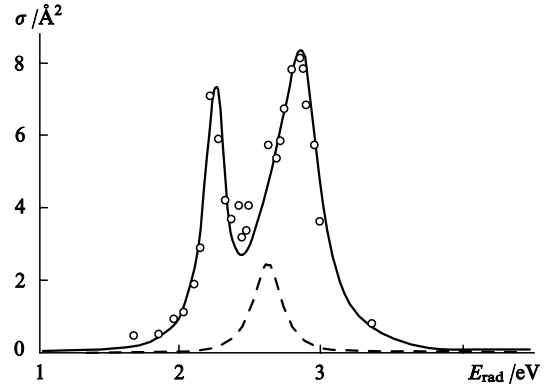


Figure 3. Giant resonance for ellipsoidal Na_{11}^+ clusters.[56] The lower-energy peak corresponds to vibrations along the ellipsoid axis and the higher-energy peak corresponds to perpendicular vibrations. The dashed line corresponds to spherical Na_9^+ clusters.

the resonance dependences of absorption cross-sections on the radiation energy for the ellipsoidal Na_{11}^+ and spherical Na_9^+ clusters.[56] The two resonance peaks on the curve for the ellipsoidal Na_{11}^+ cluster imply that the oscillation frequencies along (low energies) and across (high energies) the cluster axis are different.

A shell electronic structure was also found for noble metal clusters. Although the valence bands in Cu and Ag clusters are almost twice as wide as those in alkali metal clusters, their electronic structures are similar. Due to stronger bonding of Ag atoms, the shell effects are more pronounced in the Ag cluster. The shell structure of Ag_n^- clusters ($n = 3$ to 21) was studied by photoelectron spectroscopy.[57] The greatest Ag – Ag energy was found for the Ag_{17}^- cluster, which corresponds to a filled 18-electron shell. Quantum-mechanical calculations carried out in the same study demonstrated the legitimacy of using the shell model for virtually any Ag_n^- cluster, except for Ag_7^- and Ag_9^-, which might be due to the shape of these anions.

b. Transition metal clusters

In this Section, the attention is focused on the stability and reactivity of transition metal clusters and their magnetic properties. It has been noted previously that the stability and reactivity of clusters are due to two series of 'magic' numbers, one of them being related to the geometric factor (close packing), as in ligand metal clusters, and the other being related to the electronic shell structure, as in alkali metal clusters. The properties of most ligand-free clusters of transition metals are determined by both electronic and geometric factors. In addition, for ligand-free transition metal clusters, the ability of metal atoms to exist in different oxidation states becomes especially significant; therefore, the properties of these clusters cannot be characterised by the simple shell model, as were the properties of alkali metal clusters. Exceptions are provided by Cu, Ag and Au atoms in which the *d* shell is filled and compressed, so that only *s* electrons are involved in binding.

One of the important characteristics of metal nanoclusters is ionisation energy. According to the drop model, it should increase with a decrease in the cluster size according to the $1/R$ law. However, the ionisation energy of Fe_n, Co_n and Nb_n clusters calculated using this model proved to be markedly lower than the value obtained in experiments. In addition, for small clusters with $n < 25$, the ionisation energy was shown to vary irregularly with size: the ionisation energies for clusters with even numbers of atoms are greater than those for odd numbers of atoms. The deviation from the drop model points to a difference between the electron *d* bands formed during the variation of n (even or odd).[58,59]

Let us follow the variation of the properties of a cluster depending on its size and structure taking niobium clusters as

‡ Of course, the 'electronic magic numbers' do not coincide with the Kini 'magic' numbers[29] (see above).

examples. The reactivity of Nb_n clusters was studied in the reactions with N_2 and D_2.[60] Among niobium clusters with $n < 21$, Nb_8, Nb_{10} and Nb_{16} were the most stable, which correlates with minima of the ionisation potential. It was found that some Nb clusters can exist as several geometric isomers differing in reactivity.[61] The geometric structure influences most substantially the reactivity of Nb_n clusters with $n = 3-35$.[62] However, the reactivity of Nb_n clusters with $n = 2-20$ is still governed by the electronic structure. Thus the photoelectron spectra of Nb_n^- clusters ($n = 6-17$) with even numbers of electrons differ from the spectra of Nb_n^- clusters with odd numbers of electrons,[63] which is related to the occupation of the electron shells. The highest transition energies were found for Nb_8, Nb_{10} and Nb_{16}.

A number of ligand-free copper sulfide clusters $[Cu_nS_m]^-$ with $n = 6-45$ and $m = 4-23$ have been prepared by laser vaporisation.[64] Different reactivities of $[Cu_{10}S_6]^-$ and $[Cu_6S_4]^-$ were noted. The former cluster is inert in gas-phase reactions with RSH (R = H, Pr, Ph), while the latter reacts with them to give addition products.[64]

The stability of the clusters was also estimated from their trend to decompose, undergo fission or store energy. The Coulomb fission (induced by repulsion of two charged clusters) and vaporisation of the Sb_n^+ and Sb_n^{2+} clusters ($5 \leqslant n \leqslant 80$) have been studied.[65] The results were interpreted using two models — the drop model taking into account vaporisation of fragments and the Coulomb model. Decomposition of a cluster depended on its charge. For Sb_n^+ clusters with $5 \leqslant n \leqslant 8$, decomposition with vaporisation of neutral dimers was observed, while for Sb_n^+ clusters with $n \geqslant 8$, decomposition with vaporisation of Sb_4 took place. The fragmentation of Sb_n^{2+} clusters followed a different route: for Sb_n^{2+} with $26 \leqslant n \leqslant 36$, asymmetric fission with evolution of Sb_5^+ and Sb_7^+ occurred, whereas for Sb_n^{2+} with $n > 40$, the fission was more symmetric ($Sb_n^{2+} \rightarrow Sb_{n-p}^+ + Sb_p^+$), the masses of the fragments differing by less than 30%. The rate of fission of Sb_n^{2+} clusters with $n < 36$ depends on the type of decomposition and varies according to the $1/n$ pattern, which is in line with the drop model. For larger clusters with $n > 40$, the decrease in the fission rate no longer obeys the $1/n$ law, indicating a deviation from the drop model. In this case, fission occurs simultaneously with vaporisation of Sb_4 fragments.

The variation of the magnetic moment of a substance on passing from an atom to a solid has been followed in relation to gas-phase ligand-free clusters of transition and rare earth metals. The magnetic moment of an isolated transition metal atom differs from the value found for a bulk sample. This is due to the facts that the bulk metal has a *d* conduction band and that the *d* electrons in delocalised states undergo exchange interactions known as itinerant exchange interactions. Thus the magnetic moment of an iron atom in mono- and binuclear iron compounds amounts to $6\,\mu_B$, while the magnetic moment of an iron atom in a bulk ferromagnet is $2.2\,\mu_B$. The magnetic moments of metal atoms and the magnetic properties of a cluster depend on the number of metal atoms in the cluster and vary over a broad range. This may be due to the possible rearrangement of the crystal lattice consisting of clusters, which does not coincide with the crystal lattice of the bulk sample. The determination of magnetic properties during cluster formation can occur in accordance with either the geometric close-packing model, as in the case of molecular ligand clusters with the 'magic' numbers 13, 55, 147, 304, 561, *etc.*, or the structure of the electron shell, as in the case of alkali metal clusters.

For Fe, Co and Ni clusters, the magnetic moments of the metal atoms in the core were found to increase with respect to the values for the same atoms in the bulk sample.[66, 67] Thus the Fe magnetic moment increased to $3.2\,\mu_B$; this was accompanied by fluctuations of the magnetic moment depending on the number of metal atoms in the cluster (Fig. 4*a*), which may be due to the geometric filling of close-packed layers. The value $\mu = 2.2\,\mu_B$, typical of Fe atoms in a bulk sample, is attained when the number of atoms (n) in the cluster has increased to 500. For Ni atoms, the lowest magnetic moments were found in the Ni_{13} and Ni_{55}

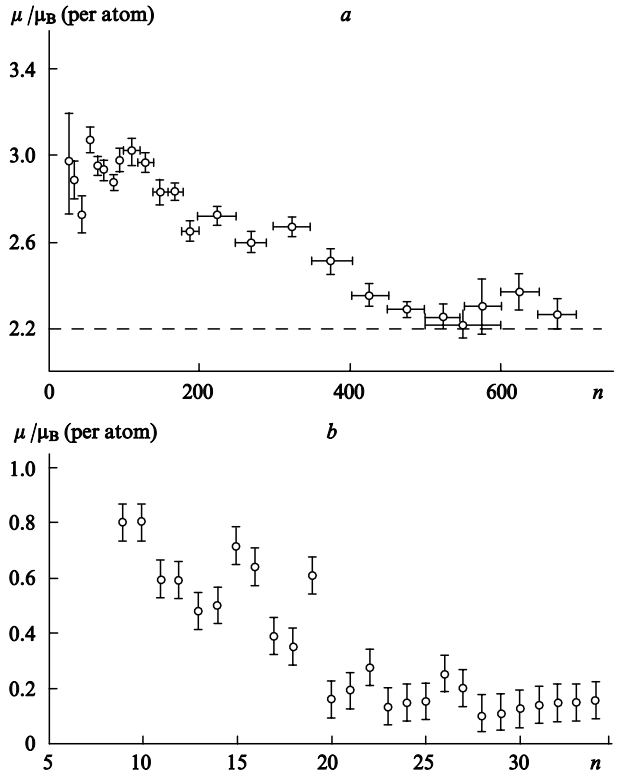


Figure 4. Magnetic moments (per atom) for Fe (*a*)[66] and Rh (*b*)[69] clusters of various sizes. The dashed line corresponds to the magnetic moment $\mu = 2.2\,\mu_B$ of bulk Fe; n is the number of metal atoms in the cluster.

clusters, which corresponds to the 'magic' numbers of close packing.[68] However, when measuring the magnetic properties, the electronic properties of the cluster and the itinerant magnetism should be taken into account. A decrease in the cluster size not only increases the magnetic moments of the atoms forming it but also gives rise to a magnetic moment of the cluster as a whole, which was observed for clusters of non-magnetic Rh (Fig. 4*b*).[69]

c. Carbon clusters

Carbon atoms readily form clusters. They are usually prepared by laser vaporisation of a graphite target. Their mass distribution is normally studied using mass spectrometry. The mass spectrum of these species has a bimodal divergence. Among small carbon clusters with $n < 24$, clusters with odd 'magic' numbers (3, 7, 11, 19, 23) of carbon atoms were the most stable, while among big clusters (fullerenes), the most stable species are those with even numbers of carbon atoms.

Small carbon clusters display enhanced stabilities when $n = 7$, 11, 15, 19 and 23, which is related to 'magic' numbers corresponding to close packing of atoms.[70, 71] The fragmentation of carbon clusters is accompanied by detachment of C_3 and C_5 fragments, pointing to high stability of these fragments. The reasons for the formation of stable carbon clusters include easy *sp*-hybridisation of carbon atoms and high strength of π-bonds.

Quantum-mechanical calculations for the molecular orbitals in carbon clusters indicate that clusters with $n \leqslant 10$ tend to have a linear structure. As the number of carbon atoms increases, the linear structure is replaced by a ring structure.[72] Thus both chain and ring species were found for the C_7^+ clusters.[70] However, the ring structure is subject to additional strain, which increases the total energy of the cluster; therefore, it is more favourable for big clusters. For C_{20}, a three-dimensional structure also becomes possible. Clusters with mixed structures were also detected. Small positively charged carbon clusters react with various diatomic molecules in the gas phase,[70, 73] and also with small

hydrocarbon molecules such as C_2H_2 ($C_n^+ + C_2H_2 \rightarrow C_{n+2}H_2$)[74] and HCN ($C_n^+ + HCN \rightarrow HC_nCN^+$).[75]

The first representatives of big carbon clusters, C_{60} and C_{70} fullerenes, were discovered in 1985 based on the mass spectra;[15] as soon as 1990, the method of fullerene preparation by vaporisation of graphite electrodes in an electric arc was developed.[16] This technique was used to prepare diverse fullerenes, which triggered extensive studies on their physical and chemical properties.

The best studied fullerene is C_{60}, shaped like a truncated icosahedron in which the pentagonal cells are coupled with hexagonal ones. This fullerene is the most symmetrical among all the fullerenes prepared. The unique feature of C_{60} is that it is the only structure in which all the carbon atoms in the five- and six-membered rings are equivalent (*i.e.*, the strain is uniformly distributed). In addition, in this fullerene, the five-membered rings are all separated from one another.

How does the so well-organised and symmetrical molecule arise? Calculations using simple kinetic models[76] describing the nucleation and growth of carbon clusters from the carbon atoms produced upon laser-induced vaporisation of graphite electrodes showed that the formation of a linear chain is energetically the most favourable. These chains interact with one another in a plasma giving rise to aggregates of 20–30 carbon atoms. During aggregation, aromatic rings or graphene layers are formed as a result of fluctuations. If the density of carbon atoms is rather high, the rings become twisted to give carbon black particles. There exists, however, a large probability that the opposite edges of the rings would meet; this yields fullerene.

The symmetrical closed structure of C_{60} and C_{70} fullerenes produces an impression that they should have low reactivity. However, a tremendous number of fullerene compounds are known. Various atoms and molecules can be attached to the carbon atoms of the fullerene cage (exohedral fullerenes); foreign atoms and molecules can be introduced inside the fullerene cage (endohedral fullerenes); the carbon atoms in the cage can be replaced by other atoms (substitution fullerenes).

The following substitution fullerenes are known: $C_{59}B$, $C_{69}B$,[77] $C_{59}N$ and $(C_{59}N)_2$.[78] The cage can also incorporate silicon and niobium atoms.[79–82] Fullerenes containing transition metal atoms $C_{59}M$ and $C_{69}M$ (M = Fe, Co, Ni, Rh, Ir) have been synthesised.[83] This was done by mixing metal and fullerene vapours. The formation of $C_{59}M$ and $C_{69}M$ fullerenes was detected in the mass spectra after photoionisation of the clusters. Substitution fullerenes have also been obtained by photoionisation of the exohedral fullerenes $C_{60}M_x$ and $C_{70}M_x$ ($x = 0–30$) with metal atoms on the surface of the cluster. It was found that, after crossing the photoionisation threshold, the metal atoms passed from the cluster surface (exohedral position) into the fullerene cage (substitution fullerenes).

Among exohedral fullerenes, fluorinated fullerenes, $C_{60}F_{60}$, are the most interesting.[84] These clusters and materials based on them are suggested to act as 'molecular ball bearings' and superlubricants. The $C_{60}M_x$ and $C_{70}M_x$ fullerenes with exohedrally attached alkali metal atoms have found extensive use. Of considerable interest are not only the structure and reactivity of these compounds but also the high-temperature superconductivity arising in them. Thus C_{60} fullerenes with a Cs/Rb component ($T_c = 33$ K) and with a Rb/Tl component ($T_c = 43$ K) have been prepared.[85] It is expected that fullerenes with an I_2 component would have $T_c = 70$ K.

The first endohedral fullerene La@C_{60} has been synthesised simultaneously with the discovery of fullerenes themselves.[86] Endohedral fullerenes can be prepared either during the fullerene synthesis by vaporisation of graphite electrodes containing a particular metal or by introducing atoms of inert gases inside the fullerene cage at high pressures and temperatures.[87,88] The size of the fullerene inner cavity increases with an increase in the number of carbon atoms; a larger fullerene cavity can accommodate several metal atoms. For example, evidence for the insertion of the La_3 cluster inside C_n fullerenes with $n \geqslant 88$ has been obtained.[89] Study of the photofragmentation of fullerenes containing K and Cs atoms showed that the minimum C_n clusters whose cavity can accommodate K and Cs atoms are C_{44} and C_{48}, respectively.[88,90]

d. Van der Waals clusters of inert gases and other small molecules

The properties of clusters formed by atoms of inert gases are dictated by weak van der Waals interactions. The stability of these clusters, like that of molecular ligand metal clusters, is associated with the 'magic' numbers characterising the geometric close packing. Clusters of inert gases with $n = 3$ are shaped like triangles, those with $n = 4$ are tetrahedra, the clusters with $n = 7$ are pentagonal pyramids, and starting with $n = 13$, the icosahedral geometry appears. The next icosahedra are formed for $n = 55$, 147, 309, 561, *etc.*, that is, for n values equal to the 'magic' numbers. For clusters with $n > 800$, a face-centered cubic packing becomes favourable.[91,92]

For rare gas clusters, effects related to photoabsorption, fluorescence, photoionisation and photofragmentation thresholds, as well as to the formation and relaxation of excitons have been studied. Fluorescence was excited by synchroton radiation.

The exciton transitions in krypton clusters have been studied. Various Kr_n clusters, atomic Kr, and a bulk sample were used (Fig. 5).[93] The Kr atomic spectrum (Fig. 5 *a*) contains two narrow bands caused by the $4p^6 \rightarrow 4p^55s$ transition (spin–orbit splitting). The spectra of Kr_n clusters (Fig. 5 *b–e*) exhibit lines corresponding to exciton transitions. Excitation of an electron in the Kr atom gives rise to a positive charge (hole). The electron and the hole form a series of hydrogen-like states, which are manifested in the fluorescence spectra as broadening, displacement, and additional lines.

Apart from the differences between the spectra of atoms, clusters, and bulk materials, differences between the spectra of atoms located on the surface and inside the cluster are also observed. For example, the spectra of Xe_mAr_n clusters ($n = 1000$) were found to contain lines corresponding to the Xe atoms located on the surface and inside the Ar_n clusters and also incorporated in the cage made of Ar atoms.[94]

In charged rare gas clusters, the charge is not delocalised over the whole cluster, as, for example, in Na_n^+, but is located on a small structural fragment (dimer, trimer, or tetramer), the rest of the cluster remaining neutral, as, for example, in $(Ar_x^+)Ar_{n-x}$ ($x = 3$, 4).[95]

Van der Waals clusters formed by H_2O, CO_2, SF_6 and C_6H_6 molecules able to form weak van der Waals polarisation contacts and hydrogen bonds are also known. For example, for the $(CO_2)_n$, $(SF_6)_n$ and $(C_6H_6)_n$ clusters, the van der Waals bonding energy is lower than 0.1 eV; for $(HF)_n$, $(H_2O)_n$ and $(CH_3OH)_3$, this value is lower than 0.3 eV.[96] Clusters with relatively small numbers of molecules, $n < 5$, can have ring structures. Small clusters with $5 < n \leqslant 20$ are non-symmetrical because side chains are attached to the ring structure, the whole cluster looking like a fragment of an amorphous or liquid structure. This trend is retained until the cluster size reaches $n = 20$. Then switching to ordered structures typical of big clusters takes place. The structures of molecular clusters are characterised by fast dynamic transitions between various conformations. The changes in the widths and positions of bands in the IR spectra of these clusters attest to the change in the number of molecules forming the clusters.[97]

Of special interest are water clusters that constitute liquid water and ice. They also participate in the formation of clouds and rains. The progress in laser spectroscopy and molecular dynamics made it possible to determine a number of properties of water clusters caused by their dynamic structure. Data on the geometric structure and hydrogen bond tunnelling in water tri-, tetra-, penta- and hexamers have been obtained.[98] Calculations[99,100] predict a planar structure for the tri-, tetra- and pentamers and a three-dimensional structure for the heptamers and larger clusters of water. The optimal configuration is characterised by the maximum number of hydrogen bonds and the minimum geo-

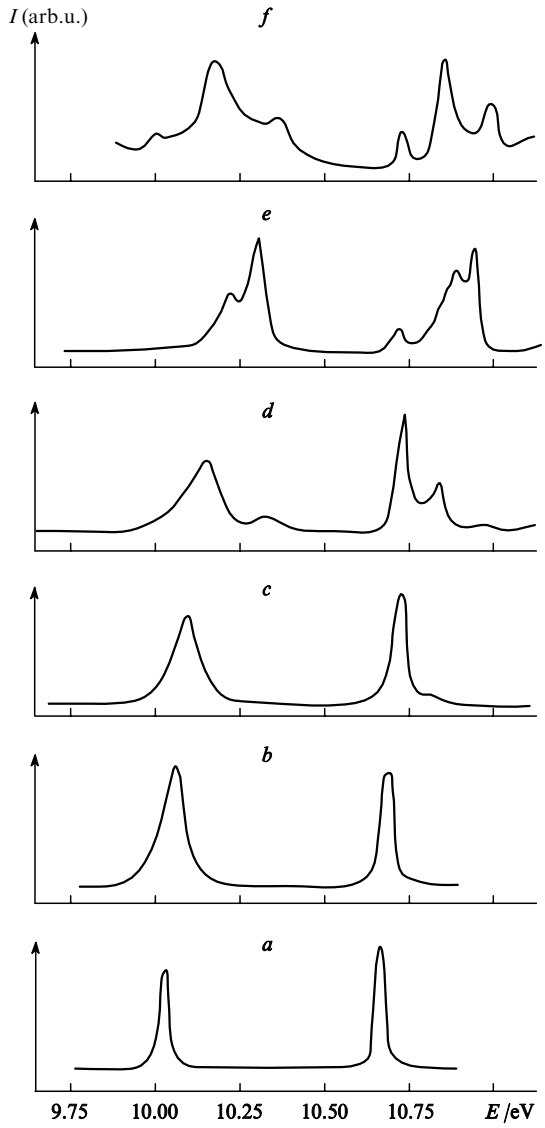


Figure 5. Fluorescence excitation spectra of atomic Kr (*a*), Kr_n clusters (*b*–*e*) with different numbers of Kr atoms, and a bulk sample (*f*).[93]
Number of krypton atoms in the cluster: 3 (*b*), 8 (*c*), 200 (*d*), 10^4 (*e*).

metric strain. IR-spectroscopic data confirm these assumptions.[98] Frequencies equal to 206, 304 and 658 cm^{-1} corresponding to the barriers to the rearrangement of the hydrogen bond configurations were found for three-, tetra- and pentamers, respectively. Water clusters are also formed upon hydration of gas-phase and colloid clusters, in particular, upon the hydration of macromolecules and proteins.

3. Colloid clusters

Colloid clusters are formed in solutions upon chemical reactions; their sizes range from 1 to 100 nm. They can exist in the liquid phase for long periods without being precipitated or coagulated, owing to weak intercluster interactions, charge repulsion and surface passivation. In terms of their behaviour towards the liquid medium, colloid clusters can be divided into two groups: lyophilic (hydrophilic) and lyophobic (hydrophobic) clusters.

Lyophilic clusters can sorb molecules from the environment and form strong solvation complexes with them. Clusters of this type are surrounded by a liquid shell, which is partially retained upon coagulation of separate clusters or on passing into a gel nanosystem. The most typical representatives of hydrophilic clusters are those formed by silicon and iron oxides and other metal oxides.

Lyophobic clusters do not adsorb solvent molecules on their surface. However, the surface can be modified by ions from solution, thus acquiring a positive or a negative charge. The giant Pd clusters the structure and the properties of which were considered in Section III.1 can be classified as colloid clusters in terms of the preparation method and the size (1.4–2.0 nm).

Normally, colloid clusters of metals are passivated with various ligands to prevent sticking together. Compounds suitable as these ligands are, for example, thiols, triphenylphosphine and its derivatives, phenanthroline.[101] Colloid clusters of semiconductors such as CdS, CdSe, CdTe, SnO_2, TiO_2, Fe_2O_3, MoS_2, HgS, InAs, GaP, GaAs, BiI_3, *etc* have been prepared.[7, 101, 102]

The weak intercluster interaction in solutions of colloid clusters does not preclude investigation of their individual properties. Among the optical properties peculiar to colloid clusters, the shift of the absorption frequency and the change in the oscillator strength following the change in the cluster size are the most impressive. As the size of the nanocluster decreases, the bands corresponding to the electronic excitation shift to higher energies and the oscillator strength is concentrated on several transitions. These effects are due to the replacement of the band spectrum corresponding to transitions between the conduction and valence bands in the bulk sample by the line spectrum of a cluster. It has also been reported that a decrease in the cluster size results in shorter lifetimes of excited states.

An expression for the calculation of the transition energy as $E \approx 1/R^2$ (R is the cluster radius) can be deduced from the quantum-size dependence $\Delta p \Delta x \geqslant h$ (p is the momentum, x is the coordinate) with the assumption that $\Delta x = R$. For semiconductors, the absorption and emission of energy are related to the formation and decomposition of the exciton (hydrogen-like bound state of a conduction electron and a hole); hence, the energy of exciton excitation is written in the form

$$E_n = \frac{h^2 n^2}{3R^2 m^*_{ef}},$$

where n is an integer, R is the cluster radius, m^*_{ef} is the effective mass of the exciton. Figure 6 shows the variation of the coefficient of light absorption by CdS colloid clusters with sizes from 6.4 to 48 nm *vs*. wavelength.[102] It can be seen that an increase in the

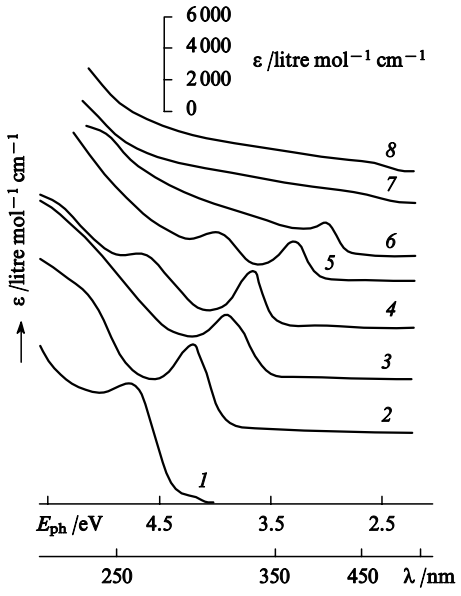


Figure 6. Absorption of light by CdS clusters *vs*. cluster size ('blue shift').[102]
Cluster size /nm: 6.4 (*1*), 7.2 (*2*), 8.0 (*3*), 9.3 (*4*), 11.6 (*5*), 19.4 (*6*), 28.0 (*7*), 48.0 (*8*). E_{ph} is the phonon energy.

cluster size entails a displacement of the absorption peak toward shorter wavelengths ('blue shift'). Similar shifts have also been observed for CdSe clusters.[103]

In the luminescence of nanoclusters caused by charge generation on exposure to light, a shift to shorter wavelengths following a decrease in the cluster size also takes place. Luminescence was observed for the ZnO, ZnS, CdS and CdSe clusters.[104–110] The change in the wavelength in the light absorption and emission spectra following a change in the cluster size can be employed in the design of frequency-tuned lasers on the basis of InAs and CdS.[111, 112]

The accumulation of the oscillator strength in several narrow bands or an increase in the oscillator strength normalised to the volume with a decrease in the cluster size should also be classified as quantum-size effects. This is caused by the increase in the overlap integral of the electron and hole wave functions. The oscillator strength corresponds to the radiation lifetime of the excited state at low temperature, while the oscillator strength normalised to the volume corresponds to the light absorption coefficient. For bulk semiconductors, the width of the exciton band is 0.15–0.3 eV; however, in clusters, the width of transitions decreases to 0.1–0.5 meV as a result of quantum restriction, which leads to the accumulation of the integral oscillator strength and to substantial growth of the exciton absorption of nanoclusters.[103, 113]

For clusters, the radiation lifetime of fluorescence was found to decrease with a decrease in the cluster size.[114] For instance, the lifetime of a Eu^{2+} tracer in clusters of alkali metal halides and chalcogenides[115, 116] and in ZnS[117] was found to decrease by almost five orders of magnitude with respect to the lifetime of Eu^{2+} in the bulk material. However, in another study,[118] no decrease in the lifetime was observed for Eu^{2+} in a 4-nm ZnS cluster. Thus, the data for the Eu^{2+} tracer lifetime in ZnS clusters are contradictory. This interesting phenomenon requires further studies and collection of experimental data both for the elucidation of the quantitative relationships between the cluster size and the optical characteristics and for the production of new optical materials.

IV. Cluster nanosystems and nanostructures

In this Section, we discuss the principles and approaches to the formation of nanosystems from clusters, from separate clusters and matrices, and from a bulk material. The properties of nanostructures to be considered include the intracluster, atomic, and intercluster dynamics, structural and mechanical properties, electrical conductivity, and optical and magnetic properties.

1. The formation of nanostructures. Assembly and self-assembly

Assembly and self-assembly of nanoclusters to nanostructures is an important problem the solution of which would contribute to the design of a new generation of materials with unique properties. The properties of materials can be changed in two ways: by changing the size of nanoclusters and by changing the intercluster interactions. The assembly of a nanostructure from nanoclusters follows the same laws as the formation of crystals from atoms; however, clusters differ substantially from atoms because they have a real surface and real cluster boundaries.§ Therefore, the formation of nanosystems from nanoclusters is accompanied by generation of numerous defects and stresses, resulting in fundamental changes in the properties of the nanosystem.

Nanostructures and nanosystems can be formed from clusters of any type. However, before proceeding to consideration of the processes of formation of nanosystems from solid-state and matrix clusters, it is necessary to consider the primary cluster nucleation processes because the properties and structure of these clusters depend markedly on their interaction with the matrices.

a. Nanosystems based on solid-state clusters

Let us consider the formation of nanosystems from solid-state nanoclusters using thermal decomposition of iron salts as an example. Decomposition of iron salts at a temperature above some critical (or threshold) value starts with the formation of a mobile active reaction medium in which nucleation of iron oxide nanoclusters occurs.[119] The process of cluster formation can be compared with seed formation in a confined space in a solution or in a melt (a cage or a pore). In this case, the role of this confinement can be played by diffusion restriction, which prevents the perturbation of the concentration of the mother medium caused by the change in the cluster size from migrating over the nucleation time (t_n) by a distance longer than $L \approx (Dt_n)^{1/2}$ (D is the diffusion coefficient). It is this distance that determines the size of the cage surrounding the cluster beyond which components of the mother medium cannot migrate. For a system of non-contacting clusters, the dependence of the Gibbs energy (ΔG_f) on the cluster radius (R) for one cluster is described by the formula ¶

$$\Delta G_f = 4\pi R^2\alpha - \frac{4}{3}\pi R^3\rho\Delta\mu, \tag{3}$$

where α is the density of the surface energy of the cluster (α = const), ρ is the substance density in the cluster (the number of atoms in 1 m^3), $\Delta\mu$ is the change in the chemical potential of the system caused by the transfer of a single iron atom from the medium to the cluster. If the cluster and the surrounding medium contain N atoms of any type of which n_0 are iron atoms (n iron atoms being contained in the cluster), then for $N \gg n_0 > n$

$$\Delta\mu = \Delta\mu^0 + \ln\frac{n_0 - n}{N}. \tag{4}$$

Here $\Delta\mu^0$ is the change in the standard chemical potential upon the transfer of one iron atom from the medium to the cluster structure expressed in kT units. At the initial stage, clusters do not contact one another. Since the volume of this cluster is $V_f = (4/3)\pi R^3$ and the surface area is $S_f = 4\pi R^2$, relation (3) can be written in the form

$$\Delta G_f = \alpha S_f - \left(\Delta\mu^0 + \ln\frac{n_0 - n}{N}\right)\rho V_f. \tag{5}$$

The function ΔG_f passes through a maximum at $R = R_{cr}$ (R_{cr} is the critical radius of seeds in the nucleation) and through a minimum at $R = R_{max}$ (R_{max} is the cluster radius corresponding to a stable equilibrium state of the system) (Fig. 7).

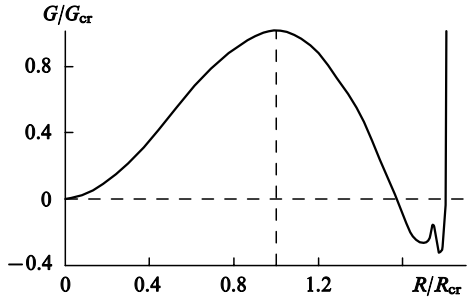


Figure 7. Change in the Gibbs energy G/G_{cr} upon nucleation, cluster growth and cluster sintering according to relations (5) and (7) in R/R_{cr} units.

§ The same boundaries appear on grinding of a bulk sample, for example, using mills or by plastic deformation.

¶ It should be noted that the thermodynamic approach is used in relation to ensembles of atoms or clusters which contain a large number of particles. However, this approach also proved effective (as will be shown below) for a limited number of particles.

Expression (5) characterises the stages of nucleation and the growth of a cluster in the system of weakly interacting non-contacting clusters. Upon further growth of clusters, they come into contact and the boundaries between them vanish (sintering). The onset of cluster sintering corresponds to a discrete transition from isolated clusters first, to weakly interacting and then, to strongly interacting clusters. If half of the distance R_t between the cluster centres at the stage of sintering is equal to R_t = const, the surface area (S_s) and the volume (V_s) of the cluster which has formed contacts with k neighbours can be calculated fairly accurately using the expressions

$$S_s = 4\pi R^2 + k2\pi R(R_t - R), \tag{6}$$

$$V_s = \frac{4}{3}\pi R^3 + k\frac{1}{3}\pi(-2R^3 + 3R^2R_t - R_t^3).$$

Correspondingly, the change in the Gibbs energy at the stage of sintering, *i.e.*, when $R > R_t$, is

$$\Delta G_s = \alpha S_s - \left(\Delta\mu^0 + \ln\frac{n_0 - n}{N}\right)\rho V_s. \tag{7}$$

Thus, the profile of the variation of free energy of the system per one cluster over the whole range of R is determined by relation (5) for $R < R_t$ and by relation (7) for $R > R_t$. As an example, Fig. 7 presents the $\Delta G(R/R_{cr})$ plot for $R_t = 1.75\,R_{cr}$. The curve given in the Figure has three minima separated by two maxima. The first minimum at the point $R = 0$ corresponds to the initial state of the mother medium; the second minimum at $R = R_{max}$ matches the first stable state, namely, the equilibrium state of the cluster having formed but not contacting (this is possible when $R_{max} < R_t$); the third minimum matches a system of sintering clusters each of them having k contacts. Correspondingly, the first maximum at $R = R_{cr}$ corresponds to the potential barrier to nucleation, while the second one corresponds to the potential barrier to sintering. Figure 8 shows the shape of the potential barrier to sintering for $k = 6$ and for different R_t. In a system densely populated by clusters, at $R_t \leqslant 1.7\,R_{cr}$, sintering occurs without a barrier; in a system less densely populated by clusters, at $R_t = 1.75R_{cr}$, the transfer to sintering requires overcoming a potential barrier, and in an even less densely populated system, at $R_t = 1.8R_{cr}$, sintering does not occur at all because in this case, this process is associated with an increase in the free energy.

The differential thermal analysis (DTA) and differential thermal gravimetry (DTG) curves recorded during thermal decomposition of iron oxalate $Fe_2(C_2O_4)_3 \cdot 5\,H_2O$ in air exhibit two minima at T_d = 200 and 260 °C.[120] The first minimum in both curves corresponds to dehydration of the iron complex with its partial decomposition giving rise to CO and CO_2. When $T_d > 200$ °C, a mobile medium starts to form, in which nucleation and growth of iron oxide clusters takes place. The second minimum is apparently due to further removal of CO and CO_2 and the onset of sintering of iron oxide clusters. The cluster size can be estimated from the specific surface area (BET) or using data of X-ray diffraction analysis, atomic force microscopy (AFM) and Mössbauer spectroscopy. The AFM images of iron oxide-based cluster systems formed at T_d = 265 °C are shown in Fig. 9 *a*,*b*. The contacting clusters which undergo sintering can be readily seen in Fig. 9 *a*.

Figure 10 shows how the thermodynamic model of nucleation and cluster growth and sintering (the upper section of the Figure)

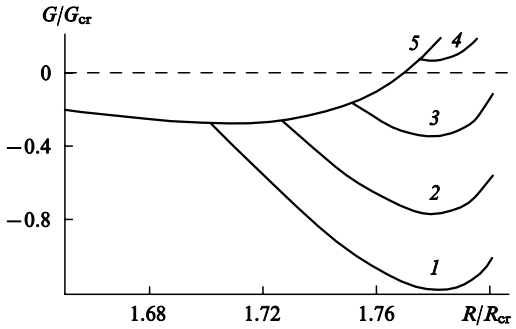


Figure 8. Change in the Gibbs energy G/G_{cr} in the region of the onset of cluster sintering *vs.* R/R_{cr} at different R_t values (which is half the distance between the cluster centers).
$R_t = 1.7R_{cr}$ (*1*), $1.73R_{cr}$ (*2*), $1.75R_{cr}$ (*3*), $1.77R_{cr}$ (*4*), $1.78R_{cr}$ (*5*).

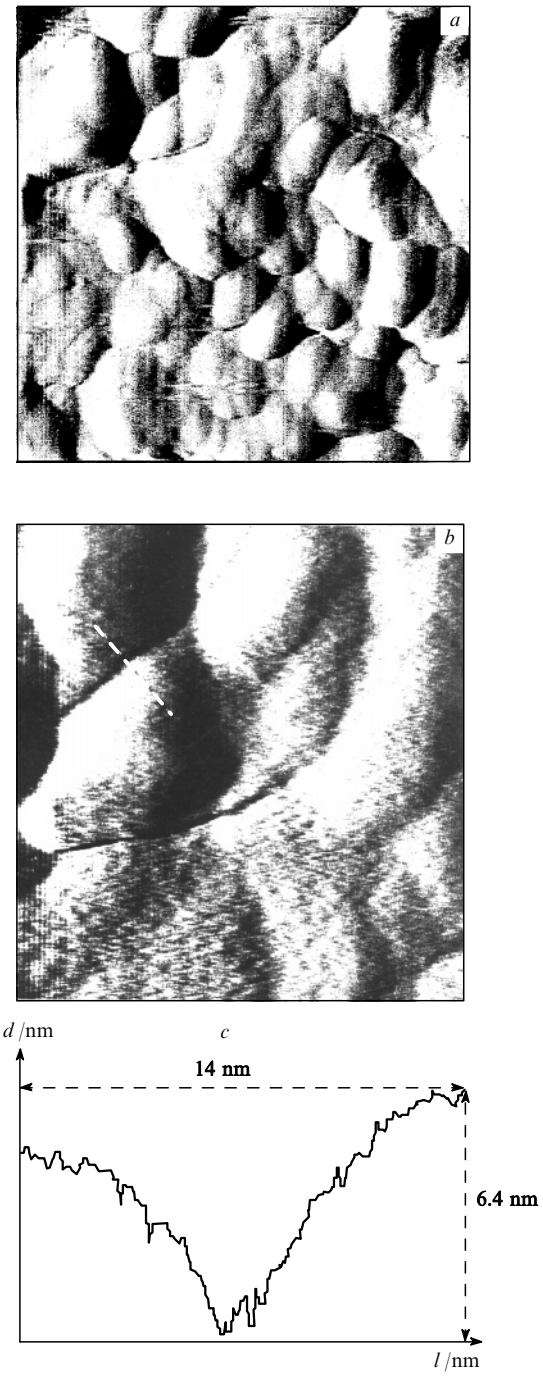


Figure 9. Computer images of a nanocluster system of strongly interacting iron oxide clusters obtained by an atomic-force microscope with a resolution of 500 (*a*) and 150 nm (*b*); and surface relief (*c*) along the dashed line drawn in the upper left section of Fig. 9 *b*. The line is 14 nm long; the maximum relief depth is 6.4 nm.

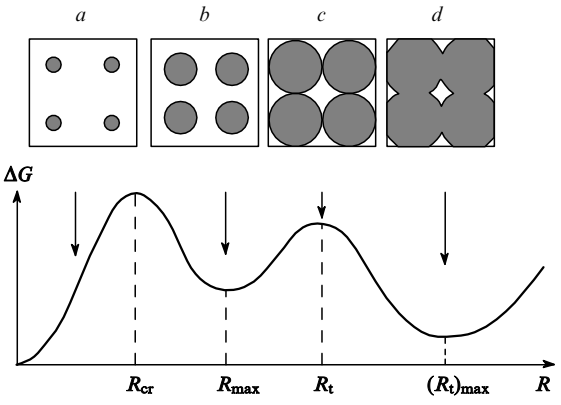


Figure 10. Scheme of cluster formation, growth and sintering; (*a*) formation of seeds, (*b*) maximum size (5–6 nm) of a stable cluster in a weakly interacting system of clusters, (*c*) onset of sintering; (*d*) formation of a system of strongly interacting clusters. The arrows match steps *a*–*d* to the curve for the change in the Gibbs energy obtained upon thermal decomposition of iron oxalate.

interprets the experimental data on iron oxalate thermolysis (the low section of the Figure). The subcritical range of cluster sizes ($R < R_{cr}$) corresponds to the stage of fluctuation nucleation of clusters; in this range, the function $\Delta G(R)$ increases (Fig. 10 *a*). In the region of $R > R_{cr}$, the enlargement of clusters is accompanied by a decrease in the free energy; it proceeds spontaneously and ends in the formation of a stable cluster with the size $R_{max} = 5-6$ nm and a nanosystem formed by weakly interacting clusters (Fig. 10 *b*). When the distance between the centres of neighbouring clusters ($2R_t$) approaches the value $2R$, sintering starts (Fig. 10 *c*). In the region of $R_{max} < R < R_t$, the function $\Delta G(R)$ increases, which forms a potential barrier to the sintering with a maximum at $R = R_t$. With further increase in R ($R > R_t$), sintering occurs spontaneously and is accompanied by a decrease in the Gibbs energy. The second potential well in the $\Delta G(R)$ curve corresponds to a system of strongly interacting clusters (Fig. 10 *d*). When $R > (R_t)_{max}$, the potential well disappears and further sintering becomes impossible because it would be accompanied by an increase in the Gibbs energy ($\Delta G > 0$). Since the R_{max} and R_t values are dictated by experimental conditions, the outcome of the topochemical reaction depends on the reactor temperature, duration of sintering and the previous history of the sample.

Thus, the formation of a nanosystem includes two main stages: first, a nanosystem of weakly interacting clusters is formed (this stage starts with nucleation and ends in cluster sintering) and subsequently it is converted into a nanosystem of strongly interacting clusters (this stage starts with cluster sintering). Figure 9 *a* corresponds to a nanosystem formed by strongly interacting clusters† with sizes of 20–50 nm. The appearance of strong intercluster interaction and the sintering bring about substantial interfacial stresses. These stresses (p) are generated by the 'neck' formed due to the surface tension (the region where the clusters are contacting):[121] $p = 2\alpha/x$ (α is the surface tension, x is the radius of the neck formed upon cluster sintering). Assuming that $\alpha = 1\ \mathrm{N\,m^{-1}}$ for iron oxide[122] and $x \approx 1$ nm, we obtain $p \approx 10^9-10^{10}$ Pa.

Excessive pressure also develops due to the presence of defects and dislocations at the interface; for ~10-nm clusters, it reaches 10^9 Pa.[6,123–125] The stress and pressure developing in a system of strongly interacting nanoclusters are important factors determining the formation and properties of the nanostructure.

A system of strongly interacting solid-state clusters can also arise upon mechanical treatment of bulk samples. Thus plastic deformation of Ni and Cu bulk samples gave nanosystems of Ni and Cu clusters with an average size of 100 and 50 nm, respectively.[126–128] Titanium nanoclusters with sizes of up to 30–40 nm[129] have been prepared by imposing pressure with shear on the titanium carbide $TiC_{0.62}$.

Crystallisation of multicomponent alloys is of considerable interest. Thus crystallisaton of amorphous Fe–Cu–Nb–Si–B alloys at 700–900 K affords a cluster system consisting of an amorphous matrix with 10-nm α-Fe clusters and ~1-nm Cu clusters uniformly distributed in the matrix.[130,131] Crystallisation conditions can be altered by preliminary treatment of the alloy. In this case, α-Fe clusters with sizes of up to 5 nm were obtained.[130,131] Crystallisation of rapidly solidifying amorphous alloys Al–Cr–Ce–M (M = Fe, Co, Ni, Cu) with Al concentrations of more than 90% yields icosahedral Al nanoclusters, which occur in an amorphous matrix.

b. Nanoclusters prepared using matrices

In this Section, we shall find out how a matrix influences the properties of nanoclusters formed in it. The formation of nanocluster seeds from a supercooled liquid or a supersaturated solution in an infinite space has been extensively studied and discussed, in particular, from the thermodynamic standpoint.[132–134]

The Gibbs energy for this process is calculated using an equation[132–134] similar to equation (3) introduced for solid-phase reactions

$$\Delta G = 4\pi\alpha R^2 - \frac{4}{3}\pi R^3 \rho \Delta\mu. \qquad (8)$$

For a solution with the finite concentration $c = n_0/N$ (n_0 is the number of atoms of a dissolved substance, *e.g.*, iron, N is the number of solvent atoms), the $\Delta\mu$ value is found from the relation

$$\Delta\mu = \Delta\mu^0 + \ln\frac{n_0}{N} = \Delta\mu_0\,. \qquad (9)$$

Thermodynamic estimation of the influence of a pore on the features of the formation of a nanocluster in it has been reported.[135] For a closed pore in which a cluster of n atoms is formed,

$$\Delta\mu = \Delta\mu^0 + \ln\frac{n_0 - n}{N}, \qquad (10)$$

where $\Delta\mu^0 = \mu_l - \mu_s$ is the difference between the chemical potentials of the liquid and solid standard states. Thus, the Gibbs energy for cluster formation in a closed pore can be written as

$$\Delta G = \frac{4}{3}\pi\rho R^3\left[\frac{3\alpha}{\rho R} - \left(\Delta\mu_0 + \ln\frac{n_0}{n_0 - n}\right)\right]. \qquad (11)$$

The pattern of the $\Delta G(n)$ dependences describing the formation of a cluster in an infinite space and in a closed pore is shown in Fig. 11. The curves describing the change in the Gibbs energy upon the formation of nanoclusters in an infinite space have a maximum at the points n_{min} corresponding to the critical volume of formation of a stable cluster seed (Fig. 11, curves *1*, *2*). For a supersaturated solution (Fig. 11, curve *1*) or a supercooled melt, the n_{min} value is found from Eqn (8). As the initial concentration n_0/N decreases, the n_{min} value shifts to greater n [$(n_{min})_2$ in curve *2*].

The formation of a cluster in a closed pore is illustrated by curves *3* and *4* (Fig. 11). The limited concentration of the solute inside the pore entails the existence of a limiting volume of the cluster n_{max}; after this volume has been reached, cluster growth becomes energetically unfavourable and ceases. One more important factor influencing cluster formation and growth in a pore is pore heterogeneity. Heterogeneity of a pore changes the condi-

† The change in the type of intercluster interaction changes many properties of the nanosystem; this will be discussed in the Section dealing with the properties of nanostructures.

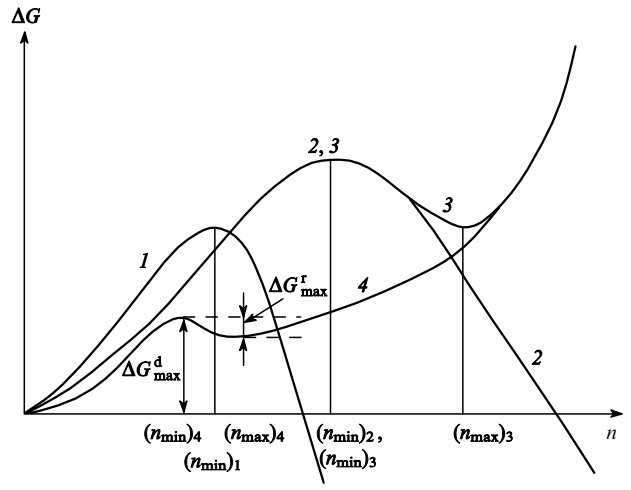


Figure 11. Funcion $\Delta G = f(n)$ characterising the growth of a cluster with an increase in n;
(*1*) in a supersaturated solution having a macrovolume, (*2*) in a solution with finite concentration c, (*3*) in a pore; (*4*) in a pore with allowance for the heterogeneity factor K.

tions of cluster formation and decreases the energy barrier to the formation of a stable seed of a cluster having the critical volume.[135]

Now we shall consider the variation of ΔG_{max} as a function of cluster size (n). In the region of $n \ll n_0$,

$$n_{min} = \frac{32\alpha^3}{3\rho^2\Delta\mu_0^3}. \quad (12)$$

It follows from Eqn (11) that an increase in the concentration n_0/N decreases the cluster critical volume (size). The height of the energy barrier to the formation of a stable cluster equals

$$\Delta G_{max} = \frac{16\pi\alpha^3}{3\rho^2\Delta\mu_0^2}. \quad (13)$$

However, in the region of $n_{min} \ll n < n_0$

$$n_{max} = n_0 \frac{\Delta\mu_0}{2 + \Delta\mu_0}. \quad (14)$$

Thus, the maximum size of the clusters (n_{max}) in a pore is always smaller than n_0 and, for a constant concentration, it increases with an increase in the pore size. When estimating n_{max}, one should take into account the influence of pore heterogeneity and the fact that the probability of formation of several clusters in one pore increases with an increase in the pore size from 10 to 100 nm and further; naturally, this results in smaller n_{max} (in large pores, $n_{max} \ll n_0$).

As noted above, pore heterogeneity decreases the energy barrier to cluster formation. The Gibbs energy of both the formation (ΔG^d_{max}) and decomposition (ΔG^r_{max}) of clusters can be considered. With allowance for the heterogeneity factor K ($K < 1$), which depends on the contact angle between the cluster and the pore surface,

$$\Delta G^d_{max} = \frac{16\pi\alpha^3 K}{3\rho^2\Delta\mu_0^2}. \quad (15)$$

The pore also influences the ΔG^r_{max} value, *viz*., decreases it. As a consequence, with a decrease in n_{max} (especially for pores of $\sim$10 nm), $\Delta G^r_{max} < \Delta G^d_{max}$.

The surface and the volume of a pore influence as well the rate of cluster formation, which increases due to a decrease in the energy barrier and the heterogeneity factor.[134, 135]

The nucleation and the formation of iron hydroxide clusters in organic sorbents — styrene and divinylbenzene copolymers (polysorbs) with a specific surface area of up to 1000 $m^2\ g^{-1}$ and a pore size of 7 to 50 – 100 nm have been investigated.[135, 136] The pore surface in polysorbs bears no functional groups; therefore, the influence of chemisorption on cluster formation can be neglected. Polysorbs were impregnated with ferric chloride solutions with different concentrations and purged with air containing an ammonia admixture (0.008% – 0.08%). As a result the irreversible chemical reaction

$$FeCl_3 + H_2O + NH_3 \longrightarrow Fe(OH)_3 + NH_4Cl + NH_4OH,$$

resulting in the formation of iron hydroxide took place in the polysorb pore. This changed the pH of the medium and induced the growth of insoluble iron clusters in the pore.

Changes in the intensity (ε) of spectral lines in the Mössbauer spectra of iron hydroxide clusters were used to investigate the influence of various parameters (pore size, concentration of ammonia in air, concentration of $FeCl_3 \cdot 6\,H_2O$) on the size of the resulting clusters. Figure 12 shows the dependence of ε on the size (d) of the pore in polysorb at different ammonia concentrations in air.[135] It was found that a decrease in the pore size results in a corresponding decrease in the cluster size [*e.g*., according to Eqn (14)] and, hence, in a decrease in the intensity of spectral lines. For large pores, a decrease in ε with an increase in the iron chloride concentration was also observed, which can be due to the formation of several smaller clusters within one pore. A substantial increase in the rate of cluster formation with respect to that in a macro-volume was noted, which is consistent with the heterogeneity factor and Eqn (15).

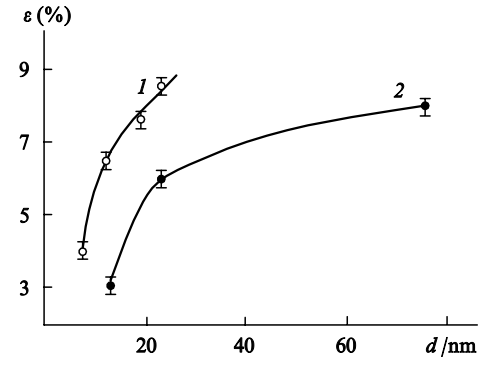


Figure 12. Line intensity in the Mössbauer spectrum of iron oxide clusters formed in the polysorb pores *vs*. pore diameter ($T = 300$ K) at an ammonia concentration in air of 0.08% (*1*) and 0.008% (*2*).

Yet another active matrix widely used to prepare nanoclusters is porous active carbon. The deposition of metal salts, for example, iron oxalate $Fe_2(C_2O_4)_3 \cdot 5\,H_2O$, on an active carbon substrate followed by annealing and reduction under a hydrogen atmosphere gives rise to a mixed heterogeneous system of Fe_3O_4, γ-Fe_2O_3 and metallic iron clusters on a carbon substrate. Depending on the duration of the reduction with hydrogen, the size of oxide clusters ranges from 7 to 12 nm, and the size of iron (α-Fe) clusters is 3 – 7 nm.[137] It is noteworthy that a nanosystem of these clusters possesses a self-forming property: the reduction by hydrogen is accompanied by hydrogenation (carbon burning) accompanied by an increase in the pore size. The size and composition of nanoclusters are also markedly affected by the nature of the carbon surface.[138, 139]

c. Colloid nanosystems

Nanostructures prepared from colloidal solutions and sols by sol – gel technology can be used in conductive systems, optics and catalysts. Systems consisting of zirconium, titanium or aluminium alkoxides [$Zr(OPr^i)_4$, $Ti(OBu^i)_4$, $Al(OPr^i)_3$] and iron or cobalt complexes are fairly promising.[140] Based on them, supported catalysts represented by nanocluster systems have been prepared, for example, FeO/ZrO_2, FeO/TiO_2, FeO/Al_2O_3. The cluster size was varied by changing the concentrations of components and the heating temperatures. However, clusters prepared by sol – gel technology are unsuitable for the design of assembled nanostructures because of the large scatter in the nanocluster size. It is more promising to assemble nanostructures from clusters prepared using direct and reverse micelles.[21, 22, 141, 142] These clusters are distinguished by narrow size distributions.

Since reverse microemulsions are characterised by high mobility and great interfacial surface area, they can act as a universal medium for numerous chemical syntheses including those giving rise to metal, metal sulfide and other clusters. In a microemulsion, drops constantly collide due to the Brownian motion, coalesce and again split, which results in the continuous exchange of their contents.

Thus Ag_2S clusters are prepared using mixtures of two types of reverse micelles, the aqueous phases of which contain Na_2S and Ag-surfactant, respectively. Upon collision, these micelles coalesce, which is accompanied by the exchange of the contents of the aqueous media. This exchange yields solid Ag_2S particles. The size of a new-phase particle is limited by the size of the drop. The size of Ag_2S clusters was found to increase from 3.0 to 5.8 nm with an increase in the size of water drops.[21] In this case, the model of nucleation in a pore considered in Section IV.1.b is also valid. To release the nanoclusters from the micelle, the micelle is destroyed by thiols, the resulting nanoclusters are dissolved in an appropriate solvent, the solution is filtered, and the solvent is evaporated. This procedure permits preparation of nanoclusters with a size of up to 10 nm passivated by thiols (*e.g.*, dodecanethiol). Two- and three-dimensional nanostructures are formed from these clusters on various substrates.

Characteristic features of the formation of nanostructures from Ag_2S clusters have been described.[141, 142] The researchers observed the self-assembly of clusters to give ordered two- and three-dimensional structures. Organised nanostructures have also been obtained from metallic Ag, Co, Au and semiconductor nanoclusters.[143 – 147] Alkanethiols, alkylphosphines and dithiols were used as nanocluster surface passivators.

Figure 13 presents two photomicrographs of the Ag_2S nanostructure prepared from passivated nanoclusters with a size of 5.8 nm. The photomicrograph shown in Fig. 13 *b* clearly demonstrates that the nanoclusters are strictly assembled to give a nanostructure rather than arranged randomly. Like conventional crystals, this structure can contain dislocations and defects (they are marked by arrows in photomicrograph 13 *a* obtained with a smaller magnification).

Two-dimensional nanostructures (2D structures) are closely packed monolayers, while 3D structures have a face-centred cubic (FCC) lattice.

The procedure for the preparation of monodisperse nanoclusters using microemulsion systems makes it possible to vary the size of the initial nanoclusters, a sort of 'atoms'. Figure 14 presents three photomicrographs of the nanostructures prepared from Ag_2S nanoclusters with a size of 3.0 (*a*, *b*), 4.0 (*c*, *d*) and 5.8 nm (*e*, *f*). Despite the difference in the shape of the aggregated nanostructures (Fig. 14 *a*,*c*,*e*), the type of organisation is the same

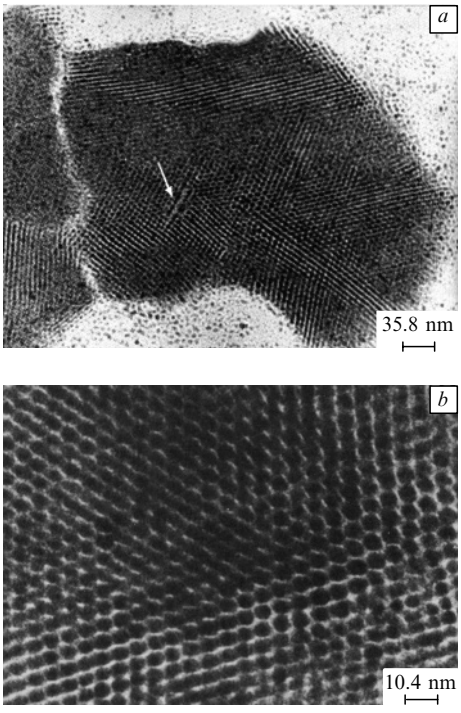


Figure 13. Photomicrographs of Ag_2S nanocluster structures with a resolution of 35.8 (*a*) and 10.4 nm (*b*). The white arrow marks a defect in the nanostructure 'crystallinity'.[21]

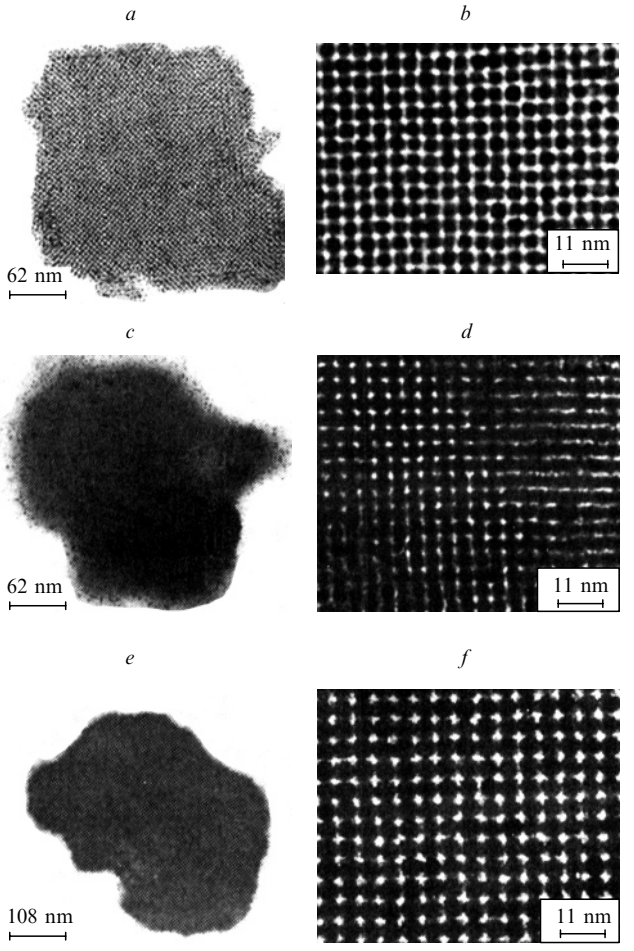


Figure 14. Photomicrographs of nanocluster structures formed from Ag_2S clusters with different sizes: 3.0 (*a*, *b*), 4.0 (*c*, *d*) and 5.8 nm (*e*, *f*).[21]

and corresponds to the body-centred cubic (BCC) lattice (Fig. 14 *b*,*d*,*f*).

In this case, assembly and self-assembly of nanoclusters to give a BCC crystal lattice is induced, apparently, by van der Waals forces acting between separate nanoclusters having a nearly spherical shape.

d. Assembling of fullerenes, fullerides, fullerene-like structures and nanotubes

Fullerenes are fairly convenient structural materials for the formation of nanostructures because they are perfectly monodisperse and spherical. The organisation and self-organisation of colloid and gas-phase fullerenes to nanostructures (fullerides) is induced by heating, pressing, *etc*. In aqueous solutions, the star hexaanion derivatives $C_{60}[(CH_2)_4SO_3]_6^-$ form spherical aggregates comprising four molecules.[148] The shape, the size and the structure of aggregates were studied by small-angle neutron and X-ray scattering. An unusual stability of these aggregates was noted: their volume and shape do not depend on the fullerene concentration or on the inter-aggregate interaction.

Larger aggregates were formed from colloid solutions of C_{60} fullerene in benzonitrile at C_{60} concentrations of more than 100 μmol litre^{-1} (at lower C_{60} concentrations, only separate fullerene molecules are present in the solution).[149] In this case, the average size of the aggregate reached $\sim$250 nm. These aggregates, existing as dynamic systems,‡ were detected using picosecond photolysis. No aggregates of this type are formed in benzene or decalin up to concentrations of 500 μmol litre^{-1}. Apparently, the formation of aggregates is influenced by solvent polarity and the symmetry of the molecules being joined. Indeed, the non-symmetrical C_{70} molecule does not form aggregates either in polar benzonitrile or in nonpolar benzene or decalin.

The preparation and study of the nanocrystals of fullerene fluorides $C_{60}F_x$, $C_{60}F_{36}$ and $C_{60}F_{48}$ present considerable interest.[84, 150, 151] It was found that at room temperature, the crystals of $C_{60}F_{36}$ have a BCC lattice, while those of $C_{60}F_{48}$ crystallise with a body-centred tetragonal lattice. The data of high-temperature (T = 353 K) X-ray diffraction *in situ* point to a phase transition in a $C_{60}F_{48}$ nanocrystal: the body-centred tetragonal lattice is transformed into a face-centred cubic lattice.

The parameters governing the formation of fullerene nanostructures (crystals) are the pressure and the temperature. Thus crystallisation of C_{60} fullerene at 1.56 GPa and 423 K affords a crystal lattice the structural elements of which are dumb-bell-shaped $C_{60}-C_{60}$ dimers.[152] (This reaction is similar to the mechanochemical reaction of C_{60} with KCN.[153]) An increase in the temperature induces decomposition of the dimers to give an orthorhombic polymeric structure of C_{60} molecules, which is converted into a polymeric tetragonal structure at $T \approx 723$ K.

Carbon nanotubes (NT) are also used for the formation of nanostructures. A nanotube is a graphene sheet rolled into a hollow cylinder. The chirality and the diameter of this tube can be characterised by the vector $\mathbf{c} = n\mathbf{a} + m\mathbf{b}$, ($\mathbf{a}$, $\mathbf{b}$ are the unit vectors of the hexagonal cell and m and n are integers). Depending on the mode of rolling, nanotubes can be either achiral zigzag-like (two sides of each hexagon are parallel to the NT axis, $m = 0$), or armchair-like (two sides of each hexagon are normal to the NT axis, $n = m$), or chiral helix-like (each pair of the hexagon sides is arranged at an angle other than 0 or 90 ° to the NT axis). The form of the nanotubes influences substantially the properties of nanostructures (metallic or semiconducting). By varying and combining two types of nanotubes, for example, zigzag and armchair nanotubes, one can create single-electron devices with different conductivities, for example, diodes.[154] The size (length) of nanotubes also influences the properties of nanostructures formed from them. Depending on the nanotube size, the properties of nanosystems vary from semiconductor properties with a real forbidden gap (quantum dots, 0D) to metallic properties for a unidimensional system (quantum wire, 1D). According to quantum-mechanical calculations, transition from (0D) to (1D) structures takes place if the nanotube becomes more than 10-nm long.

‡ Aggregates of C_{60} are unstable and undergo constant assembly and destruction of the type $nC_{60} \leftrightarrows (C_{60})_n$.

e. Nanofilms

Nanofilms are two-dimensional structures. There exist numerous expedients for film deposition or growth on metallic, oxide, chalcogenide and other substrates. The method used most widely to prepare organised films is deposition of atoms or molecules from the gas phase onto the surface of a single crystal and design of epitaxial or polycrystalline atomic or molecular layers from them.

Considerable progress has been attained in the synthesis of films from fullerenes on substrates of various materials including metals,[155, 156] semiconductors,[157–159] layered materials,[160, 161] insulators,[162] *etc*. However, the question of what factor dictates the type of the structure being formed (face-centred, hexagonal or close-packed) still remains open. It can only be concluded that weak interaction of the fullerene molecules with the substrate favours the formation of an ordered layer of C_{60} molecules, whereas strong chemisorption of C_{60} on the substrate surface gives rise to a disorganised, disordered structure. The structure of a thin film of fullerene molecules formed on the graphite surface has been studied.[163] It was shown by computer simulation that the C_{60} film supported on graphite has a hexagonal structure.

The films deposited on a substrate can also have a nonuniform, islet structure. The formation of films of gas-phase clusters on a substrate depends on the time, temperature and deposition velocity. The final state of the film is determined by the average size and density of the cluster islets: the larger the islets, the smaller the density.

The rate of atom diffusion is known to be low at low temperatures; therefore, relatively small clusters with high density are formed. The same considerations are valid for the formation of films from clusters. The formation of nanostructures from antimony clusters on the amorphous surface of carbon has been studied as a function of the number of Sb atoms in the cluster (n = 4–2200).[164] (The antimony clusters were prepared by condensation of antimony vapour in a helium cell cooled with liquid nitrogen.) The dependence of the average size (N) of the cluster islet structure on the average size (n) of the primary antimony cluster passes through a minimum at $n = 350 \pm 50$. This was interpreted as being due to the fact that the size distribution of the islet structure becomes narrower as the cluster size approaches the optimum value ($n = 350 \pm 50$). As the size of the primary antimony cluster increases, the rate of its diffusion over the substrate surface decreases; hence, the probability of coalescence of the primary clusters to an islet nanostructure also decreases. Each large primary cluster (from $n > 400$ to $n = 2200 \approx N$) is adsorbed on the surface and retained unchanged for some densities of the primary beam. From small clusters with $n < 350$, it is possible to form islet structures with large N (> 3000), owing to higher diffusion rates.

An effective method for the formation of nanofilms from clusters is deposition from plasma as well as chemical and physical vapour deposition (CVD and PVD).[8, 165] In plasma deposition, the film thickness and the size of crystallites are controlled by variation of the gas pressure and discharge parameters. Dudko *et al*.[166] and Barg [167] prepared chromium films on a copper substrate with an average size of crystallite clusters of $\sim$20 nm. The increase in the film thickness to 500 nm resulted in its crystallisation. The ion-plasma deposition of titanium carbide and nitride also results in the formation of nanocrystalline films.[165] The use of magnetron sputtering of the initial substances allows the substrate temperature to be decreased by 100–200 °C; this extends the scope of the preparation of nanotubes. This procedure was employed to produce Ni_3Al films with a crystallite size of 20 nm.[168]

The preparation of nanofilms from colloid solutions has been considered in the previous Section in relation to the formation of silver sulfide-based nanostructures.[21] It has been noted [21] that hexagonal ordering of clusters (3 – 5 nm) is observed even within a monolayer. Generally, to prepare assembled nanofilms from colloid solutions, it is necessary to have monodisperse nanoclusters, which are self-assembled into a film due to weak van der Waals intercluster interactions.

In recent years, a procedure has been developed for the formation of films on a liquid surface (Langmuir – Blodgett) and transferring them onto a solid surface. This method permits the formation of superlattices and nanometer layers of organic molecules with a specified pattern of layer alternation.

The organisation of nanofilms by chemical assembling and molecular layering methods has been described.[27] In the synthesis of highly organised structures by the chemical assembling method, the key role is played by the chemical reactions taking place between the functional groups located on the surface of a solid (substrate) and the adsorbed molecules with specified composition. This procedure is used, for example, to apply organised layers of metal oxide clusters.

f. Compacted nanosystems

Compacting of gas-phase, colloid or molecular clusters by pressing followed by the high-temperature sintering of nanoclusters gives rise to nanosystems.[169, 170] The most densely organised nanostructures are produced from the smallest monodisperse clusters. Thus a nanostructure based on titanium nitride were prepared by pressing nanoclusters with a size of 8 – 25 nm with subsequent sintering.[171] To preserve a small size of crystallites in nanosystems, low sintering temperatures and doping additives hampering the crystal growth are required. An example is provided by WC – Co nanocrystalline solid alloys, which consist of WC nanoclusters (50 nm) dissolved in a Co matrix.[172, 173] Tungsten carbide (up to 1 mass %) is added to retard the crystal growth.

A magnetic-pulse method is also used to compact nanosystems.[174] In this case, pressing occurs on exposure to pulse compression waves and is accompanied by local heating due to the fast energy evolution upon the friction of particles during packing. The magnetic-pulse pressing allows the generation of pulse compression waves with an amplitude of up to 5 GPa and a duration of several microseconds. The use of pulse pressures results in a higher compaction density compared to that reached by static pressing. Apparently, this is due to the generation of intercluster pressures, which enhance the intercluster interactions. The magnetic-pulse method was used, for example, to press Al_2O_3 [175] and TiN [176] nanoparticles. An increase in the temperature of magnetic-pulse pressing was found to be more efficient than an increase in the pressure (cold pressure). With a pulse pressure of 4.1 GPa and a temperature of 870 K, nanosystems with a grain size of 80 nm and a density of 83% of the theoretical one were prepared. Upon a decrease in the temperature to 720 K, the density decreased to 81%.

2. The properties of nanocluster systems

As noted above, isolated nanoclusters possess unique properties related to their nanometer size. However, in most cases, nanoclusters are interacting with one another; this can not only induce a quantitative change in their properties but also provoke the appearance of new properties. The assembly and self-assembly of clusters to give nanocluster systems changes many properties of the clusters. The most vivid properties of nanosystems such as structural phase transitions (in particular, in ferroelectrics and fullerenes) and optical, electric and magnetic (giant magnetoresistance, quantum magnetic tunnelling, magnetic phase transitions) properties are related to the atomic and cluster dynamics.

It is pertinent to consider both the intracluster atomic dynamics and the intercluster dynamics in a nanosystem where the cluster moves as a a single whole.

a. Intracluster atomic dynamics

The intracluster atomic mobility (in relation to the melting dynamics) is studied using microscopic and quantum-statistical methods as well as methods based on the use of thermodynamic models and computer simulation of motions (molecular dynamics and Monte Carlo method). The most important and characteristic parameters of motion are the mean square displacements of atoms in the cluster

$$\langle \bar{r}^2(t)\rangle = \frac{1}{N}\langle [x(t) - x(0)]^2\rangle \tag{16}$$

$\{\langle [x(t) - x(0)]^2\rangle$ is the mean-square displacement along the x axis in which the displacement is time averaged$\}$ and the diffusion coefficient

$$D = \frac{1}{6}\,\frac{\mathrm{d}\langle \bar{r}^2(t)\rangle}{\mathrm{d}t}\,.$$

At longer times, $\langle \bar{r}^2(t)\rangle = 6Dt$.

Before we proceed to the consideration of the microscopic approach, it is necessary to discuss two points: (i) whether the concept of phonons determining the dynamics of solids is applicable to clusters and (ii) what changes in the vibrational and rotational spectra would occur upon a decrease in the nanocluster size. The point is that in crystals constructed of nanoclusters, the lattice is not strictly periodical, unlike that in molecular crystals (because the substantial influence of the surface should be taken into account for clusters); therefore, phonons cannot be considered as plane waves with the energy E and momentum q. However, a cluster can be regarded as a single giant molecule with $3N$ degrees of freedom (N is the number of atoms in the cluster). All the natural frequencies ω corresponding to the vibrations of this 'molecule' and eigenvectors can be found. Thus, the vibrational states can be numbered in terms of frequencies ω_i rather than momenta. The mean square displacement of an atom can be found from the formula [119]

$$\langle r^2\rangle = \frac{\hbar}{NM}\sum_i \frac{\bar{n}_i + 1/2}{\omega_i}\,, \tag{17}$$

where M is the atom mass, $\bar{n}_i$ is the averaged number of vibrations.

For large clusters, the density of phonon states $\rho(\omega)$ should be introduced and the summation over frequencies should be replaced by integration. In this case, we obtain

$$\langle r^2\rangle = \frac{\hbar}{NM}\int\left(\frac{1}{2} + \frac{1}{\exp(\hbar\omega/kT) - 1}\right)\frac{\rho(\omega)}{\omega}\,\mathrm{d}\omega\,. \tag{18}$$

The form of the function $\rho(\omega)$ depends on the phonon spectra and on the model of the atomic cluster mobility chosen. In the case of the Debye model,

$$\rho(\omega) = \frac{9N\omega^2}{\omega_{\max}^3}$$

and

$$\langle r^2\rangle = \frac{9\hbar^2}{4Mk\theta_{\mathrm{D}}}\left(1 + \frac{4T^2}{\theta_{\mathrm{D}}^2}\int_0^{\theta_{\mathrm{D}}/T}\frac{u\,\mathrm{d}u}{\exp(u-1)}\right), \tag{19}$$

where θ_{D} is the Debye temperature, $u = \hbar\omega/kT$. At high temperatures, $T \gg \theta_{\mathrm{D}}$

$$\langle r^2\rangle = \frac{9kT}{M\omega^2}\,, \tag{20}$$

$$\langle x^2\rangle \approx \frac{3kT}{M\omega^2}\,.$$

For the Einstein model,

$$\rho(\omega) = 3N\delta(\omega - \omega_{\mathrm{E}})$$

(δ is the δ function, ω_{E} is the Einstein frequency) and

$$\langle x^2\rangle = \frac{\hbar}{2M\omega_t}\mathrm{cth}\left(\frac{\hbar\omega_E}{2kT}\right). \quad (21)$$

Before we consider the phonon spectra of small particles, it is necessary to calculate the density of states function $\rho(\omega)$ for the vibrations in clusters. Specific features of the spectra of clusters are due to the presence of a large number of surface atoms. It is known that atoms on the cluster surface are more weakly attached to the lattice and, hence, their vibration frequencies are lower. Therefore, the vibrational spectrum of the cluster exhibits a large number of low-energy vibrations, which results, in accordance with (18)–(21), in an increase in $\langle r^2\rangle$. However, clusters are characterised by limiting phonon wavelengths stipulated by the cluster size, *i.e.*, the phonon spectrum loses some of the low-frequency vibrations, and $\langle r^2\rangle$ decreases. Thus, the phonon spectrum of the cluster becomes discrete. However, if the Debye dependence is assumed for the contribution of the density of phonon states [$\rho(\omega) \sim \omega^2$], the effect of cutting of the phonon spectrum would be insignificant, and the overall effect for the isolated clusters would still be related to an increase in $\langle r^2\rangle$.

Even a simple model of the atomic cluster mobility predicts unusual cluster properties. If a cluster is regarded as a sphere consisting of two parts — the surface layer and the inner core — a characteristic Einstein frequency and the mean square displacement of atoms can be attributed to each part, $(\omega_E)_s$ and $\langle x^2\rangle_s$ for the surface and $(\omega_E)_i$ and $\langle x^2\rangle_i$ for the inner core. In this case,

$$\langle x^2\rangle_s = \frac{\hbar}{2M(\omega_E)_s}\mathrm{cth}\left[\frac{\hbar(\omega_E)_s}{2kT}\right]$$

and

$$\langle x^2\rangle_i = \frac{\hbar}{2M(\omega_E)_i}\mathrm{cth}\left[\frac{\hbar(\omega_E)_i}{2kT}\right].$$

According to the Lindemann criterion, melting of a substance starts when $\langle x^2\rangle_m \simeq 0.1a^2$ (a is the average distance between the atoms); the difference between melting of the surface layer and the inner core of the cluster should be taken into account because $\langle x^2\rangle_s$ is greater than $\langle x^2\rangle_i$ owing to the decrease in the number of atomic bonds for the surface atoms.[177] Figure 15 shows the temperature dependences of $\langle x^2\rangle_s$ (curve *1*) and $\langle x^2\rangle_i$ (curve *2*). Due to the difference between the $\langle x^2\rangle_s$ and $\langle x^2\rangle_i$ values, the $\langle x^2\rangle_m$ point where melting starts would be matched by different melting points for the surface $(T_m)_s$ and internal $(T_m)_i$ atoms. Moreover, apart from the regions corresponding to the solid and liquid states of the system, a transient region appears corresponding to the solid and liquid states existing simultaneously (see Fig. 15).

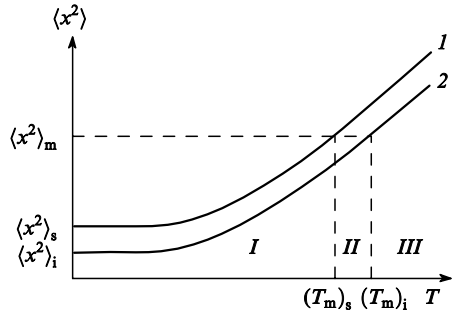


Figure 15. Temperature dependence of $\langle x^2\rangle$ for atoms on the cluster surface (*1*) and inside the cluster core (*2*). The subscripts s and i denote the surface and the cluster core, $\langle x^2\rangle_m$ are the mean-square displacements corresponding to the Lindemann criterion, $(T_m)_s$ and $(T_m)_i$ are the melting points of the surface layer and the cluster core; (*I*) is the region corresponding to the solid, (*II*) is the region corresponding to the solid–liquid transition state, (*III*) is the region corresponding to liquid.

Now we shall consider the quantum-statistical method for the investigation of the atomic mobility.

The change in the thermodynamic state of a cluster can be described by the free energy function $\Delta G = \Delta E - T\Delta S$ (E is the internal energy of states of the cluster, S is entropy). The entropy of the cluster can be calculated from the formula

$$S = -kT\ln Z,$$

where $Z = \sum g_i \exp(E_i/kT)$ is the function of distribution of states (here, g_i and E_i are the degeneracy and the energy of an ith level). Numerous studies have been devoted to the calculation of the Z value by quantum-statistical methods (see, for example, a number of studies [178–180]). The energy distribution of states for a solid cluster differs substantially from that for a liquid. At low temperatures, the density of states is greater for a solid than for a liquid; however, at high temperatures, the situation is reversed; as a consequence, the temperature of the equilibrium transition (T_{eq}) from the solid to the liquid state appears. Thus, at low temperatures, the energy change ΔE is determined by the vibrational and rotational energy levels of a solid. As the temperature increases, the entropy factor, *i.e.,* the disorder of motions, starts to play the crucial role, which is typical of a liquid. The T_{eq} value (or the melting point of the cluster) depends on the model chosen for the calculation of states for the solid and the liquid and on the number of states, *i.e.*, on the cluster size. When $T = T_{eq}$, the system contains both the solid and liquid phases.

The degree of disorder of the solid or liquid state can be characterised, for example, by the non-rigidity parameter (γ).[181] The variation of the Gibbs energy $G(T,\gamma)$ of a cluster system as a function of γ showed that the freezing point (T_f) and the melting point (T_m) of a cluster system do not coincide, *i.e.*, there is a region of coexistence of the solid and liquid states.

Yet another approach to the study of the dynamics of cluster melting is based on computer simulation of melting using Monte Carlo or molecular dynamics methods.[182–184] To determine the $\langle r^2\rangle$ and $\langle x^2\rangle$ parameters, one should solve a set of equations for the movement of clusters in a field with a specified attraction potential between atoms or molecules. The calculations can be carried out for a constant energy or temperature. In addition to the $\langle r^2\rangle$ and $\langle x^2\rangle$ parameters, this approach gives the time-averaged mean kinetic energy (temperature) over all the degrees of freedom of the cluster atoms

$$T = \frac{2\bar{E}}{(3N-6)k}$$

and the relative averaged change in the bond length (δ)

$$\delta = \frac{2}{N(N-1)}\sum_{ij}\frac{(\langle r_{ij}^2\rangle - \langle r_{ij}\rangle^2)^{1/2}}{\langle r_{ij}\rangle}.$$

By analysing these values, one can draw a conclusion about the cluster dynamics, in particular, about the melting–freezing phase transition. Figure 16 presents the computer simulation data for the Ar_{13} cluster.[185] The temperature at which δ sharply increases, which is interpreted as melting of the cluster in accordance with the Lindemann criterion, can be clearly seen in the Figure. The dependence of $\langle T\rangle$ on the system energy in the solid and liquid states indicates that the melting E_m and freezing E_f energies of the Ar_{13} cluster are different. The results of calculations of $\langle r^2\rangle$ for Ar_{13} also point to a substantial difference between the solid and liquid states. For the solid state, $\langle r^2\rangle$ reaches a flat plateau after 100 time intervals of simulation, whereas for the liquid state, $\langle r^2\rangle$ increases in accordance with the diffusion equation.

The organisation of the $(C_{60})_n$ structure on a graphite substrate and phase transitions in it have been studied by computer simulation.[163] A nanosystem in the ground state consists of hexagonal monolayers parallel to the substrate surface. The most stable structures were formed for n = 7, 19, 37, 61. Raising

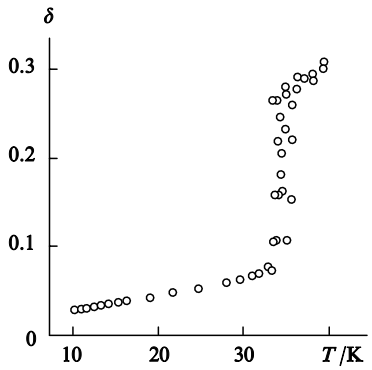


Figure 16. Temperature dependence of the mean-square change in the distance (δ) between the closest neighbours in the Ar_{13} cluster.[185]

the temperature had induced sublimation of C_{60} before the system passed into the state where the solid and the liquid phase coexisted. Study of the thermal stability of the $(C_{60})_{55}$ nanosystem near the graphite substrate demonstrated that, due to the low mobility of C_{60} clusters, this system did not undergo noticeable structural changes prior to the onset of sublimation.

Melting of clusters can also be considered within the framework of the thermodynamic formalism.[177,186–191] The state of the clusters formed during solid-state reactions or from solutions and melts is determined by the free energy $G = f(\alpha,\mu,R)$ [see Eqns (3) and (8)]. The difference between the free energies of the cluster in the liquid and solid states is

$$\Delta G = 4\pi R^2\Delta\alpha + \frac{4}{3}\pi R^3\rho\Delta\mu, \tag{22}$$

where $\Delta\alpha = \alpha_l - \alpha_s$ is the difference between the surface energies, $\Delta\mu = \mu_l - \mu_s$ is the difference between the chemical potentials for the liquid and solid states of the cluster. It is obvious that for melting, $\Delta\alpha < 0$ and $\Delta\mu > 0$. The $\Delta G(R)$ curves are shown in Fig. 17. The critical cluster size corresponding to the transition from the solid to liquid state ($\Delta G = 0$) is calculated from the formula

$$R_{cr} = \frac{3\Delta\alpha}{\rho\Delta\mu}. \tag{23}$$

When $R < R_{cr}$, a cluster occurs in the liquid state. It follows from Eqn (23) that the solid–liquid transition state cannot be realised for separate atoms in a matrix (for $\Delta\alpha = 0$), when a cluster has not yet formed. Meanwhile the $\Delta\alpha$ value should be the greatest for a free cluster. Any intercluster interactions would decrease this value and, hence, the R_{cr} value, which determines the region of possible fluctuations of the solid and liquid states.

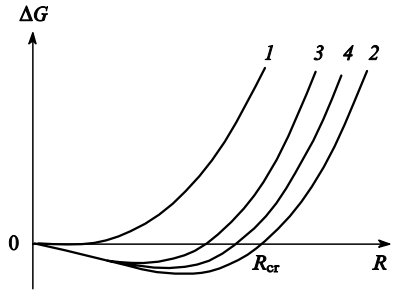


Figure 17. Change in the Gibbs energy for an ensemble of separate atoms in a solid (*1*), for an isolated cluster (*2*) and for a system of interacting clusters (*3*, *4*) occurring in the solid and liquid states *vs*. cluster size.
(*3*) Clusters interacting with one another, (*4*) clusters after treatment with surfactants.

Cluster stability can be characterised by the change in the pressure $\delta p = p_0 - p$ or temperature $\delta T = T_0 - T$ which corresponds to a given difference between the chemical potentials $\Delta\mu = f(p,T)$ and brings the phases to equilibrium at a specified cluster size (p_0 and T_0 are the pressure in the medium and the melting point for the bulk material).

If the function $\Delta\mu = f(p,T)$ is replaced by its series expansion in terms of δp at the point p_0, then, with allowance for the fact that $\partial\mu_l/\partial p = V_l$, $\partial\mu_s/\partial p = V_s$ (V_l and V_s are the molecular volumes of the cluster in the liquid and solid states),[192] we have

$$\Delta\mu \approx -(V_l - V_s)\delta p. \tag{24}$$

Using the Clapeyron–Clausius formula

$$\frac{\delta p}{\delta T} = \frac{q}{T_0}(V_l - V_s),$$

where q is the latent heat of the phase transition, we obtain

$$\Delta\mu \approx -\frac{q\delta T}{T_0}. \tag{25}$$

Substitution of Eqn (25) into Eqn (23) gives a hyperbolic variation of the phase transition temperature for a cluster *vs*. its radius

$$\frac{\delta T}{T_0} \approx -\frac{3\Delta\alpha}{\rho q R}. \tag{26}$$

Dependence (26) indicates that the melting point of a cluster decreases with a decrease in the cluster size. Dependence (22) shown in Fig. 17 allows one to conclude that at a given temperature and pressure of the medium, the initially stable structure of the cluster ($\Delta\mu > 0$) becomes metastable with respect to the liquid phase at $R < R_{cr}$.

Analysis of the experimental data on the atomic dynamics of clusters attests mainly to an increase in the mean square displacements in the metal and oxide clusters compared with the displacements in bulk samples.[119] Thus a decrease in the probability of the Mössbauer effect and an increase in the mean square displacements of atoms $\langle r^2\rangle$ was observed for the W, β-Sn, Fe and α-Fe_2O_3 clusters.[119] An exception is provided by the Au clusters with a size of 6–20 nm for which the probability of the Mössbauer effect was found to increase and $\langle r^2\rangle$ was found to decrease with a decrease in the cluster size; this was explained by the long-wavelength restriction of the phonon spectrum. Study of thin oxide films on the surface of β-Sn and Fe clusters also points to an increase in $\langle x^2\rangle$ for atoms located on the surface.[119] Apart from the increase in the $\langle x^2\rangle$ values, an important feature of atomic dynamics on the surface is the anisotropy of the atomic vibrations. Anisotropy of the atomic vibrations along the surface and normal to the surface has been observed for iron and tin atoms deposited on the extensive surface of η-Al_2O_3, silica gels and zeolites.

A decrease in the melting point (down to room temperature) with a decrease in the cluster size has been observed for gold, tin and CdS nanoclusters.[193–195] An electron microscopy study of tin films[194] has also revealed the separation of the melting and freezing points and the existence of a specific solid $\rightleftharpoons$ liquid state in which clusters possess an enhanced mobility in the transient temperature range.

In several publications, melting of iron oxide nanoclusters has been studied.[135,190,191] It was noted that melting of these clusters is accompanied by an increase in the mean square displacements of atoms. Figures 12 and 18 present the Mössbauer spectroscopy data for iron hydroxide clusters formed in polysorbs with pore diameters of 7.5 to 0.75 nm and for the nanosystem formed from the iron oxide clusters prepared by thermal decomposition of iron oxalate. For iron hydroxide clusters (see Fig. 12), the intensity of

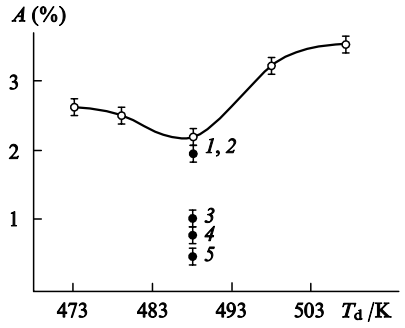


Figure 18. Spectral surface area of the Mössbauer spectrum of a nanosystem formed from iron oxide clusters prepared by decomposition of iron oxalate *vs*. temperature of thermal decomposition T_d.
The light dots are experimental data. The dark dots correspond to the surfactants: (*1*) ethanol, (*2*) isopropanol, (*3*) the surfactant Twin-65, (*4*) butanol, (*5*) SDS.

the spectral line sharply decreased upon an increase in the polysorb pore size. According to nucleation conditions [135] [see Eqn (13)–(15)], a decrease in the pore size leads to a decrease in the cluster size in the pore. The curve shown in Fig. 12 corresponds to the onset of cluster melting, which is attributable to an increase in the intracluster atomic mobility. For the γ-Fe_2O_3 nanocluster system, the dependence of the spectral surface area A on the temperature of thermal decomposition of iron oxalate (T_d) has a minimum at $T_d \approx 488$ K (Fig. 18). According to Mössbauer spectroscopy, the T_d value is related to the mean size of the γ-Fe_2O_3 cluster prepared by decomposition of iron oxalate. It was found that the cluster size increases from 2 to 4 nm as the temperature T_d changes from 488 to 508 K. The right-hand branch of the curve in Fig. 18 is related to a decrease in A (following an increase in T_d) and an increase in the atomic mobility in the γ-Fe_2O_3 cluster, similarly to the observed decrease in A in the iron hydroxide clusters formed in polysorb pores. It should be noted that the Mössbauer spectra of iron hydroxide and iron oxide clusters contain no 'broad component' corresponding to the movement of the cluster as a whole, which is due to the restricted diffusion of clusters in the pores. This will be discussed in the Section 'intercluster dynamics.' Thus, changes in the spectral surface area are associated with the change in the atom mobility within the cluster.

The left-hand ascending branch in the curve $A = f(T_d)$ (Fig. 18) is related to further decrease in T_d and, correspondingly, to a decrease in the size of clusters down to their disappearance to give separate atoms, dimers and trimers of Fe^{3+} (see Fig. 17, curve *1*). Thus, the minimum in the $A = f(T_d)$ curve observed at $T_d = 488$ K appears to be due to the onset of formation of an iron oxide cluster.

As noted above, the atomic cluster mobility is strongly influenced by the intercluster interactions. They decrease the surface energy. However, the intercluster interactions and strain can be reduced due to the action of surfactants or mechanochemical treatment. It can be seen from Fig. 18 that the spectral surface area markedly decreases after the action of surfactants. Thus, weakening of the intercluster interaction results in an increase in the intracluster atomic mobility and in a decrease in the melting point. Relation (26) can be used to estimate the R_{cr} value, corresponding to the onset of melting of γ-Fe_2O_3 clusters and to compare it with the $R(V)$ value observed experimentally from Mössbauer spectra. Using the values $\rho = 5.18 \times 10^6$ g m^{-3} (see Ref. 196), $\Delta\alpha \approx 1$ J m^{-2} (see Ref. 197) and $q \approx 2 \times 10^{-19}$ (see Ref. 136), we obtain

$$R = \frac{aT_0}{\delta T},$$

where $a = 0.1-1.0$ nm. As a result, for $T_m = 300$ K, we have $R \approx 0.1-1.2$ nm, which is in good agreement with the value $d = 2$ nm found from the Mössbauer spectrum.

It is also noteworthy that the existence of the specific solid–liquid transition state in which atoms possess enhanced mobility can provide an interpretation for the effect of adsorption decrease in the material strength (Rehbinder effect)[198] at the atomic-molecular level due to wetting and deformation of its surface under the action of a surfactant.

For nanosystems prepared by compacting, changes in $\langle r^2 \rangle$ and in the heat capacity were noted. Thus the low-temperature heat capacity in the region of T from 0.06 to 10 K for a compacted nanosystem of copper clusters with nanocluster sizes of 6.0 and 8.5 nm was 5–10 times higher than the heat capacity of bulk copper. An increase in the heat capacity of a nanostructured copper [199] is attributable to an increase in $\langle r^2 \rangle$ on the surface of nanoclusters.

Study of the phonon spectra of a compacted system of Ni clusters with a size of 10 nm prepared by neutron scattering showed an increase in the density of phonon states at low frequencies (below 14 MeV) [200] with respect to coarsely crystalline Ni. Calculation of the heat capacity based on these data demonstrated its increase (1.5–2-fold) for a nanosystem with respect to the bulk material. A Ni nanosystem formed from 70-nm clusters [130, 201] also has a higher heat capacity (by 10%–25%) up to 600 K, which is attributed to a decrease in the Debye temperature.

A model calculation of nanosystems with cluster sizes of 1.1, 2.0 and 2.8 nm using the Lennard-Jones potential showed [202] diffusion of the phonon spectrum to both high- and low-frequency regions, most of the additional vibrational modes being located at grain boundaries. The results point to a substantial increase in the heat capacity with a decrease in the cluster size in the region of $T \approx 100$ K, which is due to the predominant contribution of the low-frequency vibrations at grain boundaries.

Thus, joining of nanoclusters into a nanosystem smoothes only partially the dynamic characteristics of nanoclusters.

b. Intercluster dynamics

Convenient nanosystems for study of the movement of a cluster as a whole are represented by cation exchange resins, for example, styrene–divinylbenzene copolymers with different degrees of cross-linking (1%, 2% and 12% — samples A, B and C, respectively) and different sets of nanopores containing iron oxide nanoclusters with a size of 3 nm.[203–205] Due to the cross-links, which restrict the diffusion of iron hydroxide nanoclusters in the copolymer, nanoclusters are placed in cages with a varied size. The Mössbauer spectra of iron hydroxide clusters in polymeric systems with different degrees of cross-linking are presented in Fig. 19. These spectra in the velocity range of ± 100 mm s^{-1} exhibit a narrow component and a broad component.

The movement of iron hydroxide clusters can be described in terms of the model of limited diffusion of particles in the field of a potential. The form of the potential and the diffusion rate can be found from the temperature dependence of the surface area of the narrow component and from the shape of the broad component.[206] The Mössbauer spectrum consists of Lorentzian components with non-broadened (narrow) lines having the intensity

$$A_0 = z^{-2}\left|\int \exp(i\mathbf{k}^*\mathbf{R}) \exp\left(-\frac{U(\mathbf{R})}{kT}\right) d^3\mathbf{R}\right|^2.$$

Here $z = \int \exp(U(\mathbf{R})/kT) d^3\mathbf{R}$, $\mathbf{k}^*$ is the radiation wave vector, $\mathbf{R}$ is the cluster radius.

Analysis of the $A = f(T)$ function provides the possibility of reproducing the movement potential $U(\mathbf{R})$. Study of the temperature dependence $A_0 = f(T)$ for a sample with 2% cross-linking (sample B) gives $A_0 = 0.06$ ($T = 264-243$ K) and the potential form as a square (spherical) well with elastic walls (Fig. 20). If we

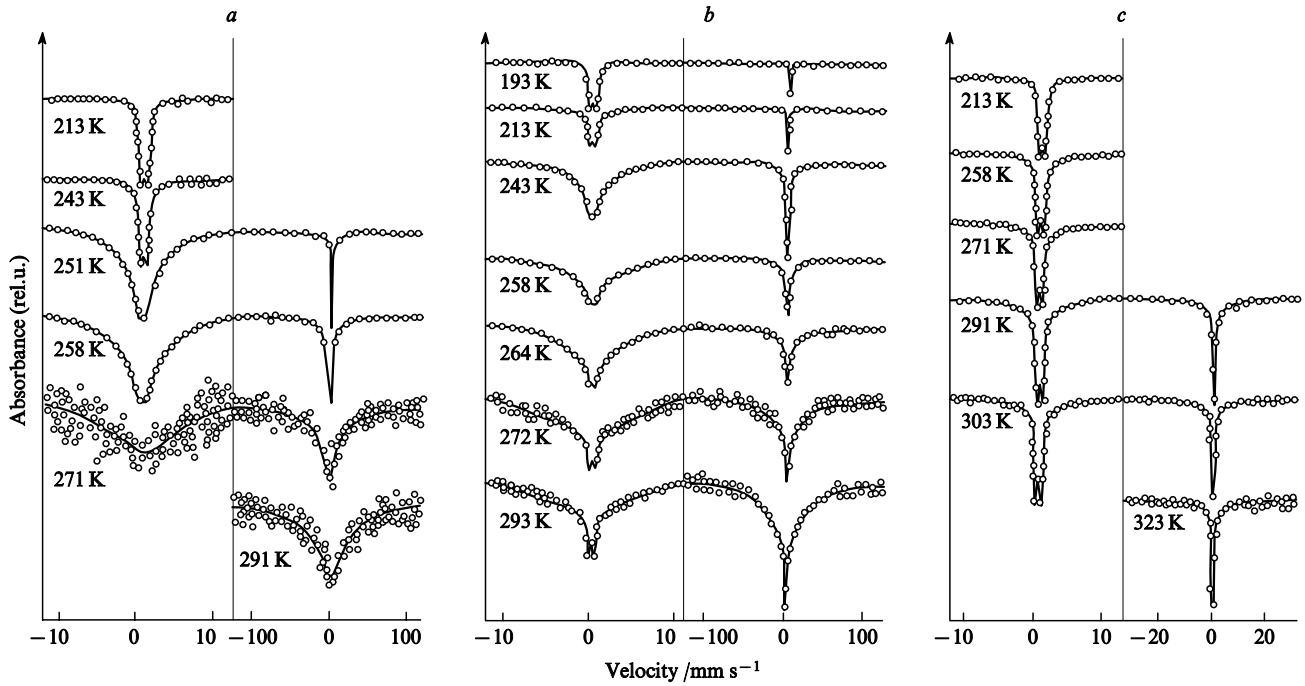


Figure 19. Mössbauer spectra of iron hydroxide in an ion exchange sulfo resin at different temperatures; (*a*) 1% (sample A), (*b*) 2% (sample B), (*c*) 12% of cross-linking (sample C).

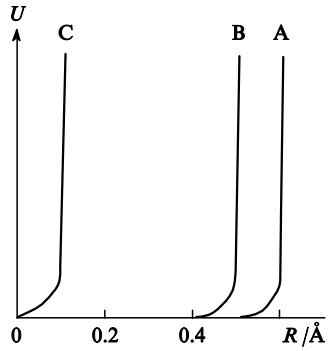


Figure 20. Shape of the potential well describing the movement of iron hydroxide clusters in samples A, B and C (see the notation to Fig. 19).

assume that in a spherical cage with radius b, only the diffusion coefficient is temperature-dependent, then

$$A_0 = \frac{g(\sin kb - kb\cos kb)^2}{(kb)^6}.$$

For $kb = 3.6$, the radius of the potential well is 0.5 Å. The spectrum calculated using these parameters is in good agreement with the experimental one.[203–205] An increase in the size of the cage (sample A) increases the well radius to 0.62 Å, while a decrease (sample C) arrests completely the cluster movement. Thus, the maximum clearance between the cluster and the network is equal to 0.62 Å. This type of motion with limited diffusion is observed for iron oxide hydroxide FeO(OH) clusters in an iron accumulating protein, ferritin.[206]

c. Structural features of nanosystems. The role of defects and stresses

Combination of clusters into a nanosystem gives rise to numerous phase boundaries and dislocations and a corresponding intercluster stress. The phase boundaries play a crucial role in considering many mechanical properties, heat conductivity, electrical conductivity and magnetic characteristics of nanostructures. The size effects and intercluster interactions also influence the structural phase transitions. The phase transitions related to the movement of atoms in a cluster were considered in the previous Section. Now we shall discuss the structural changes in a nanosystem induced by variations of the cluster size, intercluster interactions, defects and dislocations.

The intercluster interactions create stresses, excess energy and excess pressure at the cluster boundaries. The excess energy per dislocation is calculated from the formula [207]

$$E_d = \frac{Gb^2}{4\pi(1-\nu)}\ln\frac{r}{r_0}, \qquad (27)$$

where G is the shear modulus, b is the Burgers vector characterising the magnitude of the shift of an edge dislocation, $b = a_0/\sqrt{2}$ (a_0 is the lattice constant), ν is the Poisson coefficient (usually 0.3), r is the maximum distance at which the influence of dislocations is still retained, r_0 is the minimum dislocation size. With the assumption that the concentration of dislocations in a cluster is determined by the ratio of the cluster surface area to the cluster volume, the excess energy density of the cluster ε_d is

$$\varepsilon_d = \frac{Gb^2}{4\pi(1-\nu)}\frac{1}{R}\ln\frac{r}{r_0}. \qquad (28)$$

Thus, the excess energy density decreases as the cluster size R increases and approaches zero for a bulk material. It should be noted that the applicability of this approach to small nanoclusters is restricted by the thickness of the surface layer of the cluster (a), *i.e.*, Eqn (28) can be used only to calculate the excess energy of clusters with $R > a$.

When considering the influence of defects and dislocations on the properties of nanosystems constructed from nanoclusters of arbitrary sizes, one should proceed from the thermodynamic concentration of defects and dislocations, which takes into account the chemical potential and the excess energy of the cluster surface. The excess energy gives rise to excess pressure, which is equal to $\sim 10^9$ Pa for 1-nm clusters. If the pressure drop between the cluster bulk and the cluster surface is neglected, the concen-

tration of defects in the cluster (c_s) can be calculated from the relation

$$c_s = \frac{a(3R^2 - 3aR + a^2)}{R^3}, \quad (29)$$

where a is the thickness of the surface layer. It can be assumed that in the absence of pressure drop, *i.e.*, when the influence of defects inside the cluster is counterbalanced by the influence of defects on its surface, the difference between the chemical potentials in the cluster and on the surface is equal to zero

$$\Delta\mu^0(0) + kT\ln\frac{c_s}{c_0} = 0, \quad (30)$$

where c_0 is the defect concentration on the surface.

Naturally, the allowance made for the pressure drop shifts the equilibrium by

$$\Delta\mu^0(\delta p) = \Delta\mu^0(0) + V\delta p, \quad (31)$$

where V is the volume of a defect, $\delta p = 2\alpha/R$ (α is the surface tension). In this case, the new equilibrium of the system is determined by the expression

$$\Delta\mu^0(0) + V\delta p + kT\ln\frac{c}{c_0} = 0. \quad (32)$$

By solving the set of equations (30) and (32), we obtain

$$c = c_s\exp\left(-\frac{2\alpha V/R}{kT}\right). \quad (33)$$

The dependence of c on the cluster size in the R/a units is shown in Fig. 21. The maximum in the $c = f(R/a)$ curves is located at $R/a = 25$, which corresponds to $R = 10-50$ nm. It is the 10–50-nm clusters, having the maximum defect concentration and the highest excess energy, that are involved in the formation of nanosystems. This is important for the understanding of the reasons for the appearance of new properties in nanosystems. In nanostructures formed by molecular clusters from CO_2, N_2 and SF_6, an increase in the stress with an increase in the cluster size was observed.[208] Numerous studies of nanosystems by X-ray diffraction methods point to the influence of the cluster size and interfacial stresses on the structure of a nanosystem.[209] Analysis of nanocrystalline Al, Ru, Cu and AlRu systems[210,211] showed that the mean square deformation of these systems is equal to 1%–3%, which is markedly greater than the deformation of coarse-grain metals. Meanwhile, by modelling X-ray diffraction of clusters of different size,[212] it was shown that small clusters do not contribute to the elastic distortions of the crystal lattice caused by dislocations at phase boundaries. The major contribution is made by larger nanoclusters. Thus, there exists a transient region of nanocluster sizes in which the effect of stresses at phase boundaries is a maximum; this complies with the conclusions based on the thermodynamic model for the influence of defects [see relations (29) and (33)].

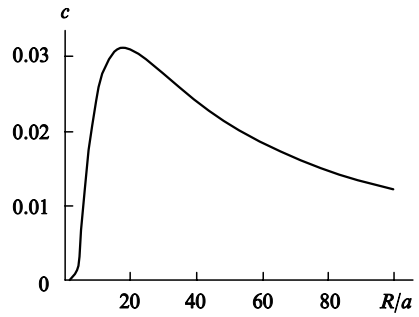


Figure 21. Density of defects c in the cluster *vs*. the cluster size (in the R/a units).

The excess stresses result in a change in the crystal lattice constant. In most cases, the lattice parameters decrease, which is attributed to the generation of additional energy at phase boundaries, to the change in the specific volume and to the appearance of excess pressure.[213–215]

Nanosystems are characterised by unusual mechanical properties: microhardness and superplasticity. At room temperature, microhardness of nanosystems is 2–7 times higher than that of the corresponding bulk materials. According to a publication,[216] the Vickers microhardness of a cluster

$$H_v \approx H_0 + k_0 d^{-1/2}$$

increases with a decrease in the cluster size. The results of microhardness measurements for nanosystems formed by Ag, Cu, Pd, Se, Fe and Ni metal clusters have been reported.[217] It was found that a decrease in the cluster size is accompanied by an increase in the nanosystem hardness. In addition, microhardness of a nanosystem depends on the conditions of its treatment. These conditions influence the structure of interfaces, cluster interactions and the cluster size. For example, relaxation and annealing of defects at the phase boundaries of the $Al_{98.5}Mg_{1.5}$ clusters, with the cluster size remaining invariant ($d \approx 150$ nm),[218] decrease the microhardness from 1.7 to 1.45 GPa. However, the cluster size is affected by annealing to a markedly greater extent. Thus annealing of a nanosystem formed by Pd clusters at 475–600 K brings about an increase in the cluster size and, hence, an almost threefold decrease in the system microhardness. Upon annealing of nanosystems of Ag ($d \approx 10$ nm) and MgO ($d \approx 10$ nm) clusters, their microhardness changed in different ways: the microhardness of the metallic nanosystem decreased[219] (apparently, due to an increase in the size of Ag clusters), while the microhardness of the oxide system remained constant up to 870 K.[220]

Yet another remarkable feature of nanosystems is superplasticity: upon stretching, the sizes of samples can increase by factors of dozens without fracture. For example, the Ni and Ni_3Al nanosystems were found to exhibit low-temperature superplasticity at $T_s = 470$ and 450 °C, respectively (these temperatures are almost three times as low as the melting point).[221] The superplasticity of oxides and ceramics presents considerable interest from both theoretical and practical standpoint. The results of a study[222] indicate that the superplasticity of nanosystems manifests itself for cluster sizes from 1 nm to 1 μm; the cluster size should not change on thermal treatment. For example, in two-phase systems, the growth of clusters of one phase caused by heat treatment is suppressed due to the presence of the other phase. It is also believed that the system superplasticity is affected by the presence of the amorphous phase.[223]

The high strength and the superplasticity of nanosystems can be explained by using the extremal dependence of the defect density and excess energy on the nanocluster size which we obtained. Indeed, nanosystems composed of small nanoclusters with sizes $d < 10$ nm contain few defects and dislocations and display exceptionally high hardness. Meanwhile, in nanosystems formed by clusters with intermediate size ($10 < d < 100$ nm), the number of dislocations is maximal, which ensures their record plasticity.

Thus, superhard materials can be produced by using nanosystems composed of nanoclusters with $d < 10$ nm, while manufacture of superplastic materials requires nanosystems composed of nanoclusters with $10 < d < 100$ nm.

The stresses arising at phase boundaries play one more important role — they act as growth stimulators for assembled nanosystems. The self-assembly and the growth of superlattices of the $Si_{0.84}Ge_{0.16}$ alloy under the action of stress induced by alternating absorption of layers of silicon and germanium atoms at the Si(001) plane at 380 °C has been considered.[224] Computer simulation using an elastic field of stress forces arising on the layer surfaces showed that the stresses are different for the layers formed by atoms differing in size. The superlattice $Si_{0.84}Ge_{0.16}$

formed under the action of stresses had equal distances between the layers (*i.e.*, a regular alternation of layers was observed) and a regular arrangement of atoms within a layer. The period of the $Si_{0.84}Ge_{0.16}$ superlattice was 3 nm.

Considerable interest is also aroused by structural phase transformations in nanosystems. It was found that the nanometer size results in stabilisation of many non-equilibrium structures. Thus nanoclusters with a size of several nanometers constructed from unstable Fe(C) and γ-Fe phases are known. They are stable even at room temperature, whereas in the bulk materials, these phases are stable only at temperatures of 800 and 1000 °C, respectively.[225] Stable CdS nanoclusters with the rock salt structure are also known, whereas bulk CdS can be stabilised only at high pressures.[226] The stabilisation of structures not equilibrated at a given temperature due to the formation of small clusters with $d < 10$ nm can be explained by the action of the surface energy and pressure created by the surface tension, which reaches a value of several Gigapascals for 1–2-nm clusters.

Non-equilibrium states of a cluster system can also be stabilised by external pressure. The phase transitions induced by high pressure (1.5 GPa) in the crystal of C_{60} (fullerite) but absent at normal pressure have been studied.[152] It was found that crystallisation of C_{60} at room temperature yields a crystal lattice with dumb-bell-shaped $(C_{60})_2$ dimers in the lattice points.§ An increase in the temperature (> 423 K) gives an orthorhombic C_{60} structure, which passes into a tetragonal structure at 723 K.

Now we shall consider one more example of phase transitions in nanocrystalline ferroelectrics. A ferroelectric transition accompanied by a first-order structural phase transition was observed in $BaTiO_3$ [227] and $PbTiO_3$ [228] crystals. This transition is characterised by a critical temperature T_C (similar to the Curie point for ferromagnets) above which the substance passes into the paraelectric state. Spontaneous polarisation in ferroelectrics results from first-order phase transitions, due to the tetragonal distortion of the crystal lattice (change in the $c:a$ ratio). At temperatures above T_C, the tetragonal crystal lattice is transformed into a cubic lattice; then $c:a \to 1$.¶

The influence of the cluster size on the ferroelectric transition was studied in relation to the $PbTiO_3$ nanosystem. This system was prepared by precipitation from a solution of clusters with sizes of 20–100 nm. For the $PbTiO_3$ crystal, the effect of the cluster size on the temperature and character of the phase transition was studied by X-ray diffraction analysis and differential scanning calorimetry (DSC). The X-ray diffraction study (Fig. 22 *a*) showed that the $c:a$ ratio changes upon phase transition. It was found that, as the cluster size decreases, the $c:a$ ratio decreases; however, even for the smallest of the clusters studied (with $d = 23$ nm), the $c:a$ ratio does not reach unity. The extrapolation $c:a \to 1$ gives the d_{cr} value, *i.e.*, the cluster size at which the spontaneous polarisability disappears, the lattice symmetry becomes cubic, and the nanosystem passes into a paraelectric state. The DSC data indicate that the phase transition temperature (T_C) decreases as the cluster size decreases from 80 to 30 nm (Fig. 22 *b*), the phase transition is gradually smeared and for clusters with $d = 26$ nm, no phase transition is observed. The decrease in T_C amounted to 20 °C. Despite the absence of obvious indications of the transition, in the case of the crystal consisting of clusters with $d = 26$ nm, one should still assume the presence of a residual smeared ferroelectric transition, which cannot be observed, apparently, due to the scatter of particles over sizes and the diffusion character of the transition itself.† It should be noted that the T_C value is also influenced by the intercluster interaction, which determines not only the T_C value but also its scatter.

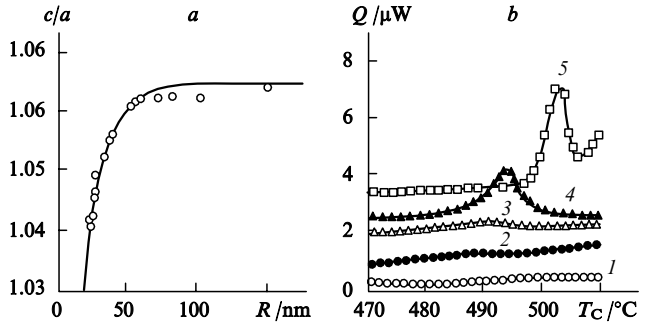


Figure 22. Ratio c/a (tetragonal distortion) (*a*) and temperature of phase transition (*b*) in the crystal of the $PbTiO_3$ ferroelectric *vs.* the cluster size.[228]
(*a*) X-Ray diifraction data; (*b*) differential scanning calorimetry data (scanning 5 K/min) obtained for clusters with $R = 26$ (*1*), 31 (*2*), 39 (*3*), 57 (*4*) and 81 nm (*5*).

The structure-magnetic properties of nanocluster systems depend largely on the presence of defects and dislocations. As noted above, the formation of a nanosystem is accompanied by the appearance of interfaces (or phase boundaries). Under some conditions, these phase boundaries can participate in the nucleation of nanoclusters. Thus the magnetic properties of cluster nitride phases arising upon nitriding of an iron catalyst in a flow of ammonia at 200–350 °C were studied by Mössbauer spectroscopy. When the nitrogen concentration in the cluster catalyst is 1 mass % – 2 mass %, phases of defect ε-iron nitride are formed in the catalyst. During low-temperature annealing (200 °C) in air, the nitrogen atoms are segregated at phase boundaries, resulting in a decrease in T_C of the nitride phase. Nitrogen is accumulated on the defects. An increase in the temperature of annealing to 400 °C results in normal gradient concentrational diffusion of the nitrogen atoms over the cluster, resulting in their uniform distribution and an increase in T_C. The equilibrium segregation of nitrogen atoms near the phase boundaries decreases the magnetic stability of the defect regions and serves as a peculiar method for 'magnetic decoration' of the stress fields by defects.[230]

Let us consider yet another example of the influence of phase boundaries and defects on the magnetic properties of the copper nanostructure with an admixture of iron atoms. Plastic deformation of the copper samples with iron dissolved therein [231] afforded copper clusters with a size of 130–150 nm and ~3-nm iron clusters.‡ The annealing of this system at a temperature of < 1000 K results in the diffusion of iron atoms along the grain boundaries and in enlargement of iron clusters; simultaneously, the magnetic properties of the system change. As the temperature rises (> 1000 K), the solubility of iron in copper increases, and normal concentrational diffusion starts; this results in vanishing of the clusters and uniform dissolution of iron atoms in copper.

The magnetic susceptibility of paramagnetics is influenced by the presence of vacancies in the crystal lattice. For nanocrystalline Pd prepared by plastic deformation (pressure with shear),[6] the magnetic susceptibility was found to increase, which was attributed to an increase in the density of electronic states at the Fermi level. This increase is possible due to the presence of vacancies in the lattice formed by palladium clusters.

d. Optical and electric properties of nanocluster systems

Specific optical and electric properties arise in nanocluster systems owing to the effects associated with the restriction of the electron

§ The same dimers are formed in the mechanochemical reaction.[153]

¶ As noted above, nanosystems composed of clusters with $d < 10$ nm contain fewer defects and dislocations. The minimisation of the crystal lattice energy with a decrease in the cluster size results in the transition from a crystal lattice with lower symmetry to a lattice with higher symmetry.[229]

† The residual smeared ferroelectric transition appears to occur also in the crystals formed from clusters smaller than 26 nm, down to 7 nm.

‡ Iron clusters can be located, for example, at grain boundary junctions.

free path (quantum restrictions) and with the appearance of discrete energy levels in the valence band and the conduction band, which changes the selection rules for optical transitions. It is possible to create one-electron nanocluster systems in which the number of discrete energy levels increases, as the cluster size decreases; in this case, the energy of electron transition from one electronic level to another increases according to the relation $e^2/2c$ ($c \approx d$). This energy can become greater than the kinetic energy of an electron (kT) and thus stimulate tunnel transitions. The development of these systems provides new potentialities for the manufacture of rectifier devices, diodes, *etc*.

It has already been noted that the nanocluster semiconductors CdS, CdSe and InP exhibit a 'blue shift' of frequency. For example, in the case of CdSe, the energy of electron transition changes from 1.7 eV (red region) to 2.4 eV (green region) as the cluster size diminishes from 20 to 2 nm.

The preparation of light-tunable diodes based on CdSe nanoclusters has been described.[232, 233] In one study,[232] CdSe nanoclusters were assembled as a thin film on the surface of a luminescent polymer (poly-*p*-phenylenevinylene, PPV). The polymer was grown on an indium oxide–tin layer able to let carriers as holes pass through. In addition, a nanocrystalline CdSe layer was coated with a Mg–Ag film for electron injection. When a voltage was applied to this system, electroluminescence was observed. The electroluminescence wavelength can be changed by varying the size of nanoclusters.

An increase in the oscillator strength and a decrease in the de-excitation time typical of some nanoclusters may lead to the design of non-linear optical nanosystems, for example, optical switches which modulate a laser beam from a high-power laser by weak, non-resonant pulses.

Light absorption and emission by porous silicon is attributed to the appearance of new optical transitions. In bulk silicon, electronic transitions between the excited state of the conduction band and the ground state of the valence band are forbidden. Only non-radiative transitions involving phonons are possible. In nanocrystalline silicon, non-radiative transitions are also retained but their contribution is insignificant. Radiative electronic transitions are more characteristic in this case.[234, 235]

In addition to the 'blue shift', a 'red shift' can also be observed in nanosystems. This occurs in semiconductors with a broad forbidden band. For example, a decrease in the absorption edge energy by 0.2 eV ('red shift') has been observed for the γ-Fe_2O_3 nanoclusters with $d \sim 8.5$ nm residing in the pores of a polymeric ion exchange sulfo resin.[236] The most probable reason for the 'red shift' is the appearance of strains and stresses on the surface of the clusters (due to surface tension) which form the lattice of the solid. Indeed, in a 5-nm γ-Fe_2O_3 cluster, the internal pressure ($p = 2\alpha/R$) equals 0.4 GPa.

X-Ray diffraction studies demonstrated a 0.35% decrease in the lattice volume for γ-Fe_2O_3 nanoclusters. If the compression modulus for γ-Fe_2O_3 is taken to be equal to that for Fe_3O_4, then a 0.35% compression of the γ-Fe_2O_3 lattice brings about an internal pressure of 0.35 GPa, which is in agreement with the calculated value, equal to 0.46 GPa, derived from the estimates of the influence of the surface tension. The action of pressure is known to induce a phase transition of a semiconductor to the conducting state. Thus, when magnetite Fe_3O_4 is kept under a pressure of 5 GPa, it passes to the conducting state. Since the forbidden gap (E_g) for γ-Fe_2O_3 is 2.1 eV and that for Fe_3O_4 is 2 eV, then the decrease in the width of the forbidden gap in γ-Fe_2O_3 induced by high pressure is 0.15 eV, which is in good agreement with the results obtained in the optical experiment.

The optical properties of a nanosystem depend on its organisation and on the intercluster interaction. Light absorption by silver nanoclusters prepared using reverse micelles has been studied.[142] This procedure yields nanoclusters with a very narrow size distribution (2 to 8 nm), the surface of which can be stabilised by thiols, and then they can be used for assembling two- and three-dimensional structures. Nanosystems incorporating silver nanoclusters with sizes of 4.5, 5.2 and 6.1 nm were prepared. Two- and three-dimensional systems were formed on a graphite substrate by applying a drop or several drops of a colloid solution of silver nanoparticles in hexane. It was found that coating of the surface of silver nanoclusters by dodecanethiols influences their optical properties: the absorption band of the plasmon peak shifts to lower energies (from 2.85 to 2.73 eV) and its width increases (from 0.9 to 1.3 eV). These data were interpreted on the basis of the model of light absorption by clusters proposed in a study.[54] The shift of the absorption band was attributed to the electronic plasmon absorption inside the cluster, while band broadening was ascribed to the change in the dielectric constant of the medium (intercluster absorption). Simulation of the absorption spectra of a 2D nanosystem showed that a decrease in the cluster size in an isolated medium (reverse micelle) results in a substantial increase in the width of the absorption band due to the restriction of the electron free path, while placing the clusters in media with different dielectric constants ε_m stimulates the shift of the absorption band, an increase in ε_m resulting in a substantial decrease in the absorption energy. Thus, the shift of the absorption band observed for silver nanoclusters can be explained by the increase in the dielectric constant upon the assembly of a 2D hexagonal network of silver clusters.

Optical investigations (Fig. 23) of the nanosystems formed show that their properties depend on the degree of structure perfection and the preparation procedure. Application of one drop of a colloid solution on the substrate gives rise to a 2D nanosystem with a hexagonal network of silver clusters (Fig. 23, curve *2*). The absorption spectrum of nanoclusters in this system differs from the spectrum of these clusters in solution: the plasmon absorption band shifts by 0.27 eV and its width increases from 0.8 eV (in solution) to 1.0 eV (in the nanosystem).

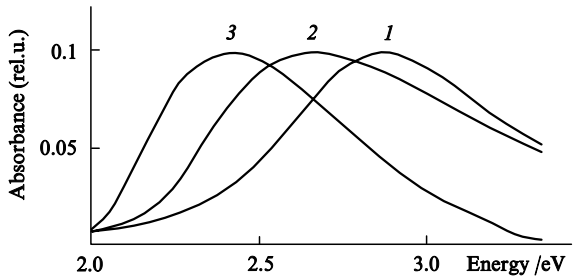


Figure 23. Variation of the plasmon absorption width and peak shift in a colloid solution and in nanosystems containing 4.5-nm silver clusters formed on a carbon substrate.[142]
(*1*) Initial colloid solution with $[Ag_n] = 2.5 \times 10^{-3}$ mol litre^{-1}; (*2*) two-dimensional cluster system formed on a substrate after deposition of one drop of a colloid solution; (*3*) three-dimensional cluster system formed after deposition of three drops of a colloid solution.

An increase in the concentration of nanoclusters in a colloid solution or deposition of several drops of the colloid solution on a graphite substrate afford a more perfect, three-dimensional, face-centred cubic structure.

For the 3D structure (Fig. 23, curve *3*), further shift (by 0.47 eV with respect to that in solution) of the absorption band toward lower energies is observed; however, the width of the plasmon peak diminishes to 0.7 eV. The narrowing down of the absorption band is a result of the increase in the electron free path. This implies that an electron penetrates the barrier between the nanoclusters (a ~2-nm thick coating). The possibility of electron tunnelling between metal surfaces by such a long distance [237] is an important feature for the design of new materials for lasers, optics and electronics.

The restriction of the electron free path in small clusters and the presence of intercluster boundaries impart new electric properties to nanosystems obtained on the basis of nanoclusters. For

example, metals or semiconductors pass into a non-conductive state. This transition is due, first, to a decrease in the carrier density as a result of the restriction of the electron wavelength and the appearance of discrete electronic levels and, second, to a decrease in the conductivity as a result of electron scattering at phase boundaries and generation of dielectric charges. Indeed, a 7–20-fold increase in the electric resistance was observed for nanocrystalline copper in the region of $T < 275$ K.[238] The high resistivity of cobalt films (2- to 50-nm thick) was mainly attributed [239] to the effects of electron localisation. The influence of the phase boundaries between nanoclusters on the electric properties of nanosystems may be due to long-range stress fields and to the dynamic state of the atoms.

In recent years, substantial progress in the fabrication of 3D, 2D and 1D electronic nanosystems (see, for example, Ref. 41) used to produce single-electron transitions, unidimensional nanowires, *etc.* has been made. The 3D organisation of nanoclusters is the most obvious. The 3D nanosystems are prepared by crystallisation of clusters (instead of atoms). For example, nanocrystalline copper was prepared in this way. However, the researchers were able to crystallise only large copper clusters (~40 nm) passivated by thiols.[143] Crystallisation of copper selenide clusters $Cu_{146}Se_{75}(PPh_3)_{10}$ was also performed.[240] The crystals thus obtained can be used in semiconductor devices. The idea of producing an organised 3D cluster structure from clusters linked by spacer molecules proved fruitful. The spacers allow one to control the distance between the clusters; this can be accompanied by spontaneous crystallisation. An advantage of this approach is that it provides the possibility of changing the energy barrier to passage of an electron through the cluster. Figure 24 shows the change in the Coulomb barrier between the Au_{55}^* clusters depending on the spacer length and nature.[41]

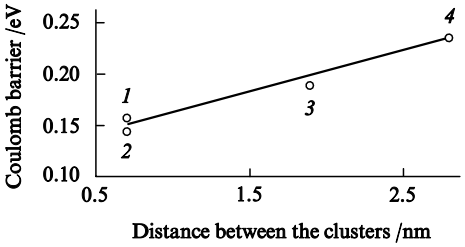
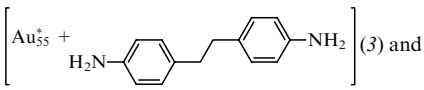
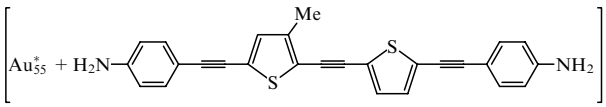


Figure 24. Coulomb barrier *vs.* distance between the clusters.[41]
The dots on the straight line correspond to the $Au_{55}(PPh_3)_{12}Cl_6$ (Au_{55}) (*1*) and $Au_{55}(PPh_2C_6H_4SO_3Na \cdot H_2O)_{12}Cl_6$ (Au_{55}^*) (*2*) clusters and the systems



(*3*) and



(4).

Two-dimensional cluster structures are usually assembled using molecular clusters stabilised by ligands. Perfect layers of gold clusters with alkanethiol coatings which virtually did not interact with the substrate and were self-assembled due to van der Waals forces have been prepared.[241] If the interaction of the clusters with the substrate is enhanced, the structure loses its perfection. However, 2D cluster structures cannot be used in conducting devices or in a tunnelling microscope without proper fixing on the substrate. Study of Au and Pd clusters on various substrates (gold, mica, glass, silicon) demonstrated that chemical fixing of clusters on the support can be easily attained, whereas a perfect organisation of the 2D structure is achieved with difficulty.[41] The point is that self-assembly requires that the building blocks be free and mobile; however, when the clusters are attached to the substrate surface, the mobility decreases. The binding between the adsorbed cluster and the substrate can be weakened by treating the substrate with a surfactant. Thus deposition of the $Au_{55}(Ph_2PC_6H_4SO_3H)_{12}Cl_6$ clusters onto a single-crystal Au(111) surface modified by aminothiols improved the ordering of the 2D layer.

The assembly of the 2D layers for electronic devices is performed in the presence of spacer molecules, which allow one to control the distances between the clusters. These nanostructures are prepared by dissolution of clusters with appropriate spacers in Langmuir–Blodgett films; the cluster ligands and the spacer molecules should be complementary.

Of great interest from the practical standpoint are unidimensional cluster structures, nanowires. They are formed as whiskers at atomic steps of the surfaces. A nanowire from gold clusters was prepared using porous membranes based on alumina with 7-nm channels in which clusters consisting of Au_{55} cores stabilised by ligands were placed.[242]

Nanowires are also prepared from carbon nanotubes. The conduction of nanotubes can be switched (from the metallic to the semiconductor type) by changing their helical structure.[154] Electronic devices are assembled by combining nanotubes with different structures. The combination of carbon nanotubes in pairs of 'armchair' (A) and 'zigzag' (Z) types was considered.[154] Calculation of the switching from the metallic type of conduction (A state) to the semiconductor type (Z state) showed an asymmetry along the tube axis, which provides a rectifier effect. This result is in line with experimental data [243] on the rectifying effect of nanotubes.

e. Magnetic properties

The magnetic properties of nanocluster systems are influenced by both size effects and intercluster interactions and the cluster organisation. One of the best known and well-studied phenomena is superparamagnetism, *i.e.*, the change in the direction of the magnetic moment of the cluster as a whole due to thermal fluctuations without losing the magnetic ordering. The formation of magnetic domains in cluster systems depends on both the individual properties of the clusters (magnetic anisotropy) and the intercluster interactions. Therefore, magnetisation processes in these systems depend appreciably on the defectiveness of the cluster structure and on phase boundaries.

The magnetic quantum tunnelling effects and giant magnetoresistance also present interest. The new effects include the first-order magnetic phase transitions in nanoclusters and nanocluster systems in which the magnetic ordering and magnetisation disappear by a jump upon an increase in the temperature or a decrease in the cluster size.

Superparamagnetism. The phenomenon of superparamagnetism consists in the generation of measurable thermal fluctuations of the magnetic moment of the cluster upon a decrease in the cluster size to 1–10 nm. The fluctuation time ($\tau = 10^{-9}$–10^{-10} s) can be calculated using a simple equation

$$\tau = \tau_0 \exp\left(\frac{K_a V}{kT}\right), \qquad (34)$$

where K_a is the magnetic anisotropy constant of the cluster, V is the cluster volume. The observation of superparamagnetism depends on the time of measurement (τ_{meas}) of the magnetic characteristics, namely, magnetisation and magnetic susceptibility. If $\tau < \tau_{meas}$, the system is referred to as a superparamagnetic system. If $\tau > \tau_{meas}$, the superparamagnetic state cannot be detected. In this connection, Mössbauer spectroscopy with a characteristic time of measurement $\tau_{meas} = 10^{-8}$ s (the time of Larmor precession of the ^{57}Fe nuclear spin in the magnetic field) has become a unique method for the investigation of superparamagnetism. The superparamagnetic relaxation of the magnetic moment with $\tau \approx 10^{-8}$–10^{-10} s causes line broadening in the Mössbauer spectra and disappearance of the magnetic hyperfine

structure. Mössbauer spectroscopy makes it possible to estimate the relaxation times in the range of $10^{-8}-10^{-10}$ s and cluster sizes in the range from several nanometers to tens of nanometers.

One more important characteristic of a nanosystem is the magnetic anisotropy constant. This value is related to the magnetic structure and the shape of the cluster. In addition, it characterises the state of the surface, defects and intercluster interactions. Thus for γ-Fe_2O_3 nanoclusters formed in the pores of a sulfo resin with a size of ~ 7 nm, the magnetic anisotropy [236] is 4.4×10^5 J m^{-3}, which is much higher than the value $K_a = 4.7\times10^3$ J m^{-3} for a bulk sample.

It is known that ferromagnets have a magnetic domain structure below the critical temperature. In the absence of an external magnetic field, a system formed from ferromagnetic clusters has a minimum magnetic energy (E_m), which consists of the exchange and dipole energies and the energy of magnetic anisotropy

$$E_m = E_{ex} + E_d + E_{an}\,.$$

The exchange interaction (E_{ex}) lines up the magnetic moments parallel to one another; it is responsible for the uniform magnetisation of domains, and the dipole interaction (E_d) induces antiparallel arrangement of the magnetisation vectors of neighbouring domains, thus decreasing E_m.

As the cluster size decreases below some critical value, the fragmentation of a cluster into domains becomes energetically unfavourable; in this case, a system of single-domain clusters with single-phase magnetisation is formed. Transition of a ferromagnetic cluster from the single-domain state with single-phase magnetisation into a multidomain state changes superparamagnetic properties.[244, 245] When the cluster size increases ($R > R_{cr}$), the energy of anisotropy $U = E_{an} = K_aV$ decreases to zero, which is accompanied by a corresponding decrease in the relaxation time τ and the change in the superparamagnetic properties.

A cluster having the critical size R_{cr} occurs in a state of uniform magnetisation, its magnetic moment being constant over the whole volume $\mathscr{M}(r,\theta,\varphi) = \mathscr{M}_0$ (r is the radial coordinate, θ and φ are the polar and azimuthal angles). When $R > R_{cr}$, the uniform magnetisation state is no longer energetically the most favourable, and rearrangement of $\mathscr{M}$ over the whole particle bulk takes place. It was found [244, 245] that

$$R_{cr} \simeq 2.085\sqrt{\frac{3I}{4\pi}}\,,$$

where I is the exchange integral. The height of the potential barrier was calculated [244] using the formula

$$U = \frac{K_a}{2}\int\left(\cos^4\omega - 3\cos^2\omega\sin^2\omega + \frac{3}{8}\sin^4\omega\right)\mathrm{d}V, \qquad (35)$$

where ω is the function $\omega(R,\theta)$, characterising the deviation of the magnetic moment of the cluster from the uniform magnetisation state. For a nanosystem with a cubic symmetry ($\omega \ll 1$),

$$U_{cub} = \frac{K_a}{2}\int(1-5\omega^2)\mathrm{d}V. \qquad (36)$$

If one compares expressions (35) and (36) with the relation for the calculation of the total moment of the cluster

$$\mathscr{M} = \mathscr{M}_0\int\cos\omega\;\mathrm{d}V \approx \mathscr{M}_0\int\left(1-\frac{\omega^2}{2}\right)\mathrm{d}V, \qquad (37)$$

it turns out that a minor deviation of $\mathscr{M}$ from $\mathscr{M}_0$ (by $\omega^2/2$) gives an order of magnitude higher change in the energy of the anisotropy of the potential barrier. Note that for clusters with a uniaxial symmetry, in which the magnetisation state deviates from the uniform state, the U value does not decrease sharply with the cluster size

$$U_{rel} = \frac{K_a}{2}\int\left(1-\frac{3}{2}\sin^2\omega\right)\mathrm{d}V. \qquad (38)$$

The superparamagnetic behaviour of a nanocluster system formed by Fe–Ni and Fe clusters with a size of 10–25 nm has been studied.[244, 245] To separate the clusters and to weaken the magnetic dipole interaction between them, clusters with a filler and with a content of iron clusters equal to 10% were studied. The data of Mössbauer spectroscopy indicate that the superparamagnetic relaxation time for 11.5-nm clusters is shorter than the relaxation time of 10.5-nm clusters; subsequently, τ increases in proportion with K_aV, which is consistent with the beginning of the deviation from uniform magnetisation.

Magnetisation and quantum magnetic tunnelling. The state of the cluster surface, cluster shape and intercluster interaction influence substantially the magnetisation curves of a nanosystem and the coercive force. Calculations of the relaxation time upon transition of the system into the state with uniform magnetisation show an increase in the energy of anisotropy and the related coercive force following a decrease in the cluster size.[244] The magnetic hysteresis curves for nanocrystalline Ni and Co [246] indicate that the coercive force H_c in cluster nanosystems subjected to plastic deformation is several times as great as H_c for bulk materials. Low-temperature annealing leads to a decrease in H_c with the cluster size remaining invariant, due to the annealing of defects, while high-temperature annealing results in lower H_c and larger clusters. Thus, the increased coercive force of nanocrystalline metals and alloys is related to the stresses and defects at the cluster boundaries and to the single-domain state of the clusters.

The influence of arrangement of Co nanoclusters on the magnetisation curves has been investigated.[22] The colloid Co clusters with sizes of 5.8–8.0 nm were arranged into a 2D hexagonal lattice on a graphite substrate. Studies of the superparamagnetic properties of this system demonstrated shifting of the blocking temperature § of the assembled structure ($T_b = 63$ K) towards higher values with respect to T_b for the colloid solution ($T_b = 58$ K). The increase in T_b is due to the increase in the energy barrier K_aV as a result of intercluster interactions. The total saturation magnetisation of the nanocrystalline system was found to decrease to $M_s = 80$ emu g^{-1} with respect to that of bulk cobalt ($M_s = 162$ emu g^{-1}). The decrease in M_s is due to the presence of the stabilising ligand layer around the Co clusters, which decreases the total magnetic moment of the cluster due to the exclusion of electrons of the Co atoms located on the surface. Attention is drawn to the difference between the magnetisation curves and hysteresis loops for colloid solutions of clusters and organised nanosystems (Fig. 25). Magnetic saturation is achieved for the fields $H = \sim 2$ T only in the case of the organised nanosystem, which implies collective rotation of the magnetic moments of nanoclusters.

The superparamagnetic behaviour of nanoclusters has been considered so far as a thermally activated process with an energy barrier of about K_aV. However, in organised nanosystems, quantum-tunnelling transitions accompanied by a discrete change in the magnetisation of the whole nanocluster system are also possible. These effects were observed for the $[Mn_{12}(CH_3COO)_{16}\cdot(H_2O)_4O_{12}]\cdot 2\,CH_3COOH\cdot 4\,H_2O$ single crystal, which is constructed from acetylacetonate manganese nanoclusters (Mn^*_{12}) with identical sizes.[45] This nanosystem exhibits unusual magnetisation and magnetic hysteresis curves (see Fig. 2). The hysteresis loop is stepwise and consists of vertical and flat sections. In the flat sections of the hysteresis loop, the relaxation time of the magnetic moment is longer than the time of the measurement ($\tau_{meas} \approx 600$ s). In the sloping sections, the relaxation time is close to the time of measurement, which gives rise to several

§ Blocking temperature is the temperature at which no thermal fluctuations take place over the period of magnetisation measurement.

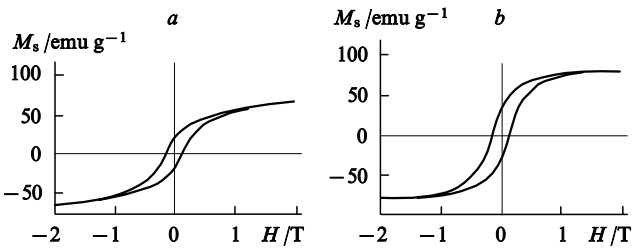


Figure 25. Magnetisation curves for Co nanoclusters with $d = 5.8$ nm; (*a*) a colloid solution in pyridine ($T = 3$ K), (*b*) a nanosystem organised on the graphite surface.[22]

minima in the curves for the dependence of τ on the external magnetic field (Fig. 26*a*). The dependence of $\Delta M/\Delta H$ on H provides exact magnitudes of the fields at which the relaxation times have a minimum. The relaxation time oscillates with respect to the applied field with a minimum corresponding to the steps in the hysteresis loop. Figure 26*b* gives the experimental τ values obtained at different temperatures for the H_0 values corresponding to the minima in the $\tau = f(H)$ curve (Fig. 26*a*): H_0 varies from 0 to 2.64 T with the step $H_{n+1} - H_n = \Delta H = 0.44$ T. At these points discontinuous change in τ is observed. They correspond to the sequence of intersection of electron levels with the spin $S = 10$. Calculation using the formula $\Delta H = D/g\mu_B = 0.44$ T (D is splitting of the level in the crystal field, g is the gyromagnetic ratio) gives $D = 0.60$ K, which coincides with the value $D = 0.61$ K,

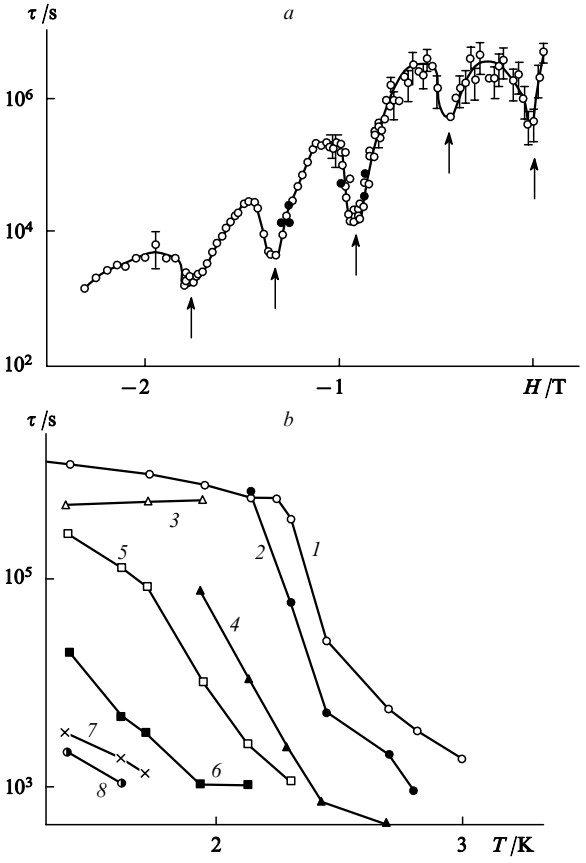


Figure 26. Relaxation time of the magnetic moment of the Mn_{12}^* cluster *vs.* the strength of the external magnetic field (*a*) and *vs.* temperature at different H_0 values (*b*).[45] The measurements were carried out at $T = 2.1$ K; (*a*) the arrows mark the H_0 values at which the steps are observed when the electron levels coincide; (*b*) H_0 values (in T): (*1*) 0, (*2*) 0.44, (*3*) 0.60, (*4*) 0.88, (*5*) 1.32, (*6*) 1.76, (*7*) 2.20, (*8*) 2.64.

reported in a study.[247] Thus, relaxation of the magnetic moment is accelerated when tuning by the magnetic field results in coincidence of the electron levels. This is indicative of quantum tunnelling in the magnetic cluster system, which is possible only when the levels of all clusters contained in the molecular crystal strictly coincide. The decrease in the relaxation time with an increase in temperature (Fig. 26*b*) is apparently due to the electron tunnelling through excited levels with lower Boltzmann occupancy. The probability of tunnelling depends on the width and the height of the barrier. Each minimum of the relaxation time corresponds to the resonance tunnelling from a given level with a time of the order of the measurement time.

An attempt has been made[248] to find out whether quantum tunnelling occurs in large clusters, for example in iron oxide hydroxide clusters, which constitute the core of the protein ferritin. The superparamagnetism phenomenon in such a large cluster (maximum size 6 nm) is usually observed at temperatures above 10 K (depending on the size of the ferritin core). Nevertheless, at low temperatures (5 and 12 K), the hysteresis curve for magnetisation of this cluster in the field with $H = 0$ also displays a step. It is obvious that for this system, coincidence of levels upon tuning by a magnetic field is impossible, which precludes quantum tunnelling. However, at one point ($H = 0$) with doubly degenerate levels, tunnelling is still possible. In addition, the blocking temperature of this system depends on the external magnetic field according to a non-trivial pattern. The temperature increases for low fields, passes through a maximum and decreases for high fields with $H > 0.3$ T. The increase in T_b for low fields is attributed to the violation of the quantum tunnelling condition at $H \neq 0$, while the decrease observed at high fields is ascribed to the decrease in the activation barrier to thermal fluctuations. It should be noted that in this experiment, the $\Delta M/\Delta H = f(H)$ curves have a standard shape, pointing to the absence of the quantum character of transitions.

Giant magnetoresistance effects. The giant magnetoresistance effect (GMR) in clusters is a great decrease in the resistance of the cluster material (by 1000%) when it has been inserted in a magnetic field, whereas the magnetoresistance of a bulk sample changes slightly (for example, the resistance of permalloy, 80% Ni–20% Fe, increases by 3% in a magnetic field). The GMR effects were observed in a study of the magnetic properties of various metallic[249–252] and oxide[253–257] nanosystems, the mechanisms of GMR origination for nanocrystalline metals and metal oxides being different.

Magnetic nanoclusters are prepared by dissolving one metal (for example, Fe or Co) in the matrix of another (conducting) metal (for example, Cu or Ag); these two components should be poorly soluble in each other. In a nanosystem consisting of a conducting metallic matrix and magnetic clusters, the conduction electrons of the matrix are scattered on the magnetic moments of the clusters. When a magnetic field is applied, the direction of the magnetic moments of the clusters changes; this changes their interaction with the conduction electrons of the metallic matrix and, hence, the conductivity. The magnitude of the GMR effect is determined by the ratio of the electron free path (l) to the distance between the neighbouring magnetic clusters, which depends on the concentration of the dissolved metal. When the free path is long, an electron undergoes numerous scattering events before it enters into interaction with the magnetic cluster (the direction of the cluster magnetic moment does not influence the electron scattering and no GMR is observed). If the free path is relatively short, magnetic clusters can be involved in the percolation processes of the matrix and can interact strongly with one another, which also eliminates GMR.

For a system consisting of Co clusters dissolved in an Ag matrix,[251] the change in the Co concentration from 10% to 50% is accompanied by a substantial change in the electric resistance of clusters in the magnetic field (Fig 27). The most pronounced effect is observed when the Co concentration is $\sim 20\%$, which is

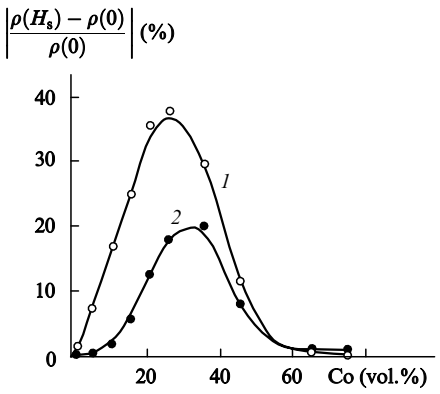


Figure 27. Giant magnetoresistance effect in the Co–Ag nanosystem *vs.* the Co concentration at $T = 5$ (*1*) and 300 K (*2*) in a 0.5-T magnetic field.[251]

attributed to the optimal size of the Co clusters in the Ag matrix. The GMR effect increases with a decrease in temperature.

To interpret the appearance of GMR, the two-current model is used. According to this model, electron scattering on the cluster magnetic moment in a disordered system is equivalent in two directions (for example, up and down). In a system ordered by a magnetic field, one direction, namely, that along the field, has a lower resistance than the other direction; this results in an overall decrease in the resistance. The change in the resistance ($\Delta\rho$) correlates with the change in the size of the magnetic cluster (d): $\Delta\rho \sim 1/d$.

Nanosystems that contain magnetic clusters are promising for controlling the magnetic field of conduction valves. A model system with epitaxially deposited Co(2.5 nm)–Cu(2.2 nm) nanofilms and with a Pb monolayer as an interlayer [252] demonstrated high sensitivity with respect to relatively weak fields (up to 0.05 T), which is of interest for practical purposes.

An even more pronounced effect (decrease of resistance by several orders of magnitude) was observed for perovskite structures of manganites.[253] These are ceramic samples, and, at first sight, in is difficult to distinguish a nanostructure in them. However, as will be shown below, the results of magnetic measurements in this type of system are interpreted resorting to cluster models. The results of studies of the $La_{0.67}Ca_{0.33}MnO_x$ films on $LaAlO_3$ substrates [253] are shown in Fig. 28. In the manganite,

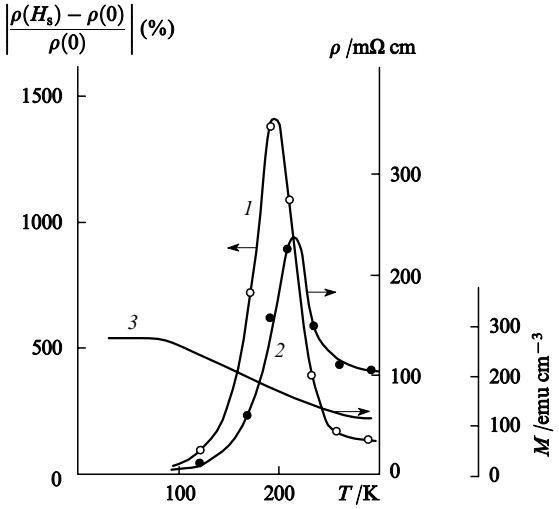


Figure 28. Temperature dependence of the giant magnetoresistance $|\rho(H_s)-\rho(0)/\rho(0)|$ (curve *1*), the resistance (ρ) (curve *2*) and magnetisation (M) (curve *3*) for $La_{0.67}Ca_{0.33}MnO_x$.

unlike metals or alloys, GMR does not cover the whole range of temperature measurement but occurs only in the vicinity of the phase transition from the semiconductor to metallic state (at $T = 220$ K). The most pronounced GMR effect induced by switching on a magnetic field with $H = 4-6$ T is achieved at $T \approx 190$ K, *i.e.*, near the point of transition to the metallic state. However, the temperature dependence of the magnetic moment of the manganite indicates that no sharp magnetic phase transition occurs at $T = 190-220$ K, magnetisation decreasing from the maximum value (saturation at $T = 100$ K) to $M \approx 100$ emu cm^{-3} (at room temperature). This indicates that the GMR is mainly influenced by the semiconductor–metal phase transition rather than the magnetic phase transition.

The GMR value is sensitive to the temperature of annealing and to the concentration of oxygen. Thus GMR measurements for a film prepared at 640 °C gave a smeared GMR peak with a maximum $\Delta\rho/\rho = 500\%$ at $T = 100$ K; for a film annealed at 700 °C in an O_2 atmosphere for 0.5 h, the peak $\Delta\rho/\rho = 1400\%$ was observed at $T \approx 200$ K; further increase in the annealing temperature to 900 °C resulted in a shift of the $\Delta\rho/\rho$ maximum to $T = 280$ K. The giant magnetoresistance observed in ceramics will undoubtedly find practical application.

The mechanism of the formation of GMR in ceramics differs apparently from that for metals. The spin dynamics in manganites of the $La_xCa_yMn_zO_3$ type in which the Mn atoms have been partly replaced by Fe has been studied by Mössbauer spectroscopy.[254–257] A $La_{0.75}Ca_{0.25}Mn_{0.98}Fe_{0.02}O_3$ sample prepared by sintering of salts and oxides was employed.[254] Figure 29 shows the Mössbauer spectra of this compound at different temperatures. Typically, in the region of GMR, the spectrum is separated into the paramagnetic central doublet and the magnetic HFS.[253] Broadening of the HFS lines points to a relaxation type of behaviour of the magnetic moment in the compound $La_{0.75}Ca_{0.25}Mg_{0.98}Fe_{0.02}O_3$, which is similar to the superparamagnetism observed for cluster nanosystems. However, ceramics consist of coarse grains, whose size is beyond the nanometer range.

Data on inelastic neutron scattering (INS) [258] attest that this compound is a ferromagnet at low temperatures; however, when the temperature rises, an inelastic component appears in the INS spectra. As the point of transition of the ceramics from the metallic to the paramagnetic state ($T_c = 250$ K) is approached, this component starts to predominate. This result suggests that in the region of transition of the ceramics from the semiconductor to metallic state, the GMR arises due to the appearance of fluctuating nano-sized regions, which possess ferromagnetic ordering. The size of these regions increases as the temperature decreases. An increase in the size of the region in which the ceramic passes from the paramagnetic to the metallic state is accompanied by an increase in the superparamagnetic relaxation time and the ultimate transition to the magnetically ordered, ferromagnetic state. The temperature range in which this magnetic transition takes place covers tens of degrees but it is in this region that the scattering of conduction electrons changes and the GMR effect arises due to the change in the relaxation time of the magnetic moment, the distances between the fluctuating clusters, and the cluster size (at temperatures below the phase transition temperature, there are no ferromagnetic nano-sized regions, whereas at high temperatures, there is no metallic electrical conductivity).

Magnetic phase transitions. In isolated nanoclusters and nanosystems, magnetic phase transitions are observed; usually, they are second-order phase transitions.¶ The magnetic phase transitions are characterised by Langevin dependences of magnetisation,[259] by disappearance of the magnetic order and spontaneous magnetisation at the Curie (T_C) and Neel (T_N) temperatures, respectively, and by smooth curves for the variation of the magnetisation with temperature. (Nanosystems can also possess superparamagnetism, resulting in an effective lowering of T_C and T_N.)

¶ These transitions are similar to those observed in bulk magnets.

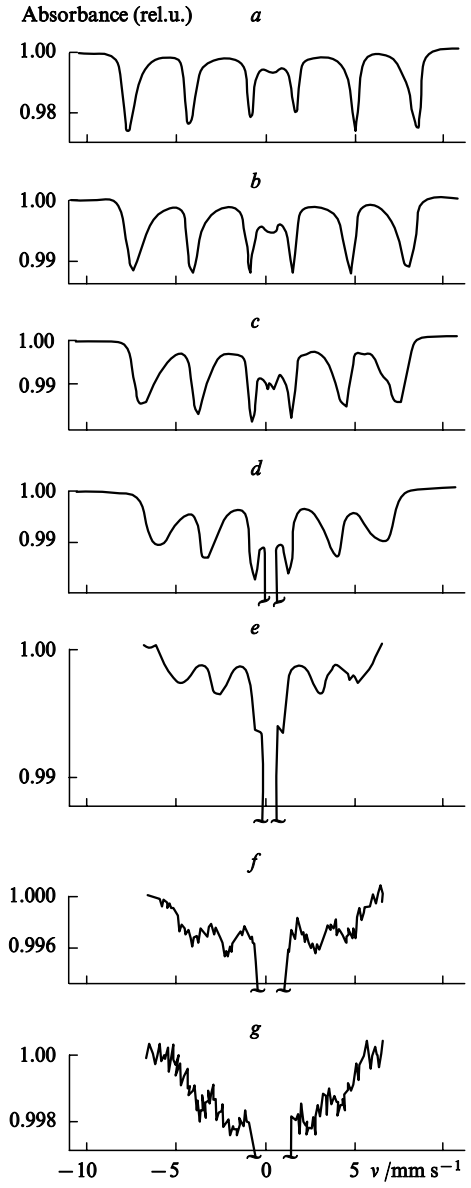


Figure 29. Mössbauer spectra ($a-g$) of a ceramic $La_{0.75}Ca_{0.25}Mn_{0.98}$-$Fe_{0.02}O_3$ sample at different temperatures.[254]
Temperature /K: 78 (*a*), 100 (*b*), 120 (*c*), 150 (*d*), 185 (*e*), 200 (*f*) 210 (*g*).

For several metal oxide clusters, in addition to second-order magnetic phase transitions, first-order magnetic phase transitions were also observed. In this case, a nanosystem lost abruptly the spontaneous magnetisation at some temperature T_{cc} or at some critical cluster size, below which the cluster passed into the paramagnetic state (not the superparamagnetic state). It is difficult to observe the first-order magnetic phase transitions in clusters by magnetisation measurements due to the scatter of clusters over sizes (this scatter results inevitably in smooth variations of the nanosystem magnetisation, and it is difficult to distinguish it from the superparamagnetic behaviour). However, Mössbauer spectroscopy can draw a distinction between the paramagnetic and magnetically ordered states; therefore, it is widely used to study the magnetic phase transitions.

The stepwise magnetic phase transitions were observed for iron oxide-based nanoclusters and nanosystems.[120, 260–263] Note that first-order magnetic phase transitions also take place in some bulk transition metal and rare earth metal oxides and alloys.[259] They are interpreted using a thermodynamic model.[264]

A thermodynamic model for magnetic phase transitions in nanoclusters has been proposed.[261] A cluster is assumed to exhibit a pronounced magnetostriction effect, *i.e.*, to change its volume on passing from the magnetically ordered to the paramagnetic state. Meanwhile, the Curie point of a substance depends on its volume

$$T_C = T_0\left(1 + \beta\frac{V - V_0}{V_0}\right), \tag{39}$$

where β is the magnetostriction constant of a substance, V and V_0 are molecular volumes of a substance in the magnetically ordered and paramagnetic states. The change in the Gibbs energy density on passing from the magnetically ordered state to the paramagnetic state is written in the form

$$\Delta G_V = -\frac{1}{2}NkTm^2 + \frac{1}{2}\eta\left(\frac{V - V_0}{V_0}\right)^2 + 2\frac{\alpha}{R}\frac{V - V_0}{V_0} + \frac{1}{2}NkT\left(\ln\frac{1 - m^2}{4} + m\ln\frac{1 + m}{1 - m}\right), \tag{40}$$

where N is the number of atoms with the spin 1/2, $m = M/M_s$ is the relative magnetisation value (M_s is the saturation magnetisation), η is the volume compressibility, and α is the surface tension. The first term in Eqn (40) corresponds to the exchange energy density in the molecular field approximation, the second term reflects the deformation energy, the third term corresponds to the surface energy, and the fourth one matches the entropy term for the temperature dependence of magnetisation.

Minimisation of the free energy and solution of the set of equations $d\Delta G_V/dV = 0$, $d\Delta G_V/dm = 0$ gives

$$\frac{T}{T_{c0}} = m\left(\frac{1}{3}\gamma m^2 + 1\right)\left(\frac{1}{2}\ln\frac{1 + m}{1 - m}\right)^{-1}, \tag{41}$$

where $T_{c0} = T_0(1 - \beta\eta p)$ shows the change in T_0 due to pressure ($p = 2\alpha/R$), $\gamma = (3/2)NkT_0\eta\beta^2(1 - \beta\eta p)^{-1}$.

Figure 30 presents the temperature dependence $m = f(T/T_{c0})$ for different values of the parameter γ, which determines the character of the magnetic phase transition. For $\gamma < 1$, the phase transition corresponds to a second-order magnetic transition and when $\gamma \geqslant 1$, it is a first-order magnetic transition. The γ value can be represented as $\gamma = T_{cc}/T_{c0}$, where $T_{cc} = (3/2)NkT_0^2\eta\beta^2$. If the cluster size $R \leqslant R_{cr}$, then for $\gamma \geqslant 1$, the cluster passes from the magnetically ordered to the paramagnetic state upon a first-order phase transition.

$$R_{cr} = \frac{2\alpha\beta\eta}{1 - T_{cc}/T_{c0}}. \tag{42}$$

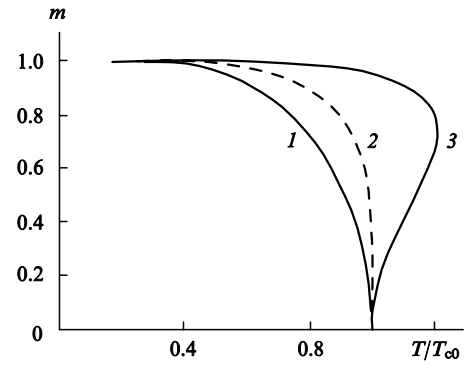


Figure 30. Temperature dependence of the cluster magnetisation for different γ (see the text).
(*1*) $\gamma < 1$, (*2*) $\gamma = 1$, (*3*) $\gamma > 1$.

For larger clusters, only the second-order phase transition can take place. It can also manifest itself as superparamagnetism at temperatures $kT > K_aV$.

The first- and second-order magnetic transitions were observed, for example, for the ferrihydrite $Fe_5HO_8 \cdot 4H_2O$ clusters formed in the polysorb pores.[261] The matrix method allows two cluster systems to be produced, namely, a system with isolated clusters and that with clusters interacting with one another (if several clusters occur in a pore). Figures 31 and 32 show the Mössbauer spectra of the ferrihydrite clusters obtained in 13- and 20-nm polysorb pores. The spectrum recorded at 4.2 K corresponds to a quadrupole doublet and consists of two parts — the central component and the magnetic hyperfine structure with relatively narrow lines (with allowance for the disorder of the cluster structure). As the temperature is raised, some of the HFS of the spectrum is converted into a paramagnetic doublet, without entering the intermediate states corresponding to the superparamagnetic behaviour. The results presented in Figs 31 and 32 suggest that a jumpwise first-order magnetic phase transition occurs in ferrihydrite clusters in the temperature range of 4.2–6 K. An increase in the iron concentration results in an increase in the cluster size; nevertheless, the spectral pattern at 4.2 and 6 K does not change.

In the spectra recorded at 10 K (Fig. 32 *c*) for large clusters ($c = 1.2 \times 10^{-3}$ mol litre^{-1}) formed in a 13-nm pore, the absorption line is broadened, which corresponds to the intermediate forms (between the quadrupole doublet and HFS), peculiar to superparamagnetism. Thus, at 10 K, a second-order magnetic transition is observed for large clusters, in addition to the first-order phase transition. For smaller clusters ($c = 1.2 \times 10^{-3}$ mol litre^{-1}, Fig. 31 *b*), line broadening is barely observed and the second-order magnetic transitions (superparamagnetism) do not show themselves. The appearance of superparamagnetism at 10 K made it possible to estimate the critical cluster size from the broadening of the HFS lines in the spectrum (Fig. 32 *c*), using relation (34): $R_{cr} \approx 2$ nm.

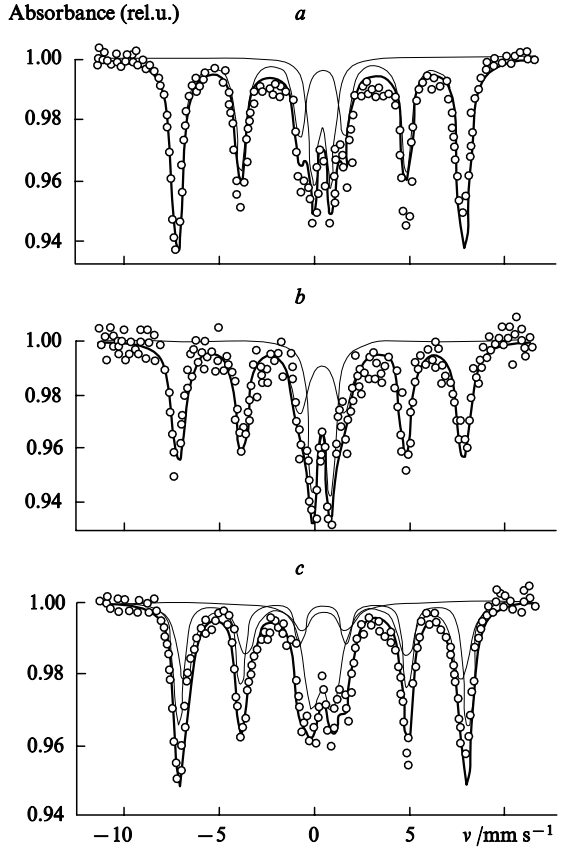


Figure 31. Mössbauer spectra of ferrihydrite clusters ($c = 1.2 \times 10^{-3}$ mol litre^{-1}) in polysorb pores with sizes of 13 (*a*, *b*) and 20 nm (*c*). Here and in Figs 32 and 33, the thick lines show the results of computer processing of the spectrum and the thin lines show its separation into components.
Temperature /K: (*a*) 4.2, (*b*) 10, (*c*) 42.

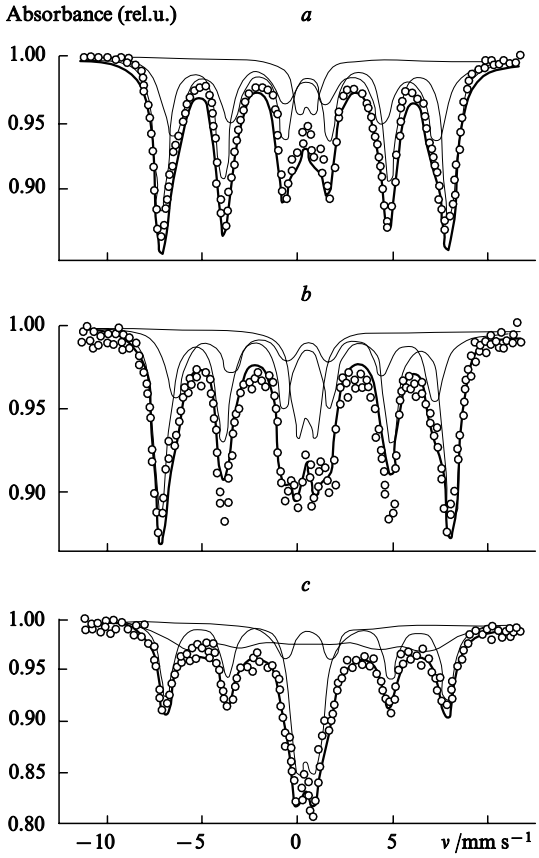


Figure 32. Mössbauer spectra of ferrihydrite clusters ($c = 1.2\,10^{-2}$ mol litre^{-1}) obtained in polysorb pores with a size of 13 nm at different temperatures.
Temperature /K: (*a*) 4.2, (*b*) 6, (*c*) 10.

Estimation of the size of the cluster formed in a pore from the concentration of iron atoms ($c = 1.2 \times 10^{-3}$ mol litre^{-1}) gives the value $R \approx 1-2$ nm (for an isolated cluster). Thus, these data and the data obtained on the basis of superparamagnetic relaxation can be used to estimate the R_{cr} value ($R_{cr} \approx 1.5-2$ nm).

Further growth of clusters and enhancement of their interactions is accompanied by appearance of second-order magnetic transitions: the HFS lines are markedly broadened and the first-order phase transition can no longer be distinguished against the background of the second-order transitions. Estimation of the R_{cr} size using relation (42) gives $R_{cr} \approx 1$ nm, which coincides in order of magnitude with the results obtained in experiments.

The effects similar to a first-order magnetic phase transition were also observed in the α-Fe_2O_3 nanoclusters,[265] in the α-FeOOH – α-Fe_2O_3 system,[266, 267] and in proteins, ferritin and hemosiderin, which include the magnetic core $(FeOOH)_8 \cdot (FeOOPO_3H)$.[268]

Yet another parameter determining the character of the magnetic phase transition is the external excess pressure. It has been noted above that the critical temperature of phase transition decreases upon an increase in pressure due to the change in the surface tension. A change in the external pressure by Δp entails a change in the magnetic transition temperature for the cluster by the value

$$\frac{\Delta T_{c0}}{T_0} = \frac{\Delta p}{2\alpha/R - 1/\beta\mu}. \quad (43)$$

Thus, a decrease in T_{c0} increases the probability of the first-order magnetic phase transition. A study of two nanosystems, namely, an ion exchange sulfo resin (sulfo cation exchange resin) incorporating iron hydroxide clusters with a size of 3 nm and a globular protein (ferritin) incorporating iron hydroxide clusters with a size of 6 nm has been reported.[262] In these systems, the interaction of clusters with the polymeric and biopolymeric networks changed due to hydration. The excess pressure on the cluster was determined from the deformation of the polymeric matrix [from the increase in the water volume which accompanied its crystallisation (freezing)]. This pressure is calculated from the expression

$$\Delta p = \frac{1}{\eta_m}\frac{\Delta V}{V}. \quad (44)$$

For $\Delta V/V = 0.09$ (for water) and $1/\eta_m = 5-10$ GPa,[196] it was found that $\Delta p = 0.45-0.9$ GPa, which is comparable in magnitude with the surface pressure in a 1.5-nm cluster (~ 1 GPa). Using relation (43), one can estimate the decrease in T_{c0} under the action of pressure. Assuming that $p = 1$ GPa, $\beta = 10^2$, $\mu = 10^{-11}$ m^2 J^{-1} and $1/N \sim 10^{-28}$ m^3 (the data were taken from publications [196, 261]), we have $\Delta T_{c0} = (0.1-1.0)T_{c0}$. Thus, ΔT_{c0} can reach a value of the order of T_{c0}.

The ΔT_{c0} value was estimated from the Mössbauer spectra of the sulfo cation exchange resin (in the range of $T = 4.2-30$ K) and ferritin (in the range of 4.2–78 K).[262] Hydration followed by freezing was found to be accompanied by a decrease in T_{c0}. This value was determined from spectra in which the paramagnetic state and the magnetic HFS of the spectra were equal. The following values were obtained: T_{c0}: 9–10 K for the hydrated sulfo cation exchange resin, 13–14 K for the dry cation exchanger, 30 K for hydrated ferritin, and 30–34 K for dry ferritin. Comparison of the T_{c0} values for the dry and hydrated samples provides the temperature shift $\Delta T_{c0} \approx 3-4$ K, which is in line with thermodynamic estimates.

The first-order magnetic phase transitions induced by intercluster stresses and defects can also arise in nanosystems containing larger nanoclusters (20–50 nm). These systems are formed in solid-phase chemical reactions (see Fig. 9),[263] for example, in cluster sintering, and are subject to substantial intercluster interactions. The phase transitions observed in these systems are similar to those in the ferrihydrite clusters (1–3 nm) in a polymeric matrix. Figure 33 shows the Mössbauer spectra of the α-Fe_2O_3–γ-Fe_2O_3 nanosystem. The spectra indicate that jumpwise magnetic transitions from the magnetically ordered state (magnetic HFS) to the paramagnetic state (central doublet) can take place in this system. These magnetic transitions take place at distributed critical temperatures $T_{c0} = 120-300$ K, which are lower than the temperatures T_{c0} for bulk samples of α- and γ-Fe_2O_3 (856 and 965 K, respectively). The decrease in T_{c0} cannot be due to superparamagnetism because of the large cluster size (see Fig. 9); therefore, the calculation using relation (34) affords relaxation times several orders of magnitude longer than τ_{meas}. As a consequence, magnetisation disappears abruptly, which is related to the transformation of the magnetic HFS of γ-Fe_2O_3 into a paramagnetic doublet (Figs 33 and 34 *a*).

The presence of the first-order magnetic phase transition in the α-Fe_2O_3–γ-Fe_2O_3 nanosystem is related to the strong intercluster interactions, which bring about substantial stress in the nanosystem. This stress results in the generation of enormous pressures (up to several Gigapascals). The pressures arise during sintering [121] of the α- and γ-Fe_2O_3 clusters, the unit cells of which have different specific volumes,† and under the action of defects

† The α-Fe_2O_3 clusters have an rhombohedral structure of the corundum type and γ-Fe_2O_3 has a spinel type cubic structure.

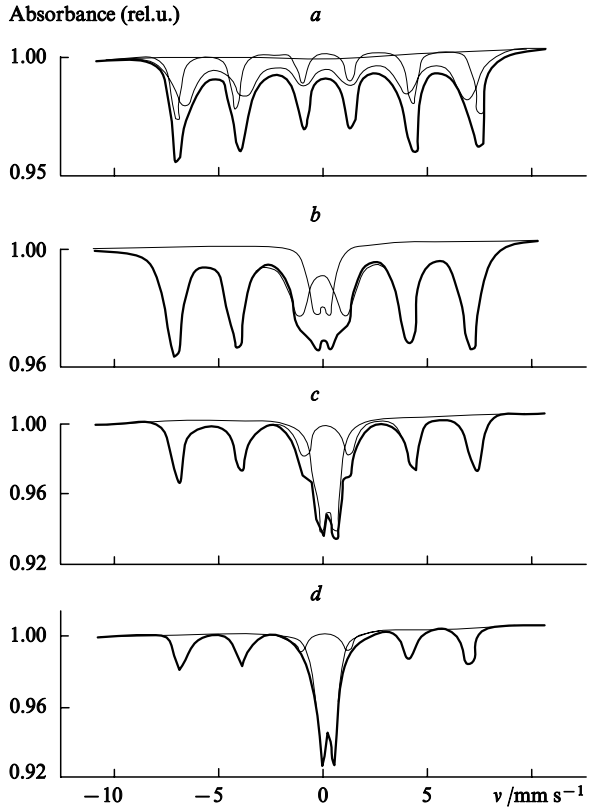


Figure 33. Mössbauer spectra of the α-Fe_2O_3–γ-Fe_2O_3 nanosystem (see Fig. 9) at different measurement temperatures.
Temperature /K: (*a*) 77, (*b*) 120, (*c*) 160, (*d*) 300.

and dislocations. As has been shown above (see Fig. 21), the density of defects has a maximum at a cluster size of exactly 20–30 nm. Further increase in the cluster size is accompanied by a decrease in the fraction of phase boundaries and defect density; thus, the cluster properties approach the properties of a bulk substance.

In addition to the first-order magnetic phase transition in this nanosystem, two more phase transitions were observed in this system, namely, a weak ferromagnetic–antiferromagnetic transition and a collective magnetic phase transition to give twined nanostructures.

Transitions from weak ferromagnetism (non-collinear antiferromagnetism) to antiferromagnetism (collinear antiferromagnetism) were observed for the α-Fe_2O_3 crystals. Weak ferromagnetism is also typical of $MnCO_3$, $CoCO_3$, MnF_2 and orthorhombic $MFeO_3$ crystals (M is a rare earth metal).[259] Weak ferromagnetism is found for antiferromagnetics with some small extent of non-collinearity of sublattice magnetisation. The non-collinearity of the magnetisation of sublattices in antiferromagnetic structures arises upon an increase in the temperature as a consequence of the instability of compensated antiferromagnetism.[269]

For bulk α-Fe_2O_3, a magnetic phase transition, known also as the Morin transition, takes place at $T_M \approx 260$ K; in this transition, the type of magnetic ordering changes jumpwise. When $T_M < 260$ K, collinear antiferromagnetism exists, while at $T > 260$ K, non-collinear antiferromagnetism (weak ferromagnetism) is observed. This transition is due to the internal symmetry of the crystal, which allows distortions in the crystal lattice at higher temperatures; this is accompanied by the rotation of spins through 90 °. The collinearity–non-collinearity phase transition for the magnetic moments of sublattices can be traced in the Mössbauer spectra as the change in the sign and the magnitude of the quadrupole splitting of the spectrum (ΔE_Q) possessing a magnetic HFS

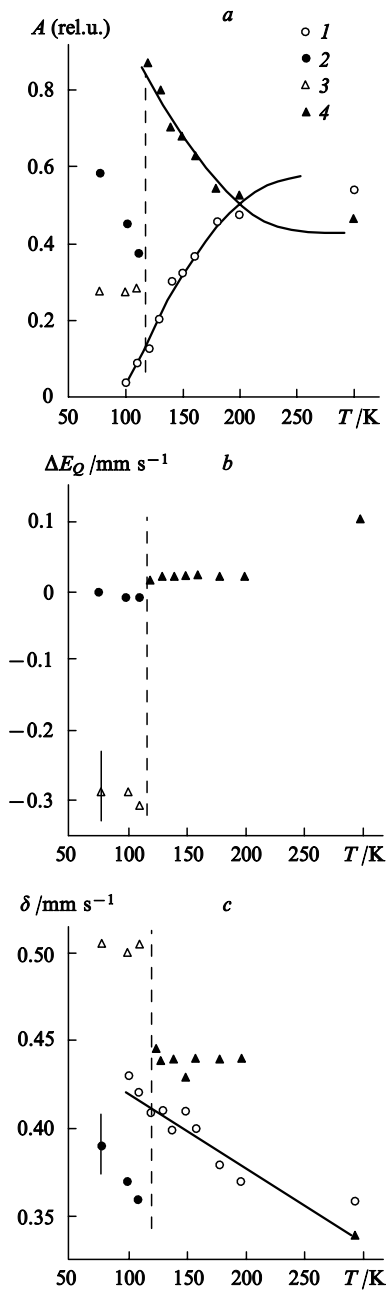


Figure 34. Results of computer simulation of the Mössbauer spectra of the α-Fe_2O_3–γ-Fe_2O_3 nanosystem: temperature dependences of the spectral surface areas (A) for various iron species (a), the quadrupole shift ΔE_Q of the magnetic HFS (b) and the isomer shift δ (c).
(1) Paramagnetic component (quadrupole doublet), (2) the magnetic component of γ-Fe_2O_3, (3) the magnetic component of α-Fe_2O_3, (4) the component corresponding to the twinning structure. The dashed line designates the region of the Morin phase transition.

$$\Delta E_Q = \frac{1}{8} e^2 q Q (3\cos^2\theta - 1),$$

where e is the electron charge, q is the crystal field gradient, Q is the quadrupole moment of the ^{57}Fe nucleus, θ is the angle between the directions of the atom spin and the electric field gradient on the nucleus. The high-temperature α-Fe_2O_3 phase is responsible for $\Delta E_Q = 0.2$ mm s^{-1}, and for the low-temperature phase, $\Delta E_Q = -0.3$ mm s^{-1}.

Now we shall consider specific features of this phase transition in the α-Fe_2O_3–γ-Fe_2O_3 nanosystem (Fig. 34 b). The low-temperature α-Fe_2O_3 phase ($\Delta E_Q = -0.3$ mm s^{-1}), exhibiting collinear antiferromagnetism at $T < 120$ K, passes into a state of non-collinear antiferromagnetism with $\Delta E_Q = 0-0.1$ mm s^{-1} at $T = 120$ K (high-temperature phase). Thus, in the nanosystem, the temperature of the Morin transition decreases to 120 K and the high-temperature phase has a lower ΔE_Q. The decrease in T_M is related to the magnetic dipole energy E_M and the exchange energy E_{exc} by a simple relation. As the cluster size decreases, the E_{exc} value decreases (because the T_{c0} value for Fe_2O_3 diminishes), and the probability of existence of the non-collinear antiferromagnetism increases. Similar examples of decrease in T_M following a decrease in the cluster size have been reported in other studies.[270, 271]

Yet another important circumstance should be mentioned. Despite the broad size distribution of nanoclusters, the phase transition in a nanosystem occurs at a fixed temperature $T_M = 120$ K. This attests to a collective transformation of the whole nanosystem, where the phase transition in one cluster initiates the phase transition in the whole sample. This type of phase transition with instantaneous collective phase transformations of the whole sample was also observed for the transformation of austenite into martensite in carbon steels (martensite transitions).[272]

Let us consider the temperature behaviour of the α-Fe_2O_3–γ-Fe_2O_3 nanosystem (from the Mössbauer spectroscopy data). At low temperatures ($T < 120$ K), both phases, α-Fe_2O_3 and γ-Fe_2O_3 exist in the system; at $T > 120$ K, the α-Fe_2O_3 and γ-Fe_2O_3 phases are converted into one common structure with the ΔE_α parameter corresponding to the α-phase, the crystal lattices of both phases being retained (X-ray diffraction data). The temperature dependence of the isomer shift δ (Fig. 34 c) demonstrates a sharp change in δ at 120 K: for the α-phase, δ decreases, while for the γ-phase, it increases jumpwise to an average value of 0.45 mm s^{-1}. These data point to collective transformations of the γ- and α-phases into an α-like phase; the retention of the crystal lattices of both phases can be explained by assuming the formation of a twinned nanostructure. Twinned structures are often formed upon crystallisation induced by mechanical deformations and during seed sintering. Twinning also occurs upon fast thermal expansion or compression and on heating of deformed crystals.[273, 274]

During the formation of the α-Fe_2O_3–γ-Fe_2O_3 nanosystem, sintering of iron oxide seeds takes place, resulting in the formation of strongly interacting clusters. It is strong intercluster interaction that appears to be responsible for the twin collective transitions in a nanosystem. As a consequence, the two-phase heterogeneous ($\alpha-\gamma$)-iron oxide nanosystem undergoes a sort of a phase temperature transition into a one-phase twinned nanostructure in which the γ-phase is attached to the α-phase. This transition is accompanied by the transfer of an electron from the γ-phase to the α-phase, which shows itself as an increase in the isomer shift.

This transition is a new feature of a heterogeneous nanosystem in which the generator of the transition, a cluster possessing a first-order collinear phase transition, induces the collective transition of the system to a twinned nanostructure. Indeed, the temperature of the twinning phase transition ($T_t = 120$ K) for this nanosystem coincides with the temperature of the antiferromagnetic–weak ferromagnetic phase transition ($T_M = 120$ K).

V. Conclusion

The unusual properties of nano-sized cluster systems have been attracting the attention of researchers for many years, and the interest in these systems has not abated. It is noteworthy that substantial progress in the study of nanoclusters and nanocluster systems has been achieved in recent years. This is due to the fact that the modern level of experiment permits not only the preparation of separate nanocluster particles but also investigation of their properties.

The main advances achieved in the design of new nanocluster systems are listed below:

— methods for the preparation of monodisperse nanoclusters and ordered nanosystems have been developed;

— ways of controlling cluster size, intercluster interaction and intercluster stress, permitting the formation and variation of the properties of nanosystems have been found;

— methods of stabilisation of nanocluster systems *via* passivation of isolated clusters have been proposed;

— methods for the production of ordered layers and superlattices using film and matrix relaxation and by the introduction of spacers have been developed.

Further progress in nanocluster chemistry would involve the synthesis of new nanostructures, creation and development of theoretical and experimental approaches to the study of mechanical, elastic, thermal, electronic, optical and magnetic properties of nanoclusters and nanosystems. The sequence nanocluster – nanosystem – nano-device should be adhered to.

The ordered systems and cluster nanocrystals manufactured on the basis of molecular clusters, fullerenes and colloid clusters can be used in nanotechnology for the design of single-electron devices, optical switches and non-linear systems, lasers with frequency tuned by changing the cluster size and quantum magnetics.

Fullerenes can be employed to manufacture unidimensional wires, rectifiers, diodes, electroluminescent light sources, field-emission cathodes and flat displays.

There appeared the possibility to produce superplastic materials by varying the mechanic properties.

The development of ordered nanolayers and superlattices opens the way to the development of single-electron devices, holographic images and superhigh-density magnetic recording.

The authors are grateful to Academician I I Moiseev, who initiated writing of this reviews and to Academicians V I Gol'dansky and L A Piruzyan, Doctors of Science V N Buravtsev and Yu M Maksimov for useful remarks.

This work was supported by the Russian Foundation for Basic Research (Project No. 00-03-3267).

References

1. I Prigogine, S Rice (Eds) *Evolution of Size Effect in Chemical Dynamics* Part 2 (New York: Wiley, 1988)
2. H Haberland (Ed.) *Clusters of Atoms and Molecules* (Berlin; Heidelberg: Springer, 1994)
3. A D Pomogailo, A S Rozenberg, I E Uflyand *Nanochastitsy Metallov v Klasterakh* (Metal Nanoparticles in Clusters) (Moscow: Khimiya, 2000)
4. I P Suzdalev *Vestn. RFFI* **1** (15) 24 (1999)
5. E L Nagaev *Usp. Fiz. Nauk* **162** (9) 49 (1992) [a]
6. A I Gusev *Usp. Fiz. Nauk* **168** (1) 55 (1998) [a]
7. R F Khairutdinov *Usp. Khim.* **67** 125 (1998) [*Russ. Chem. Rev.* **67** 109 (1998)]
8. R A Andrievskii *Usp. Khim.* **63** 431 (1994) [*Russ. Chem. Rev.* **63** 411 (1994)]
9. V I Sokolov *Izv. Akad. Nauk, Ser. Khim.* 1211 (1999) [b]
10. M N Vargaftik, N Yu Kozitsyna, N V Sherkashina, R I Rudy, D I Kochubey, I I Moiseev, in *Metal Clusters in Chemistry* Vol. 3 (Eds P Branstein, L A Oro, L A Raithly) (New York: VCH, 1999) p. 1363
11. S P Gubin *Khimiya Klasterov* (The Chemistry of Clusters) (Moscow: Nauka, 1987)
12. H Haberland, in *Clusters of Atoms and Molecules* (Ed. H Haberland) (Berlin; Heidelberg: Springer, 1994) p. 207
13. Yu I Petrov *Klastery i Malye Chastitsy* (Clusters and Small Particles) (Moscow: Nauka, 1986)
14. G B Sergeev *Vestn. Mosk. Univ., Ser. 2, Khim.* **40** 312 (1999) [c]
15. H W Kroto, J R Heath, S C O'Brien, R F Curl, R E Smalley *Nature (London)* **318** 162 (1985)
16. W Krätschmer, L D Lamb, K Fostiropoulos, D R Huffman *Nature (London)* **347** 354 (1990)
17. G Hammond, V Kuck (Eds) *The Fullerens* (Washington, DC: American Chemical Society, 1993)
18. R Taylor, D R M Walton *Nature (London)* **363** 685 (1993)
19. W E Billups, M A Cinfolini (Eds) *Buckminsterfullerenes* (New York: VCH, 1993)
20. O Lev, Z Wu, S Bharathi, V Glezer, A Modestov, J Gun, L Rabinovich, S Sampath *Chem. Mater.* **9** 2354 (1997)
21. L Motte, F Billoudet, E Lacaze, J Douin, M P Pileni *J. Phys. Chem. B* **101** 138 (1997)
22. C Petit, A Taleb, M P Pileni *J. Phys. Chem. B* **103** 1805 (1999)
23. J Evans *J. Chem. Soc., Dalton Trans* 555 (1996)
24. V G Syrkin *CVD-Metod. Khimicheskoe i Parofaznoe Okislenie* (CVD Method. Chemical and Vapour-Phase Oxidation) (Moscow: Nauka, 2000)
25. A A Chuiko, Yu I Gorlov *Khimiya Poverkhnosti Kremnezema* (The Chemistry of Silica Surface) (Kiev: Naukova Dumka, 1992)
26. G V Lisichkin, A Yu Fadeeva *Ross. Khim. Zh.* **40** 65 (1996) [d]
27. V B Aleskovskii *Khimiya Nadmolekulyarnykh Soedinenii* (The Chemistry of Supermolecular Compounds) (St. Petersburg: St. Petersburg State University, 1996)
28. V V Arslanov *Usp. Khim.* **63** 3 (1994) [*Russ. Chem. Rev.* **63** 1 (1994)]
29. P Chini *J. Organomet. Chem.* **200** 37 (1980)
30. B K Teo, N J A Sloane *Inorg. Chem.* **24** 4545 (1985)
31. J W A van der Velden, F A Vollenbroek, J J Bour, P T Beurkens, J M M Smits, W P Bosman *Recl. Trav. Chim. Pays-Bas* **100** 148 (1981)
32. V G Albano, A Ceriotti, P Chini, S Martinengo, W M Anker *J. Chem. Soc., Chem. Commun.* 859 (1975)
33. G Schmid, R Pfeil, R Boese, F Bandermann, S Meyer, G H M Calis, J W A van der Velden *Chem. Ber.* **114** 3634 (1981)
34. R G Wallenberg, J O Bovin, G Schmid *Surf. Sci.* **154** 256 (1985)
35. G Schmid *Chem. Rev.* **92** 1709 (1992)
36. R G Wallenberg, J O Bovin, A K Petford-Long, D J Smith *Ultramicroscopy* **20** 71 (1986)
37. J O Malm, J O Bovin, A K Petford-Long, D J Smith, G Schmid, N Klein *Angew. Chem., Int. Ed. Engl.* **27** 555 (1988)
38. G Schmid, B Morun, J O Malm *Angew. Chem.* **101** 772 (1989)
39. M N Vargaftik, V P Zagorodnikov, I P Stolarov, I I Moiseev, D I Kochubey, V A Liholobov, A L Chuvilin, K I Zamaraev *J. Mol. Catal.* **53** 315 (1989)
40. M N Vargaftik, I I Moiseev, D I Kochubey, K I Zamaraev *Faraday Discuss.* **92** 13 (1991)
41. G Schmid *J. Chem. Soc., Dalton Trans.* 1077 (1998)
42. Y Volokitin, J Sinzig, L J de Jough, G Schmid, M N Vargaftik, I I Moiseev *Nature (London)* **384** 621 (1996)
43. V I Gol'danskii, L I Trakhtenberg, V N Flerov *Tunnel'nye Yavleniya v Khimicheskoi Fizike* (Tunnel Effects in Chemical Physics) (Moscow: Nauka, 1986)
44. J R Friedman, U Voskoboynik, M P Sarachik *Phys. Rev. B, Condens. Matter* **56** 10793 (1997)
45. L Thomas, F Lionti, R Ballou, D Gatteschi, R Sessoli, B Barbara *Nature (London)* **383** 145 (1996)
46. N Herron, J C Calabrese, W E Farweth, Y Wang *Science* **259** 1426 (1993)
47. W Ekardt *Phys. Rev. B, Condens. Matter* **29** 1558 (1984)
48. W D Knight, K Clemenger, W A de Heer, W A Saunders, M Y Chou, M L Cohen *Phys. Rev. Lett.* **52** 2141 (1984)
49. M M Kappes, M Schar, U Rothlisberger, C Yeretzian, E Schumacher *Chem. Phys. Lett.* **143** 251 (1988)
50. D M Wood *Phys. Rev. Lett.* **46** 749 (1981)
51. C Bréchignac, Ph Cahuzac, F Carlier, M de Frutos, J Leygnier *J. Chem. Phys.* **93** 7449 (1990)
52. Z Penzar, W Ekardt *Z. Phys. D, At. Mol. Clusters* **17** 69 (1990)
53. D M Wood, N N Ashcroft *Phys. Rev. B, Condens. Matter* **25** 6255 (1982)
54. G Mie *Ann. Phys. (Germany)* **25** 377 (1908)
55. W D Knight, K Clemenger, W A de Heer, W A Saunders *Phys. Rev. B, Condens. Matter* **31** 2539 (1985)
56. C Bréchignac, Ph Cahuzac, F Carlier, M de Frutos, J Leygnier *Chem. Phys. Lett.* **189** 28 (1992)
57. H Handschuh, Chia Yen Cha, P S Bechthold, G Ganteför, W Eberhardt *J. Chem. Phys.* **102** 6406 (1995)
58. S Yang, M B Knickelbein *J. Chem. Phys.* **93** 1953 (1990)
59. M F Jarrold, in *Clusters of Atoms and Molecules* (Ed. H Haberland) (Berlin; Heidelberg: Springer, 1994) p. 315

60. A Berces, P A Hackett, L Lian, S A Mitchell, D M Rayner *J. Chem. Phys.* **108** 5476 (1998)
61. S K Nayak, B K Rao, S N Khanna, P Jena *Chem. Phys. Lett.* **259** 588 (1996)
62. S A Mitchell, L Lian, D M Rayner, P A Hackett *J. Chem. Phys.* **103** 5539 (1995)
63. H Kietzmann, J Morenzin, P S Bechthold, G Ganteför, W Eberhardt *J. Chem. Phys.* **109** 2275 (1998)
64. K Fisher, I Dance, G Willett, M Yi *J. Chem. Soc., Dalton Trans.* 709 (1996)
65. C Bréchignac, Ph Cahuzac, F Carlier, M de Frutos, J Leygnier, J Ph Roux *J. Chem. Phys.* **102** 763 (1995)
66. I M Billas, J A Becker, A Chatelain, W A de Heer *Phys. Rev. Lett.* **71** 4067 (1993)
67. I M L Billas, A Chatelain, W A de Heer *Science* **265** 1682 (1994)
68. J Shi, S Gider, K Babcock, D D Awschalom *Science* **271** 937 (1996)
69. A J Cox, J G Lounderback, S E Apsel, L A Bloomfield *Phys. Rev. B, Condens. Matter* **49** 12295 (1994)
70. S W McElvany, B I Dunlap, A O'Keefe *J. Chem. Phys.* **86** 715 (1986)
71. E A Rohlfing, D M Cox, A Kaldor *J. Chem. Phys.* **81** 3322 (1984)
72. G E Scuseria *Science* **271** 942 (1996)
73. P A Hintz, M B Sowa, S L Anderson *Chem. Phys. Lett.* **177** 146 (1991)
74. S W McElvany *J. Chem. Phys.* **89** 2063 (1988)
75. D C Parent, S W McElvany *J. Am. Chem. Soc.* **111** 2393 (1989)
76. W R Creasy *J. Chem. Phys.* **92** 7223 (1990)
77. A Muhr, R Nesper, B Schmyder, R Kotz *Chem. Phys. Lett.* **249** 399 (1996)
78. J C Hummelen, B Knight, J Pavlovich, R González, F Wudl *Science* **269** 1554 (1995)
79. K Kimura, T Sugai, H Shinohara *Chem. Phys. Lett.* **256** 269 (1996)
80. M Pellarin, C Ray, P Melinon, J Lerme, J L Vialle, P Keghelian, A Perez, M Broyer *Chem. Phys. Lett.* **277** 96 (1997)
81. D E Clemmer, J M Hunter, K B Shelimov, M F Jarrold *Nature (London)* **372** 248 (1994)
82. F Tast, N Malinowski, S Frank, M Heinebrodt, I M L Billas, T M Martin *Z. Phys. D, At. Mol. Clusters* **40** 351 (1997)
83. W Branz, I M L Billas, N Malinowski, F Tast, M Heinebrodt, T P Martin *J. Chem. Phys.* **109** 3425 (1998)
84. S Kawasaki, T Aketa, H Touhara, F Okino, O V Boltalina, I V Gol'dt, S I Troyanov, R Taylor *J. Phys. Chem. B* **103** 1223 (1999)
85. K Tanigaki, T W Ebbesen, S Saito, J Mizuki, J S Tsai, Y Kubo, S Kuroshima *Nature (London)* **352** 222 (1991)
86. J R Heath, S C O'Brien, Q Zhang, Y Liu, R F Curl, H W Kroto, F K Tittel, R E Smalley *J. Am. Chem. Soc.* **107** 7779 (1985)
87. M Saunders, H A Jiménez-Vázquez, R J Cross, S Mroczkowski, M L Gross, D E Giblin, R J Poreda *J. Am. Chem. Soc.* **116** 2193 (1994)
88. F D Weiss, J L Elkind, S C O'Brien, R F Curl, R E Smalley *J. Am. Chem. Soc.* **110** 4464 (1988)
89. Y Chai, T Guo, C Jin, R E Haufler, L P Chibante, J Fure, L Wong, J M Alford, R E Smalley *J. Phys. Chem.* **95** 7564 (1991)
90. B L Tumanskii, V V Bashilov, S P Solodovnikov, V I Sokolov, V P Bubnov, E E Laukhina,Yu I Estrin,V K Kol'tover, E B Yagubskii *Fullerene Sci. Technol.* **6** 445 (1998)
91. J A Northby *J. Chem.* 6166 (1987)
92. O Echt, O Kandler, T Leisner, W Miehle, E Recknagel *J. Chem. Soc., Faraday Trans.* 2411 (1990)
93. J Stapelfeldt, J Wormer, T Moller *Phys. Rev. Lett.* **62** 89 (1989)
94. D Scharf, J Jortner, U Landman *J. Chem. Phys.* **88** 4273 (1988)
95. W Miehle, O Kaundler, T Leisner, O Echt *J. Chem. Phys.* **91** 5940 (1989)
96. J Jortner, D Scharf, U Landman, in *Elemental and Molecular Clusters* (Eds G Benedek, T P Martin, G Pacchioni) (Berlin; Heidelberg: Springer, 1988) p. 148
97. U Buck, in *Clusters of Atoms and Molecules* (Ed. H Haberland) (Berlin Heidelberg: Springer, 1994) p. 396
98. K Liu, J D Cruzan, R J Saykally *Science* **271** 929 (1996)
99. J van Duijneveldt-van de Rijdt, F B van Duijneveldt *Chem. Phys.* **175** 271 (1993)
100. R Knochenmuss, S Leutwyler *J. Chem. Phys.* **96** 5233 (1992)
101. G Schmid, V Maihack, F Lantermann, S Peschel *J. Chem. Soc., Dalton Trans.* 589 (1996)
102. A P Alivisatos *Science* **271** 933 (1996)
103. M Mittleman, R W Schoeulein, J J Shiang, V L Colvin, A P Alivisatos, C V Shank *Phys. Rev. B, Condens. Matter* **49** 14435 (1994)
104. S Hotchandani, P V Kamat *J. Phys. Chem.* **96** 6834 (1992)
105. H C Youn, S Baral, J H Fendler *J. Phys. Chem.* **92** 6320 (1988)
106. M F Finlayson, K H Park, N Kakuta, A J Bard, A Campion, M A Fox, S E Weller, J M White *J. Lumin.* **39** 205 (1988)
107. K R Gopidas, P V Kamat *Proc. Indian Acad. Sci. Chem. Sci.* **105** 505 (1993)
108. A I Ekimov, I A Kudryavtsev, M G Ivanov, A L Efros *J. Lumin.* **46** 83 (1990)
109. T Rajh, O I Micic, D Lawless, N Serpone *J. Phys. Chem.* **96** 4633 (1992)
110. K R Gopidas, P V Kamat *Mater. Lett.* **9** 372 (1990)
111. M Grundemann *Phys. Rev. Lett.* **74** 4043 (1995)
112. T Vossmeyer, L Katsikas, M Giersig, I G Popovic, H Weller *J. Phys. Chem.* **98** 7665 (1994)
113. T Itoh, M Furumiya, T I Kehara *Solid State Commun.* **73** 272 (1990)
114. R W Schoeulein, D M Mitteman, J J Shiang, A P Alivisatos, P V Shank *Phys. Rev. Lett.* **70** 1014 (1993)
115. R L Fock, D W Taylor, K R German, A Kiel, E Buehler *Phys. Rev. Lett.* **32** 781 (1974)
116. R L Fock, D W Taylor *Phys. Rev. B, Condens. Matter* **19** 3365 (1979)
117. R N Bhargava, R N Gallagher, X Hong, A Nuemikko *Phys. Rev. Lett.* **72** 416 (1994)
118. N Murase, R Jagannathan, Y Kanematsu, M Watanabe, A Kurita, K Hirata, T Yazawa, T Kushida *J. Phys. Chem. B* **103** 754 (1999)
119. I P Suzdalev *Dinamicheskie Effekty v Gamma-Rezonansnoi Spektroskopii* (Dynamic Effects in Mössbauer Spectroscopy) (Moscow: Atomizdat, 1979)
120. I P Suzdalev, Yu V Maksimov, V N Buravtsev, V K Imshennik, A G Kazakevich, S V Novichikhin *Kolloid. Zh.* **62** 257 (2000) [e]
121. Ya G Geguzin *Fizika Spekaniya* (The Physics of Caking) (Moscow: Nauka, 1984)
122. N D Kingery, H K Bowen, D R Uhlmann *Introduction to Ceramic* (New York: Wiley, 1976)
123. A A Nazarov, A E Romana, R Z Valiev *Nanostruct. Mater.* **4** 1033 (1994)
124. R Z Valiev *Nanostruct. Mater.* **6** 73 (1995)
125. M Yu Gutkin, K N Mikaelzyan, I A Ovid'ko *Fiz. Tv. Tela* **37** 552 (1995) [f]
126. R Z Valiev, O A Kaibyshev, R I Kuznetsov, R Sh Musalimov, N K Tsenev *Dokl. Akad. Nauk SSSR* **301** 864 (1988) [g]
127. R Z Valiev, N A Krasilnikov, N K Tsenev *Mater. Sci. Eng. A, Struct. Mater.* **137** 35 (1991)
128. R Z Valiev, A V Korznikov, R R Mulyukov *Fiz. Met. Metalloved.* **73** 70 (1992) [h]
129. A V Rempel', A I Gusev, R R Mulyukov, in *Ul'tradispersnye Poroshki, Materialy i Nanostruktury* (Ultradispersed Powders, Materials and Nanostructures) (Ed. V E Red'kin) (Krasnoyarsk: Krasnoyarsk State Engineering University, 1996) p. 186
130. N I Noskova *Fiz. Met. Metalloved.* **73** 102 (1992) [h]
131. N I Noskova *Fiz. Met. Metalloved.* **76** 171 (1993) [h]
132. T Hill *Thermodynamics of Small Systems* (New York: Benjamin, 1964)
133. A W Adamson *Physical Chemistry of Surface* (New York: Wiley, 1976)
134. D W Oxtoby, in *Advances in Chemical Physics* Vol. 70 (New York: Wiley, 1988)
135. I P Suzdalev, V N Buravtsev, V K Imshennik, S V Novichikhin *Khim. Fiz.* **12** 555 (1993) [i]
136. I P Suzdalev, V K Imshennik, S V Novichikhin *Nucl. Instrum. Methods, Phys. Res. B* **76** 421 (1993)
137. V K Imshennik, I P Suzdalev, O N Stavinskaya, N I Shklovskaya, V Schuenemann, A X Trautwein, H Winkler *Microporous Mater.* **10** 225 (1997)
138. O N Stavinskaya, V K Imshennik, E I Oranskaya, I P Suzdalev, N I Shklovskaya *Zh. Fiz. Khim.* **72** 1269 (1998) [j]

139. O N Stavinskaya, V K Imshennik, S V Novichikhin, N I Shklovskaya, I P Suzdalev *Zh. Fiz. Khim.* **72** 1282 (1998) [j]
140. Yu V Maksimov, I P Suzdalev, M V Tsodikov, V Ya Kugel, O V Bukhtenko, E V Slivinskii, J A Navio *J. Mol. Catal. A, Chem.* **105** 167 (1996)
141. L Motte, F Billoudet, M P Pileni *J. Phys. Chem.* **99** 16425 (1995)
142. A Taleb, C Petit, M P Pileni *J. Phys. Chem. B* **102** 2214 (1998)
143. R L Whetten, J T Khoury, M M Alvarez, S Murthy, L Vezmar, Z L Wang, C Cleveland, W D Luedke, V Laudman *Adv. Mater.* **8** 428 (1996)
144. M Brust, D Bethell, D J Schiffrin, C J Kiely *Adv. Mater.* **7** 9071 (1995)
145. S A Harfenist, Z L Wang, M M Alvarez, I Vezmar, R I Whetten *J. Phys. Chem. B* **100** 13904 (1996)
146. J R Heath, C M Knobler, D V Leff *J. Phys. Chem. B* **101** 189 (1997)
147. S A Harfenist, Z L Wang, R L Whetten, I Vezmar, M M Alvarez *Adv. Mater.* **9** 817 (1997)
148. U-S S Jeng, T-L Lin, Ch-S Tsao, Ch-H Lee, T Canteenwala, L Y Wang, L Y Chiang, Ch C Han *J. Phys. Chem. B* **103** 1059 (1999)
149. S Nath, H Pal, D K Palit, A V Sapre, J P Mittal *J. Phys. Chem. B* **102** 10158 (1998)
150. E G Hope, J H Holloway *The Chemistry of Fullerenes* (Singapore: World Sci., 1995)
151. A A Gakh, A A Tuinman, J L Adcock *J. Am. Chem. Soc.* **116** 819 (1994)
152. V A Davydov, L S Kashevarova, A V Rakhmanina, V Agafonov, H Allouchi, R Céolin, A V Dzyabchenko, V M Senyavin, H Szwarc, T Tanaka, K Komatsu *J. Phys. Chem. B* **103** 1800 (1999)
153. G W Wang, K Komatsu, Y Murata, M Shiro *Nature (London)* **387** 583 (1997)
154. G Treboux, P Lapstun, K Silverbrook *J. Phys. Chem. B* **103** 1871 (1999)
155. Y Kuk, D K Kim, Y D Suh, K H Park, H P Noh, S J Oh, S K Kim *Phys. Rev. Lett.* **70** 1948 (1993)
156. T Hashizume, K Motai, X D Wang, H Shinohara, Y Saito, Y Makuyma, K Ohno, Y Kawazoe, Y Nishina, H W Pickering, Y Kuk, T Sakurai *Phys. Rev. Lett.* **71** 2959 (1993)
157. X D Wang, T Hashizume, H Shinohara, Y Saito, Y Nishina, T Sakurai *Phys. Rev. B, Condens. Matter* **47** 15923 (1993)
158. H Xu, D M Chen, W N Creager *Phys. Rev. Lett.* **70** 1850 (1993)
159. D Klyacko, D M Chen *Phys. Rev. Lett.* **75** 3693 (1995)
160. M Sakurai, H Tada, K Saiki, A Koma, H Funaska, Y Kishimoto *Chem. Phys. Lett.* **208** 425 (1993)
161. G Gensterblum, L M Yu, J J Pireaux, P A Thiry, R Caudano, J M Themblin, S Bouzidi, F Coletti, J H Debever *Appl. Phys.* **156** 175 (1993)
162. O Wada, Y Hanazato, M Miyamoto, S Suzuki, M Kataoka, S Isoda *Fullerene Sci. Technol.* **1** 393 (1993)
163. C Rey, J Garcia-Rodeja, L J Gallego *Phys. Rev. B, Condens. Matter* **55** 7190 (1997)
164. C Bréchignac, Ph Cahuzac, F Carlier, M de Frutos, A Masson, C Mory, C Colliex, B Yoon *Phys. Rev. B, Condens. Matter* **57** R2084 (1998)
165. R A Andrievskii *Usp. Khim.* **66** 57 (1997) [*Russ. Chem. Rev.* **66** 53 (1997)]
166. D A Dudko, V G Aleshin, A E Barg, N E Dubovitskaya, L N Larikov, A A Smekhnov *Dokl. Akad. Nauk SSSR* **285** 106 (1985) [g]
167. A E Barg *Metallofizika* **9** 118 (1995)
168. H van Swygenhoven *Nanostruct. Mater.* **6** 739 (1995)
169. R W Siegel, H Hahn, in *Current Trends in Physics of Materials* (Ed. M Yusouff) (Singapore: World Sci., 1987) p. 403
170. H Gleiter *Prog. Mater. Sci.* **33** 233 (1989)
171. T Rabe, R Wasche *Nanostruct. Mater.* **6** 357 (1995)
172. B H Kear, P R Strutt *Nanostruct. Mater.* **6** 827 (1995)
173. P Seegopaul, L E McCaudish, F M Shinneman *Int. J. Refract. Met. Hard Mater.* **15** 133 (1997)
174. G V Ivanov, N A Yavorovskii, Yu A Kotov, V I Davydovich, G A Mel'nikova *Dokl. Akad. Nauk SSSR* **275** 873 (1984) [g]
175. V V Ivanov, A N Vikhrev, A L Nozdrin *Fiz. Khim. Obrab. Mater.* **3** 67 (1997)
176. R A Andrievskii, A N Vikhrev, V V Ivanov, R I Kuznetsov, N I Noskova, V A Sazonova *Fiz. Met. Metalloved.* **81** 137 (1996) [h]
177. I P Suzdalev, V N Buravtsev, A V Volynskaya, V K Imshennik, V V Matveev *Khim. Fiz.* **14** 114 (1995) [i]
178. R M Lynden-Bell, D J Wales *J. Chem. Phys.* **101** 1460 (1994)
179. C L Cleveland, U Landman, W D Luedke *J. Phys. Chem.* **98** 6272 (1994)
180. R S Berry *J. Phys. Chem.* **98** 6910 (1994)
181. R S Berry, T L Beck, H L Davis, in *Evolution of Size Effect in Chemical Dynamics* (Eds I Prigogine, S Rice) (New York: Wiley, 1988) p. 75
182. S K Nayak, R Ramaswamy *J. Phys. Chem.* **98** 9260 (1994)
183. A Boutin, B Roussean, A H Fuchs *Chem. Phys. Lett.* **218** 128 (1994)
184. J Garcia-Rodeja, C Rey, L J Gallego, J A Alonso *Phys. Rev. B* **49** 8495 (1994)
185. R S Berry, in *Clusters of Atoms and Molecules* (Ed. H Haberland) (Berlin; Heidelberg: Springer, 1994) p. 201
186. I P Suzdalev, V N Buravtsev, V K Imshennik, Yu V Maksimov, V V Matveev, A V Volynskaya, A X Trautwein, H Winkler *Nuovo Cimento D* **18** 287 (1996)
187. I P Suzdalev, V N Buravtsev, Yu V Maksimov, A X Trautwein, H Winkler *Hyperfine Interact. (Netherlands)* **C1** 290 (1996)
188. I P Suzdalev, N I Shklovskaya *Colloid Surf. A* **108** 315 (1996)
189. I P Suzdalev *J. Radioanal. Nucl. Chem. Artic.* **190** 279 (1995)
190. I P Suzdalev, V K Imshennik, V V Matveev *Neorg. Mater.* **31** 807 (1995) [k]
191. I P Suzdalev, V N Buravtsev, V K Imshennik, Yu V Maksimov, V V Matveev, A V Volynskaya, A X Trautwein, H Winkler *Z. Phys. D, At. Mol. Clusters* **36** 163 (1996)
192. L D Landau, E M Lifshits *Statisticheskaya Fizika* (Statistic Physics) (Moscow: Nauka, 1951)
193. Ph Buffat, J P Borel *Phys. Rev. A, Gen. Phys., Ser. 3* **13** 22 (1976)
194. Y Osima, K Takaynagi *Z. Phys. D, At. Mol. Clusters* **27** 287 (1993)
195. A N Coldstein, C M Echer, A P Alivisatos *Science* **256** 1425 (1992)
196. I R Grigor'ev, U S Meilikhov (Eds) *Fizicheskie Velichiny. Spravochnik* (Physical Values. Handbook) (Moscow: Energoatomizdat, 1991)
197. B F Ormont *Dokl. Akad. Nauk SSSR* **124** 132 (1959) [g]
198. P A Rehbinder *Poverkhnostnye Yavleniya v Dispersnykh Sistemakh, Fiziko-Khimicheskaya Mekhanika* (Surface Effects in Dispersed Systems, Physicochemical Mechanics) (Moscow: Nauka, 1979) p. 142
199. G Goll, H Lohneyen *Nanostruct. Mater.* **6** 559 (1995)
200. J Trampenau *Nanostruct. Mater.* **6** 511 (1995)
201. R Z Valiev *Pis'ma Zh. Tekh. Fiz.* **15** 78 (1989) [l]
202. J Wang *Nanostruct. Mater.* **6** 747 (1995)
203. A S Plachinda, V E Sedov, V I Khromov, I P Suzdalev, V I Goldanskii, G U Nieuhaus, F Parak *Phys. Rev. B, Condens. Matter* **45** 7716 (1991)
204. A S Plachinda, V E Sedov, V I Khromov, L V Bashkaev, I P Suzdalev *Chem. Phys. Lett.* **175** 101 (1990)
205. V I Khromov, A S Plachinda, S I Kamyshanskii, I P Suzdalev *Izv. Akad. Nauk, Ser. Khim.* 886 (1996) [b]
206. I P Suzdalev, V I Goldanskii, Yu F Krupyanskii, I V Kurinov, A S Plachinda *Hyperfine Interact. (Netherlands)* **66** 177 (1991)
207. Ch Kittel *Introduction to Solid State Physics* (New York: Wiley, 1976)
208. J-B Maillet, A Boutin, S Battefey, F Calvo, A H Fuchs *J. Chem. Phys.* **109** 329 (1998)
209. I V Aleksandrov, R Z Valiev *Fiz. Met. Metalloved.* **77** 77 (1994) [h]
210. G W Neiman, J R Weertman, R W Siegel *J. Mater. Res.* **6** 1012 (1991)
211. J A Eastmen, M Fitzsimmons, L J Thompson *Philos. Mag. B* **66** 667 (1992)
212. I V Alexandrov, R Z Valiev *Philos. Mag. B* **73** 861 (1996)
213. H Muller, H G Fritsche, L Skala, in *Clusters of Atoms and Molecules* (Ed. H Haberland) (Berlin; Heidelbery: Springer, 1994) p. 114
214. X Y Qin, X Y Wu, I F Cheng *Nanostruct. Mater.* **2** 99 (1993)
215. M L Sui, K Lu *Mater. Sci. Eng. A, Struct. Mater.* **179–180** 541 (1994)
216. N J Petch *Iron Steel Int.* **174** 25 (1953)
217. R W Siegel, G E Fougere *Nanostruct. Mater.* **6** 205 (1995)
218. R Z Valiev, A V Korznikov, R R Mulyukov *Mater. Sci. Eng. A, Struct. Mater.* **168** 141 (1993)
219. Y Ishida *Nanostruct. Mater.* **6** 115 (1995)
220. T Kizuka *Philos. Mag. A* **69** 551 (1994)

221. S X McFadden, R S Mishra, R Z Valiev, A P Zhilyaev, A K Mukherjce *Nature (London)* **398** 684 (1999)
222. O D Sherby, O A Ruano, in *Superplastic Forming of Structural Alloys* (Eds E N Paton, C H Hamilton) (New York: The Metall. Soc. of AIME, 1982) p. 241
223. J G Wang, R J Raj *J. Am. Ceram. Soc.* **67** 385 (1984)
224. P Venezuela, J Tersoff, J A Floro, E Chason, D M Follstaedt, F Liu, M G Lagally *Nature (London)* **397** 678 (1999)
225. L H Schwartz, in *Application of Mössbauer Spectroscopy* Vol. 1 (Ed. R I Cohen) (New York: Academic Press, 1976) p. 37
226. J Lin, E Cates, P A Bianconi *J. Am. Chem. Soc.* **116** 4738 (1997)
227. K Uchino, E Sadanaga, T Hirose *J. Am. Ceram. Soc.* **72** 1555 (1989)
228. S Chettopadhyay, P Ayyub, V R Palkar, M Multani *Phys. Rev. B, Condens. Matter* **52** 13177 (1995)
229. P Ayyub, V R Palkar, S Chettopadhyay, M Multoni *Phys. Rev. B, Condens. Matter* **51** 6135 (1995)
230. Yu V Maksimov, I P Suzdalev, M Ya Kushnerev, R A Arents *Fiz. Met. Metalloved.* **37** 267 (1974) [h]
231. A A Rempel' *Dokl. Akad. Nauk* **347** 750 (1996) [g]
232. V L Colvin, M C Schlamp, A P Alivisatos *Nature (London)* **370** 354 (1994)
233. B O Dabbousi, M G Bawendi, O Onitsuka, M F Rubner *Appl. Phys. Lett.* **66** 1316 (1995)
234. L E Brus, P E Szajowski, W L Wilson, T D Harris, S Schuppler, P H Citrin *J. Am. Chem. Soc.* **117** 2915 (1995)
235. S H Tolbert, A B Herheld, C S Johnson, A P Alivisatos *Phys. Rev. Lett.* **73** 3266 (1994)
236. J K Vassiliou, V Mehrotra, M W Russell, E P Giannelis, R D McMichael, R D Shull, R Ziolo *J. Appl. Phys.* **73** 5109 (1993)
237. T Ung, M Giersig, D Dunstan, P Mulvaney *Langmuir* **13** 1773 (1997)
238. H Y Kai, Ph. D. Thesis, Netherland, Amsterdam Universiteit van Amsterdam, 1993
239. G I Frolov *Fiz. Tv. Tela* **38** 1208 (1996) [f]
240. D Fenske, in *Clusters and Colloids: From Theory to Application* (Ed. G Schmid) (Weinheim: VCH, 1994) p. 212
241. P Andres, J D Bielefeld, J I Heuderson, D B Yanes, V R Kolagunat, C P Kubiak, W J Mahoney, R G Osifchin *Science* **273** 1690 (1996)
242. G Hornyak, M Kröll, R Pugin, Th Sawitowski, G Schmid, J-O Bovin, G Karsson, H Hofmeister, S Hopfe *Chem. A, Eur. J.* 1951 (1997)
243. P G Collins, A Zettl, H Bando, A Thess, R E Smalley *Science* **278** 100 (1997)
244. A M Afanas'ev, I P Suzdalev, M Ya Gen, V I Gol'danskii, V P Korneev, E A Manykin *Zh. Eksp. Teor. Fiz.* **58** 115 (1970) [m]
245. A P Amulyavichus, I P Suzdalev *Zh. Eksp. Teor. Fiz.* **64** 1702 (1973) [m]
246. Kh Ya Mulyukov, G F Korznikova, R Z Valiev *Phys. Status Solidi A* **125** 609 (1991)
247. R Sessoli, D Gatteschi, A Caneschi, M A Novak *Nature (London)* **365** 141 (1993)
248. J R Friedman, M P Sarachik, J Tejoda, R Ziolo *Phys. Rev. Lett.* **56** 3830 (1996)
249. A E Berkowitz *Phys. Rev. Lett.* **68** 3745 (1992)
250. J Q Xiao, J S Jiang, C L Chien *Phys. Rev. Lett.* **68** 3749 (1992)
251. C L Chien *Annu. Rev. Mater. Sci.* **25** 129 (1995)
252. H D Chopka, B J Hockey, P J Chew, W F Egelhoff Jr, M Wuttig, S Z Hua *Phys. Rev. B, Condens. Matter* **95** 8340 (1997)
253. S Jin, T H Tiefel, M McCormack, R A Fastnacht, R Ramesh, L H Chen *Science* **264** 413 (1994)
254. M Pissas, G Kallias, E Devlin, A Simopoulos, D Niarchos *J. Appl. Phys.* **81** 5770 (1997)
255. Z W Li, A H Morrish, X Z Zhou, S Dai *J. Appl. Phys.* **83** 7198 (1998)
256. A Simopoulos, G Kallias, E Delvin, I Pangiotopoulos, M Pissas *J. Magn. Magn. Mater.* **171**–**181** 860 (1998)
257. A Tkachuk, K Rogucki, D E Brown, B Dabrowski, A J Fedro, C W Kimball, B Pyles, X Xiong, D Rosemann *Phys. Rev. B, Condens. Matter* **57** 8509 (1998)
258. J W Lynn, R W Erwin, J A Borchers, Q Huang, A Santoro, J L Peng, Z Y Li *Phys. Rev. Lett.* **76** 4046 (1996)
259. S V Vonsovskii *Magnetizm* (Magnetism) (Moscow: Nauka, 1971)
260. Yu F Krupyanskii, I P Suzdalev *Zh. Eksp. Teor. Fiz.* **67** 736 (1974) [m]
261. I P Suzdalev, V N Buravtsev, V K Imshennik, Yu V Maksimov, V V Matveev, S V Novichikhin, A X Trautwein, H Winkler *Z. Phys. D, At. Mol. Clusters* **37** 55 (1996)
262. I P Suzdalev, A S Plachinda, V N Buravtsev, Yu V Maksimov, S I Reiman, V I Khromov, D A Dmitriev *Khim. Fiz.* **17** 145 (1998) [g]
263. I P Suzdalev, Yu V Maksimov, S V Novichikhin, V N Buravtsev, V K Imshennik, V V Matveev *Khim. Fiz.* **19** 105 (2000) [i]
264. C V Bean, D S Rodbell *Phys. Rev.* **126** 104 (1962)
265. W Kundig, H Bommel, G Constabaris, R H Lindquist *Phys. Rev.* **142** 327 (1966)
266. A M van der Kraan, L I van Loef *Phys. Lett.* **20** 614 (1966)
267. T Shinjo *J. Phys. Soc. Jpn.* **21** 917 (1966)
268. S H Bell, H P Meir, D P E Dickson, J P Gibson, G A Sharp, T V Peters *Biochim. Biophys. Acta* **787** 227 (1984)
269. I E Dzyaloshinskii *Zh. Eksp. Teor. Fiz.* **33** 1454 (1957) [m]
270. Yu V Krupyanskii, I P Suzdalev *Fiz. Tv. Tela* **17** 588 (1975) [f]
271. A M van der Kraan *Mössbaur Effect Studies of Superparamagnetic α-FeOOH and α-Fe_2O_3* (Meppel: Krips Repro, 1972)
272. G E R Schulze *MetallPhysik* (Berlin: Academie-Verlag, 1967)
273. D P Hirth, J Lothe *Theory of Dislocations* (New York: McGraw-Hill, 1970)
274. J P Hirth *Acta Metall.* **22** 1023 (1971)

[a] — *Physics-Uspekhi (Engl. Transl.)*
[b] — *Russ. Chem. Bull. (Engl. Transl.)*
[c] — *Moscow Univ. Bull. (Engl. Transl.)*
[d] — *Mendeleev Chem. J. (Engl. Transl.)*
[e] — *Colloid J. (Engl. Transl.)*
[f] — *Phys. Solid State (Engl. Transl.)*
[g] — *Dokl. Chem. Technol., Dokl. Chem. (Engl. Transl.)*
[h] — *Phys. Met. Metall. (Engl. Transl.)*
[i] — *Chem. Phys. Rep. (Engl. Transl.)*
[j] — *Russ. J. Phys. Chem. (Engl. Transl.)*
[k] — *Inorg. Mater. (Engl. Transl.)*
[l] — *Techn. Phys. Lett. (Engl. Transl.)*
[m] — *J. Exp. Theor. Phys. (Engl. Transl.)*